DESIGN AND ANALYSIS OF A HIGH VOLTAGE EXPLODING FOIL INITIATOR FOR MISSILE SYSTEMS

A THESIS SUBMITTED TO
THE GRADUATE SCHOOL OF NATURAL AND APPLIED SCIENCES
OF
MIDDLE EAST TECHNICAL UNIVERSITY

BY

MUHAMMED YUSUF YILMAZ

IN PARTIAL FULFILLMENT OF THE REQUIREMENTS
FOR
THE DEGREE OF MASTER OF SCIENCE
IN
MECHANICAL ENGINEERING

JANUARY 2013

Approval of the thesis:

DESIGN AND ANALYSIS OF A HIGH VOLTAGE EXPLODING FOIL INITIATOR FOR MISSILE SYSTEMS

submitted by **MUHAMMED YUSUF YILMAZ** in partial fulfillment of the requirements for the degree of **Master of Science in Mechanical Engineering Department, Middle East Technical University** by,

Prof. Dr. Canan ÖZGEN _____
Dean, Graduate School of **Natural and Applied Sciences**

Prof. Dr. Suha ORAL _____
Head of Department, **Mechanical Engineering**

Prof. Dr. Abdullah ULAŞ _____
Supervisor, **Mechanical Engineering Dept., METU**

Examining Committee Members:

Prof. Dr. Hüseyin VURAL _____
Mechanical Engineering Dept., METU

Prof. Dr. Abdullah ULAŞ _____
Mechanical Engineering Dept., METU

Asst. Prof. Dr. Ahmet YOZGATLIGİL _____
Mechanical Engineering Dept., METU

Asst. Prof. Dr. Metin YAVUZ _____
Mechanical Engineering Dept., METU

Prof. Dr. Faruk ELALDI _____
Mechanical Engineering Dept., BU

Date: 21.01.2013

I hereby declare that all information in this document has been obtained and presented in accordance with academic rules and ethical conduct. I also declare that, as required by these rules and conduct, I have fully cited and referenced all material and results that are not original to this work.

Name, Last Name: M. Yusuf YILMAZ

Signature :

ABSTRACT

DESIGN AND ANALYSIS OF A HIGH VOLTAGE EXPLODING FOIL INITIATOR FOR MISSILE SYSTEMS

Yılmaz, Muhammed Yusuf
M. S., Department of Mechanical Engineering
Supervisor: Prof. Dr. Abdullah Ulaş

January 2013, 98 pages

Increasing insensitivity demands on designing and producing munitions necessitates utilizing primarily insensitive initiation trains specifically in missile systems. Exploding Foil Initiator (EFI) is a high voltage detonator that is used as the initiation element of rocket motor and warhead initiation trains of modern insensitive missile systems.

In this thesis, EFI prototypes are designed and manufactured with the knowledge gained from detailed literature studies. An experimental setup is constructed including firing and testing means for EFI prototypes. That experimental setup is capable of firing EFI prototypes from 500 volts to 3000 volts voltage range. Besides, it allows measuring electrical characteristics like current and voltage traces and average velocity of the flyer plates of these prototypes. Using EFI prototypes, detonation tests of HNS – IV and PBXN – 5 explosive pellets are carried out. Function times and detonation outputs of the prototypes are measured with the same experimental setup.

A numerical study which predicts electrical performance of EFI prototypes and impact characteristics of flyer plates are carried out. Numerical code is validated with the experimental results.

Key-words: Exploding Foil Initiator (EFI), Slapper Detonator, Exploding Bridge

ÖZ

FÜZE SİSTEMLERİ İÇİN YÜKSEK VOLTAJ PATLAYAN FOLYOLU BAŞLATMA ELEMANI TASARIMI VE ANALİZİ

Yılmaz, Muhammed Yusuf
Yüksek Lisans, Makina Mühendisliği Bölümü
Tez Yöneticisi: Prof. Dr. Abdullah Ulaş

Ocak 2013, 98 sayfa

Mühimmat tasarımı ve üretimi sırasında giderek artan duyarsızlık gereksinimleri, özellikle füze sistemlerinde en başta duyarsız ateşleme zincirleri kullanılmasını gerektirmektedir. Patlayan Folyolu Başlatma Elemanı, modern duyarsız füze sistemlerinin roket motoru ve harp başlığı ateşleme zincirlerinin başlatma elemanı olarak kullanılan bir yüksek voltaj detonatördür.

Bu tez çalışmasında, detaylı literatür çalışmalarından elde edilen bilgi birikimi ile özel Patlayan Folyolu Başlatma Elemanı prototipleri tasarımı yapılarak bu prototipler ürettirilmiştir. Patlayan Folyolu Başlatma Elemanı prototipleri için ateşleme ve test imkanı içeren bir deneysel düzenek kurulmuştur. Bu deneysel düzenek, Patlayan Folyolu Başlatma Elemanı prototiplerinin 500 volt ile 3000 volt arasında ateşlemesini yapabilir. Bunun yanında prototiplere ait akım ve voltaj gibi elektriksel karakteristiklerin ve uçan plakaların ortalama hızının ölçülmesine izin verir. Patlayan Folyolu Başlatma Elemanı prototipleri kullanılarak HNS – IV ve PBXN - 5 patlayıcı peletleri patlatma testleri yapılmıştır. Aynı deneysel düzenek ile detonatörün çalışma zamanı ve detonasyon çıktısı ölçülmüştür.

Patlayan Folyolu Başlatma Elemanı prototiplerinin elektriksel performanslarını ve uçan plakaların çarpma karakteristiklerini tahmin eden bir nümerik çalışma yapılmıştır. Sayısal kod deneysel sonuçlar ile karşılaştırılarak doğrulanmıştır.

Anahtar Kelimeler: Patlayan Folyolu Başlatma Elemanı, Slapper Detonatör, Patlayan Köprü

ACKNOWLEDGMENT

It is my pleasure to find a great chance to be supervised by Prof. Dr. Abdullah ULAŞ. I would like to express my deepest thanks to him for his guidance, faith and patience throughout this study.

I would like to thank to my manager Suzan KOÇ for her encouragement from the beginning till the end of this study. She stoically shared her every precious experience with me throughout the study.

I would also like to thank to committee members for their advices which guide me to have a better thesis.

I would like to thank to Osman YÜCEL, Osman AKDAĞ and Ayşe SEVER AKDAĞ for their invaluable fellowship. I further express my deepest gratitude to Mehmet Can ORAN and his fiancée Ayşem ÇAĞLAR for being great friends during such a tedious period of my life.

I would like to thank to my colleagues Funda EROĞUL, Satılmış İNAL, Arif Serdar İNAN and Halil İbrahim ÖNCÜ for their aids and patience at tough times that I faced frequently during this study. Very special thanks to my colleagues Burak KIZILKAYA, Murat AKKUŞ and Nil Ezgi DİNÇER for their priceless efforts in experimental and numerical studies of this thesis.

It is very hard to put my gratitude into words to my family. They deserve more than that ordinary appreciation for being a magnificent family. I dedicate this thesis to my father, Mustafa YILMAZ, my mother, Feride YILMAZ and my brothers İbrahim YILMAZ and İsmail YILMAZ.

This study is supported by ROKETSAN MISSILE INDUSTRIES INC.

TABLE OF CONTENTS

LIST OF TABLES

LIST OF FIGURES

FIGURES

LIST OF SYMBOLS

A	Constant for velocity calculations
C	Capacitance of the capacitor in Capacitor Discharge Circuit (CDC)
C_{0e}	Sound speed in the explosive
C_{0f}	Sound speed in the flyer plate
C_p	Specific heat capacity
CF	Constant for velocity calculations
d	Separation distance between two conductors
E	Energy
E_b	Energy up to burst
E_{bp}	Energy needed for boiling
E_{fus}	Energy needed for fusion
E_{ion}	Energy needed for ionization
E_{loss}	Loss energy before burst of the metallic bridge
E_{mp}	Energy needed for melting
E_{post}	Energy added to the system after burst of the metallic bridge
E_{pre}	Excess energy after burst of the metallic bridge
E_{RPE}	Relative percentage error
E_{vap}	Energy needed for vaporization
f_d	Oscillating frequency of current in ringdown tests
I	Current
I_{burst}	Burst current
I_p	First ionization energy
l	Length of the metallic bridge
l_{sl}	Length of the conductor in stripline
L_{cdc}	Inductance of Capacitor Discharge Circuit (CDC)
L_f	Latent heat of fusion
L_p	Inductance of voltage probe
L_{sl}	Inductance of the stripline
L_t	Total inductance of EFI system
L_v	Latent heat of vaporization
M_b	Mass of the metallic bridge
M_f	Mass of the flyer plate
M_{tamp}	Mass of the tamper
n	Polytropic gas exponent
P	Power
P_e	Pressure pulse on the explosive
P_f	Pressure pulse on the flyer plate
Q	Electrical charge
Q_0	Initial electrical charge
R_b	Dynamic bridge resistance
R_{b0}	Initial bridge resistance
R_{burst}	Resistance of metallic bridge at burst
R_{cdc}	Resistance of Capacitor Discharge Circuit (CDC)
R_{cvr}	Resistance of Current Viewing Resistor (CVR)
R_d	Total dynamic resistance of EFI system
R_{sl}	Resistance of stripline

R_{sw}	Dynamic switch resistance
R_{sw0}	Initial resistance of the switch
R_{swf}	Steady resistance of the switch
R_t	Total resistance of EFI system
t	Time
t_a	Time of arrival of the flyer plate to the exit of the barrel
t_b	Burst time
t_p	Duration of the pressure pulse
t_{sw}	Switching time
th_f	Thickness of the flyer plate
T	Temperature
T_0	Initial temperature
T_b	Burst temperature
T_{bp}	Boiling temperature
T_{fd}	Reciprocal of oscillating frequency
T_{mp}	Melting temperature
U_p	Common particle velocity
U_{pe}	Particle velocity in the explosive
U_{pf}	Particle velocity in the flyer plate
V	Voltage
V_0	Initial voltage of the capacitor
V_{burst}	Voltage at burst
$V_{corrected}$	Corrected voltage
$V_{measured}$	Measured voltage
V_f	Final velocity of the flyer plate
V_i	Induced voltage
w	Width of the metallic bridge
W	Width of the conductor in stripline
x_i	Constant for initiation criterion check calculations
x_{bc}	Calculated burst time variable
x_{bm}	Measured burst time variable

Greek Symbols:

α	First temperature coefficient of resistance
α_i	Ionization degree
ρ_0	Initial electrical resistivity
ρ_{0e}	Initial density of the explosive
ρ_{0f}	Initial density of the flyer plate
ρ_b	Density of the metallic bridge
ρ_e	Density of the explosive
ρ_f	Density of the flyer plate
ρ_{tamp}	Density of the tamper
χ	Displacement of the flyer plate
$\dot{x}$	Velocity of the flyer plate
$\ddot{x}$	Acceleration of the flyer plate

CHAPTER 1

INTRODUCTION

In recent years, a strong desire for developing insensitive munitions results a large amount of effort for decreasing the sensitivity of energetic components in missile systems. In the past, functionality of an energetic component was considered primary importance. However, this attitude has changed in a way that reliability and safety of energetic components become more vital during design period of munitions.

Reliability and safety considerations for energetic components start with the design of ignition systems in munitions. Ignition of a rocket motor and a warhead in missile systems needs special initiation mechanisms. Those mechanisms mainly consist of an energetic initiation train and a safety device that secures the initiation train by controlling the transmission of required energy to the initiation system.

In order to have a reliable and safe initiation train, design considerations should be primarily focused on the initiators. Basically there are three types of initiators which are namely, Hot Bridgewire Initiators (HBWs), Exploding Bridgewire Initiators (EBWs) and Exploding Foil Initiators (EFIs). HBWs may be classified as low voltage initiators and they are mainly used as the first energetic component in rocket motor initiation trains. A HBW basically consists of a thin metal wire which is ohmically heated by applying quite low electrical energies. EBWs are classified as high voltage detonators and they have been rarely used in missile systems. EBWs are more likely to be preferred in civil applications like oil – off shore platforms, forest service, mining and seismic studies; however, they are also used in military research.

EFIs are also classified as high voltage detonators and they are used as the first energetic component of rocket motor and warhead initiation trains in insensitive munitions. The main difference between an EBW and an EFI is EFI uses an exploding metallic foil instead of an exploding wire. The foil needs much more energy to explode comparing to the bridgewire.

EFIs can only be initiated with high voltages (e.g. > 500 volts) discharged from special circuits so they are strictly immune to electromagnetic effects and it is nearly impossible to initiate them with electrostatic discharges caused by personnel or systems they are mounted on [1]. Besides, EFIs can initiate insensitive and durable secondary high explosives like HNS-IV which cannot be initiated by other types of detonators. These reasons make EFIs safe to handle without considering additional safety precautions and eliminate the need for complex and heavy physical barriers on missile systems like Electro - Mechanical Safe and Arm Devices.

A schematic of initiation train for rocket motor and warhead of a missile is shown in Figure 1.1. As shown, Electronic Safe and Arm Device (ESAD) is the control unit for initiation of EFIs. This device contains EFI firing unit which is a special Capacitor Discharge Circuit (CDC). For rocket motor initiations, a detonation – to – deflagration transition igniter called Through Bulkhead Initiator (TBI) is used in between rocket

motor igniter and EFI. Conventionally, rocket motor igniter is a pyrotechnic device that is used to ignite the propellant in rocket motor.

On the other side, working principle of a warhead initiation train is quite straightforward. Same ESAD is used for controlling and functioning of EFI but this time the chain is fully based on detonation. So the need for a transition initiator is eliminated. Booster explosive generally consists of one secondary high explosive; however sometimes combinations of two or more high explosive chains are utilized. Detonation of booster explosive initiates the warhead.

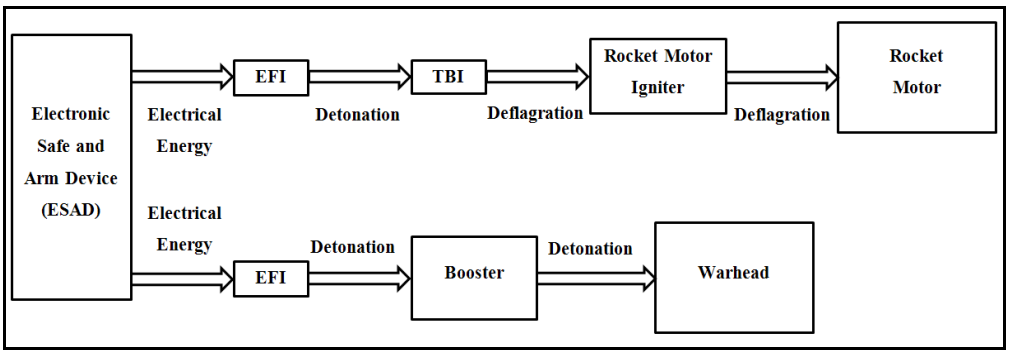

Figure 1.1 Initiation Trains for Missiles

1.1 MOTIVATION AND SCOPE OF THE THESIS

Missile production capability in Turkey has been increasing in recent years. The developments in certain parts of the missiles make Turkey a competitive country in the world. However, as it is stated above, safety and reliability of munitions have been a major concern in the market. To date, 1 W / 1 A / 5 min. safe HBWs that are developed in - house have been utilized in rocket motor initiation trains. The initiation trains in warheads have been obtained from foreign vendors.

1 W / 1 A / 5 min. safe HBWs are relatively safe initiators; however, one should be very careful in handling these kind of initiators since they can be initiated by electrostatic discharges from a human body. Besides, the initiators should not be used in radio frequency electromagnetic fields in order to prevent inadvertent firings. All of these precautions complicate working with HBWs.

Imported initiation trains are always troublesome since everlasting governmental authorizations and long export times because of the transportation of energetic materials are serious issues. Furthermore, one can be obliged to design the rest of the system according to that imported initiation train since it is very tedious to change the design of off – the – shelf components. Also there is always a strong potential that in the future foreign governments may restrict the export of the energetic materials to Turkey.

All of these above mentioned issues lead a pyrotechnics system design engineer to at least design an insensitive initiation train in - house. So it is aimed to build an insensitive high voltage initiator and to establish firing and testing means for this initiator. Following lines summarize the scope of this study.

In this study, it is primarily aimed to design EFI striplines which can later be used to initiate insensitive secondary high explosives in warhead and rocket motor initiation trains of missile systems. Another major goal is to detonate a secondary high explosive with EFI striplines.

Design process first includes getting into previous related works. A detailed theoretical knowledge is aimed to be obtained from a good number of studies. The theoretical knowledge is desired to be utilized throughout this study.

Another major objective is to construct an experimental setup for firing and testing of designed and manufactured EFI striplines. The setup is aimed to last years to be able to fire and to test other configuration parameters of next level EFI striplines. Furthermore, getting used to work with high voltage equipment and high voltage data recording are intended. It is also a primary goal to manipulate and interpret the experimental data obtained from firing and testing of EFI striplines.

This study also aims to build a theoretical numerical model to predict performance features of EFIs. It is objected that the results of this theoretical model and the experimental data show good agreement.

After all it is expected to have a full knowledge about EFIs which aids in designing another EFI easily for compensating any systems' requirements. The result of this work is aimed to be a useful small scale EFI prototype which can be used in warhead and rocket motor initiation trains.

1.2 PRESENT STUDY

During this study, a large number of literature courses for EFIs are studied out. Many of these works are great sources for inspiration that guide the present study. Theoretical knowledge obtained from related works is very useful in developing a great point of view about EFIs and it also saves a lot of time for the remaining work. Related literature data are represented exclusively in CHAPTER 2.

Several configurations for EFI prototypes are selected with the configuration parameters guided by literature. Design and manufacturing processes of EFI prototypes are explained in CHAPTER 3.

To be able to realize the effect of system parameters on the performance of EFIs, experiments are carried out with a newly constructed experimental setup. The setup is capable of measuring electrical performance and average velocity of EFI prototypes. Details of experimentation are given in CHAPTER 4.

Performance predictions of EFIs are performed with a semi-empiric thermodynamics based numerical study. Basic energy equations relating electrical energy to heat

energy are used to obtain performance of EFI prototypes for different system parameters. Structure of the numerical study is represented in CHAPTER 5.

Experimental results and results of numerical study are presented in CHAPTER 6. Figures are used to visualize the results for discussions and validation of the numerical study.

In CHAPTER 7, conclusions drawn from the study are narrated.

CHAPTER 2

LITERATURE SURVEY

There have been lots of studies on EFIs so far. This chapter begins with evolution of EFI systems in history. Fundamentals of the system are represented by defining every single component in the system and working principle of the system is introduced. Finally, related studies with the content and scope of this thesis are summarized by pointing out the most important parts of the studies.

2.1 HISTORY

Previously it was realized by Keller and Penning [2] that under the action of large electrical currents, exploding foils would be used to accelerate thin flyer plates. The phenomenon of creating very high short duration pressures with the acceleration of thin flyer plates was first utilized in materials science to study the effects of shock waves on various materials [2]. Then in 1965, Exploding Foil Initiator (EFI) also named as Slapper Detonator was invented by John Stroud at Lawrence Livermore National Laboratory (LLNL) to be used as a shock initiator for secondary high explosives [3]. Since then, many researches have been conducted in LLNL with slapper detonators under the name *Electric Gun* referring other shock initiation applications in which EFI was used [4 – 9].

Researchers from several laboratories like Sandia National Laboratory (SNL) [10 - 12] and Los Alamos National Laboratory (LANL) [13] in United States have accomplished many works on EFIs and they documented these works in detail providing lots of useful information to new researchers. Materials Research Laboratory (MRL) in Australia contributed so many experiences to literature [14 - 18]. Defence Research Establishment Valcartier (DREV) in Canada made pretty good effort for small slapper systems [19 - 20].

EFIs have been used for various reasons since their invention. For instance, *Electric Gun* stated above, was used for Equation of State (EOS) measurements for a number of metals in LLNL. It was also adapted in shock wave studies like interaction of shock waves with free surfaces and shock initiation of high explosives for determination of their sensitivities [4]. Like EBWs, EFIs can be used in civil applications such as explosive welding, explosive hardening, seismic studies, oilfield works and mining [1].

The studies at earlier stages need high levels of flyer impact pressure, so bulky EFI systems were present in the past. Throughout the years, EFI systems have been evolved getting smaller. The decrease in size makes EFIs available for use in missile systems. Today a few millimeters sized EFIs are available in the market [21].

2.2 FUNDAMENTALS OF EFI

Nappert [19] clearly visualized basic components of an EFI system shown in Figure 2.1. The figure shows a stripline type EFI which carries both transmission lines and main parts like bridge foil and barrel on it.

Figure 2.1 can be taken as the simplest schematic that is useful for understanding the structure of an EFI and its working principle. The main idea underlying an EFI operation is explained within the component descriptions given in the following lines.

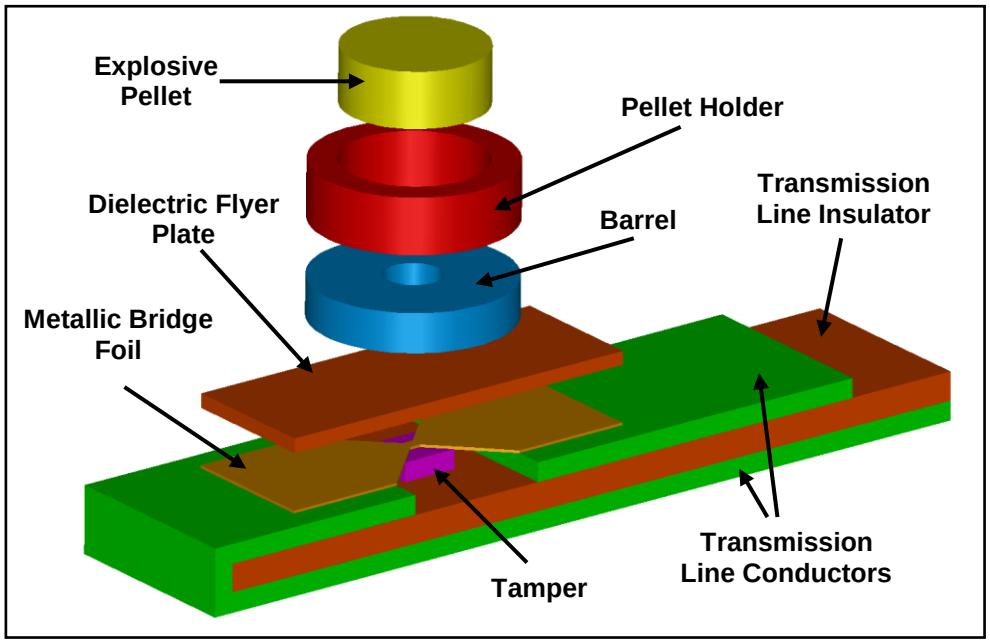

Figure 2.1 Components of EFI [19]

Metallic Bridge Foil:

It is a thin metal foil that has a narrower section called as bridge. When high voltage is discharged from a capacitor through transmission line conductors onto the bridge, ohmic heating causes the solid bridge part to melt, vaporize and finally become plasma. This process is named as explosion of the metallic foil.

Metallic foil may be any conductor in an EFI system [1]. However, a large number of works are based on aluminum and copper metallic foils. Aluminum was the most widely used metallic foil at past for large scale EFIs. It is a good conductor which is easily attainable and not very expensive. Copper has also good electrical burst

behavior which is a desired property for electrically exploded foils [3]. For small scale EFIs, it is realized that copper is chosen to be the metallic foil material. This may be due to readily available copper-Kapton® laminates that are widely used in electronics applications or the well-known process of depositing copper films on Kapton®. Kapton® is a polyimide material produced by DuPont which is described in detail in the following lines. A metallic foil is characterized with its dimensions shown in Figure 2.2.

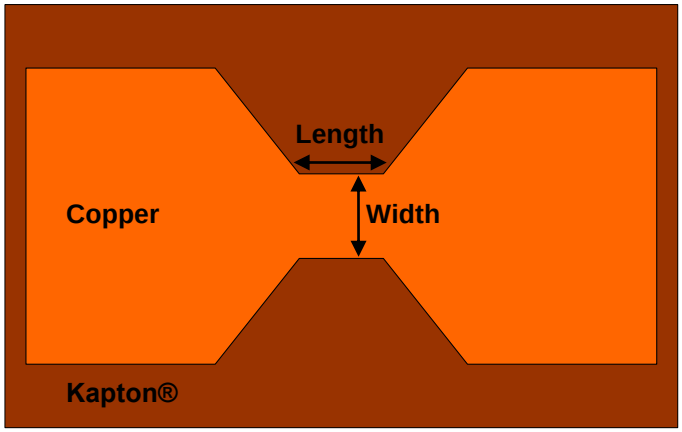

Figure 2.2 Description of Exploding Metallic Foil

Theoretically and also experimentally proved, exploding part is solely the middle narrow bridge part in a metallic foil under the action of specific large currents. Dimensions of the bridge part are the most critical parameters in system design. So far in literature, numerous different dimensions have been used regarding the energy input and output and also size of the systems. For large scale EFIs used in laboratory testing, bridge width and bridge length may be in the orders of centimeters [22], whereas in small scale EFIs dimensions lower than 1 mm is used [19, 21, 23]. Thickness of the bridge foil is another important parameter and it is observed that generally a few microns thick metallic foils have been used so far.

Tamper:

Tamper serves as a support under the metallic foil. Its main function is to direct the plasma created by explosion to the flyer plate side. In other words, it enhances the efficiency of the system by saving the energy resulted from the explosion of the metallic foil to accelerate the flyer plate [14]. Tamper is chosen to be an insulator that has a good impedance mismatch with plasma created by metallic foil at burst [14]. Several tamper materials are available like glass, Kapton® and also Teflon®. In most of the studies glass is used as a tamper material.

Flyer Plate:

Explosion of the metallic foil creates high dense plasma under the flyer plate. The flyer plate is a special dielectric plastic which is driven inside of a barrel by the plasma beneath it. Flyer plate hits the high explosive, creating an intense shock wave throughout the explosive. At the end of its flight, flyer plate is said to reach very high velocities above 4 km/s [23]. Flyer plate should also remain planar (flat) during its flight in order to achieve good shock characteristics on the explosive.

Foil material is used as Mylar® (polyester) or Kapton® (polyimide) which are trademarks of DuPont. For its stability in a wide temperature range and good insulation characteristics, Kapton® stands nearly the only material option for flyer plate. Flyer plate can be any shape as far as it covers all of the bridge part. The only critical dimension for flyer plate is its thickness because thickness of a flyer plate affects its final velocity and the pressure at the impact. Theoretically, higher thicknesses result lower velocities for the same input energy level. However, thinner flyer plates create shorter durations at the explosive interface [4]. Generally 25 μm and 50 μm thick Kapton flyer plates have been used in small scale EFIs.

Barrel:

Barrel is simply a through hole that characterizes the path and the final velocity (impact velocity on explosive) of the flyer plate. Furthermore it is vital in a way that it confines the plasma created from explosion of the metallic foil, increasing the efficiency of the system. Barrel is usually any plastic material but in cases where it acts as an electrical connector between transmission lines and metallic bridge, it should be a good conducting metal [21].

The diameter and thickness (length) of the barrel are thought to be critical design parameters. When bridge length is equal to barrel diameter, the barrel is named as a finite barrel. In finite barrel case, flyer plate shears off from the edges of the barrel and this sheared disc is accelerated through the explosive inside the barrel. On the other hand, if barrel diameter is two or more times greater than bridge length, the barrel is named as an infinite barrel. In infinite barrel case, flyer plate forms a bubble inside the barrel expanded by plasma beneath it and it is this bubble that hits the explosive at the end of the barrel. This phenomenon is explained and shown in the work by Davies *et al.* [23].

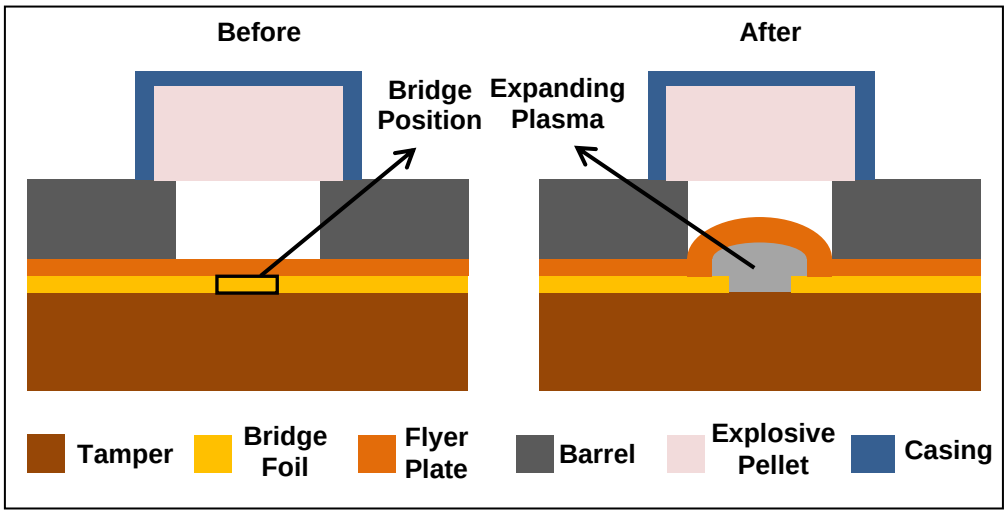

Figure 2.3 Flyer Plate Motion inside the Barrel [23]

If the barrel is too long, only tip point of the bubble hit the explosive in which case the efficiency of the system decreases. So barrel lengths should be carefully decided in infinite barrel designs [14]. For small slapper systems, barrel length is observed to be chosen under 1 mm [14, 19, 21, 23].

Explosive Pellet:

The result of EFI operation is initiation of the secondary high explosive. At the end of its flight, the flyer plate hits the explosive that is in a high density pellet form creating a shock wave. This short duration, high pressure shock wave initiates the explosive. Generally explosive pellet is contained in a proper pellet holder for the structural integrity and confinement.

EFIs do not need primer explosives in their explosive initiation trains. A very important point for EFIs is that they can initiate all secondary high explosives with proper energy input to a carefully designed system.

There have been several studies on determining the sensitivity of secondary high explosives by using flyer plate impact. PBX-9404 and TATB were tested with Electric Gun in LLNL [4]. Furthermore HNAB [24] and HNS [25] were tested at some other facilities.

Commercially available EFIs all tend to use HNS explosive of various types. HNS is one of the most insensitive explosive to impact. It is also thermally stable over 200 °C [26]. With all these properties and also good aging characteristics over years, it has been used widely in aerospace and military applications [26].

Capacitor Discharge Circuit (CDC) and Transmission Lines:

CDC is a special electrical circuit which basically consists of a high voltage capacitor, a fast acting switch and proper transmission lines. In the past, one such box covering both high voltage power supply and CDC was present in the name of firing system. Today, CDC is tended to be a separate unit from high voltage power supply. Especially during design process, this helps the designer to better control CDC parameters and make necessary revisions on the system. Additionally CDC may allow the user to measure time dependent current of EFIs from a special resistor during firing. In other words, CDC can be considered as not only a firing circuit but also a testing means.

Together with its conductors and insulators, transmission lines are the electrical paths connecting the metallic bridge to CDC. These lines should be carefully designed in order to satisfy proper transmission of the specific electrical pulse to the metallic bridge.

Flat electrical transmission lines are also referred as striplines [23]. In some of EFI designs, bridge parts are manufactured separately and then they are connected to striplines to form EFI itself [19]. However, bridge shape can be given on some part of the stripline to form an integrated design. This technique is further explained in CHAPTER 3.

In laboratory testing and generally in all ESADs, flat transmission lines are tended to be used because of their low inductance. In small slapper systems, metallic foil is known to burst within a few hundred nanoseconds from current start. Another known fact is that the rate of current rise is proportional to the ratio of charging voltage to inductance. So if CDC has a large inductance, the inertia of the metallic foil and flyer plate is overcome by magnetic forces which yield a non-planar impact of the flyer plate to the explosive [4].

Since the performances of EFIs are strictly dependent on CDC, a specific EFI should be characterized with its own CDC.

2.3 RELATED WORKS

Some of the useful information obtained from open literature about the structure of EFIs is provided previously. In this part, works mostly related with experimentation and numerical studies are represented. This part is subdivided into paragraphs every of which underlie a specific previous study.

The detailed explanations of some important parameters for an exploding foil flying plate generator were given by Richardson *et al.* [14]. The study includes characterization of nearly all components of an EFI system. The authors also formulated basic circuit and energy equations which are used in the present study to an extent. Important points from the study are;

- The authors made experiments with Kapton®, Teflon®, glass and mica tampers. From the initiation energy comparison, glass is the best material and

Teflon being the worst. Kapton® and mica are in between. Moreover, they tried different thicknesses of Kapton® as a tamper and initiation energy versus Kapton® thickness curve was obtained.

- It is stated that using infinite barrels are more advantageous than finite barrels. Finite barrels have one major disadvantage that they mask some portion the bridge causing energy to be wasted.

- It is emphasized for a specific EFI system that there is an optimum barrel length at which flyer plate reaches its maximum velocity.

- It was investigated that bridge corners should be rounded carefully in order to have uniform heating across the bridge. This would satisfy the planarity of flyer plate during its motion. Eliminating edge effects ensure a constant pressure across the width of the flyer plate which will act perpendicularly to accelerate it.

- Velocity Interferometer System for Any Reflector (VISAR) is found to be the most precise equipment for flyer plate velocity measurements. In lack of VISAR, authors preferred to make measurements with small piezoelectric sensors referring a method called Time of Arrival Method.

Waschl and Hatt [27] accomplished a study on small scale exploding bridge foils and they tried to characterize them experimentally. Their desire was to find empirical relations to final velocity of the flyer plate under various system parameters like capacitance (0.05 μF, 0.1 μF and 0.22 μF), inductance (10 nH, 35 nH, 73 nH), resistance (varying switch types – Reynolds IVARC 251-1001, EEV TGV-5, MRL planar triggered spark gap switch), Kapton® flyer plate thicknesses (13μm, 25 μm, and 50 μm) and barrel dimensions (0.25 mm and 1 mm) in this study. Square bridges with dimensions lower than 1 mm were used in the study. They performed velocity measurements with VISAR. This study has significant conclusions summarized below.

- Relationship between flyer plate velocity and a wide range of firing voltages were found to be non-linear. Referring all parameters stated above, relations are given analytically.

- Barrel diameter shows nearly no effect on flyer plate's final velocity.

- Electrical Gurney parameters are found to be dependent on capacitance. Those parameters were tabulated with changing capacitance, flyer thickness and inductance. Switch types (i.e. resistance) did not affect the performance. The tabulated information is used in Electrical Gurney model of this present study.

Nappert [19] made a detailed study on an exploding foil initiator system in Canada in 1996. His first aim was to construct a constant parameter EFI. He then characterized it by making several experiments. He used a 0.25 mm square separate 4.4 μm thick copper bridge deposited on a 25 μm thick Kapton® flyer plate. A glass tamper of 150 μm thick was used underneath the bridge. The bridge was connected to Pyralux® (laminates of copper and Kapton®, trademark of DuPont) transmission lines. A

Capacitor Discharge Unit (CDU) was constructed with a 0.1 μF capacitor purchased from Custom Elec., a Reynolds IVARC-251-001 miniature vacuum spark gap switch and a 0.005054 ohm CVR (Current Viewing Resistor) and Pyralux® transmission lines.

- Nappert made current and voltage measurements on EFI at firing voltage levels of 2000, 2400, 2700, 3200 and 3400 volts. He represented all firing data in his work.

- A model that predicts the performance of EFI system is given. In his model, Nappert used an empirical analytic expression for the dynamic resistivity of copper bridge foil. This analytic expression was based on a previous study done by Lee [28]. For flyer plate's final velocity predictions, Electrical Gurney analysis was carried on.

- Average velocity of flyer plate was measured with a Time of Arrival Detector (TOAD) simultaneously with current and voltage measurements. That detector was a piezoelectric sensor.

- Explosive tests were done with HNS - IV explosive pellets. Ionization switches were used in order to measure the detonation time of the explosive. Initiation threshold was determined by Bruceton Test.

This study belonging to Nappert has the most useful data for present study. In following parts there is further referring to Nappert's study.

Davies *et al.* [23] aimed to build a streak photography system that measures flyer plate velocities from the exit of the barrel and they used this system to characterize an EFI system with different configurations.

- Bridge thicknesses were altered; however, values were not given. Square bridge dimensions of 0.1 mm, 0.2 mm, 0.3 mm and 0.4 mm were used and barrel lengths were chosen as 0.1 mm, 0.155 mm, 0.18 mm, 0.36 mm and 0.38 mm with an infinite barrel design.

- It was observed that 0.1 mm barrel length gave the highest velocity. Davies *et al.* concluded that increasing the barrel length decreases the velocity of the flyer plate.

- Performances of EFI stripline configurations with separate bridges were poor compared to ones that have integrated bridges on striplines. This was explained by the increased inductance in separate bridge designs.

- It was expected that thinner bridge thicknesses would result higher velocities but the authors did not prove this in their experiments.

- Bridge size effects were investigated but the results did not return meaningful conclusions. However, in another paper [29] of Davies *et al.*, it is mentioned that increasing bridge dimensions results in decreasing of the flyer plate velocity due to volume of bridge material converted into plasma increases.

2.3.1 More Information for Experimentation

To characterize an EFI system and to be able to build up an empirical model for the performance predictions, electrical measurements related both EFI and CDC should be made. Current measurements can be made accurately by means of special resistors called Current Viewing Resistors (CVRs) [19, 30]. A CVR is connected in series to CDC. Current flowing through a CVR is calculated by measuring voltage on it and dividing it to CVR's resistance. CVRs that have low resistance and low inductance values are used in order not to affect system performance. As an alternative for CVR, Rogowski Coil has been used for years to measure current [15 – 16].

Ringdown test which determines the electrical characteristics of CDC is one of the vital tests. Connecting a piece of copper instead of an EFI stripline to CDC, firings are made and resulting current waveforms obtained from CVR are analyzed to find total resistance and inductance of CDC. Ringdown tests should be carried out to realize the effectiveness of a CDC and to be able to integrate electrical parameters in theoretical model. It is also noted from ringdown tests that for every firing voltage, electrical parameters are changing. Electrical characteristics of the system should be determined at every desired firing voltage [19].

Voltage measurements should be strictly carried out because burst time of metallic foil and time dependent resistivity of bridge can be obtained from voltage measurements. However, accurate voltage measurements are observed to be troublesome. There is always a possibility for inductive loop formed between the voltage probe and EFI under test. Moreover, commercial voltage probes do not contribute high bandwidth and high voltage needs together. So voltage measurements have been made with custom designed probes explained by Nappert and Fortier [20]. In their measurements, there still occurred some amount of inductive loop in the recorded data so they needed to correct the measured voltage by considering the effect of inductance of the probe. In another study by Hatt and Wolfson [16], a Tektronix high voltage probe was used for voltage measurements and the authors carried out a similar voltage correction method as in [20].

In order to determine the effectiveness of an EFI, final velocity of the flyer plate should be determined. Final velocity is the key parameter that defines the impact at the explosive interface. Apparently there are two approaches; measuring the velocity continuously or measuring average velocity. Former one is the most preferred; however, it needs more complex systems like VISAR or Fabry - Perot Interferometer [27]. These systems basically sense the light reflected from flyer plate's surface and a high speed camera is used to monitor the event. As a result, the motion of flyer plate from the beginning to the end is recorded and displacement versus time is obtained. These systems are relatively expensive and complex. For small scale systems things may get more complicated so a deep knowledge of optics is definitely needed.

Fabry - Perot Interferometer was used widely especially in LLNL for characterization of *Electric Gun* [5 – 8]. A schematic presented by Scholtes and Prinse [31] is given in Figure 2.4. Fabry – Perot Interferometer seems to be more useful than VISAR in small scale flyer plate velocity measurements. VISAR has been used especially for large scale systems [9, 16, 17].

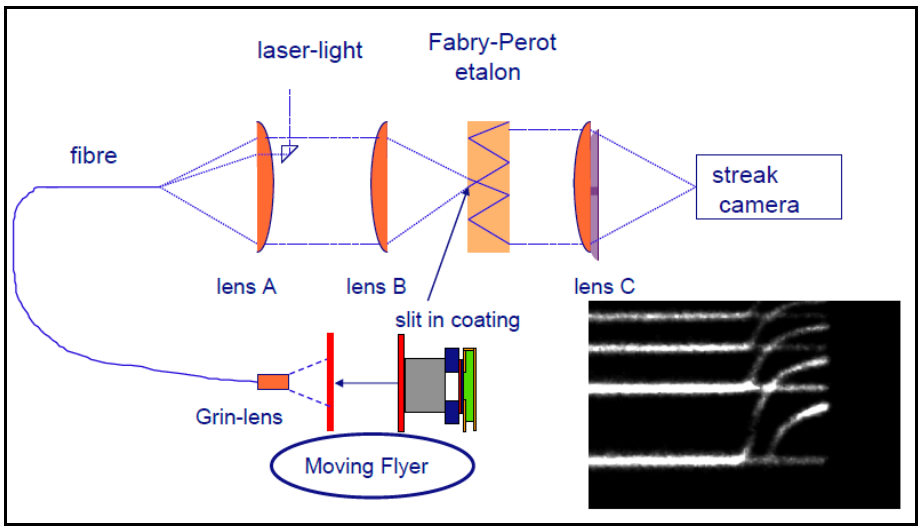

Figure 2.4 Fabry – Perot Interferometer Used in TNO [31]

Another simultaneous measurement system that has become popular in recent years is Photonic Doppler Velocimetry (PDV). Its application to flyer plate's velocity measurements is into consideration and there are efforts to utilize the method instead of Fabry – Perot Interferometer. It is cheaper than Fabry – Perot Interferometer; however, it needs room for improvement [32]. A schematic for PDV system is given in Figure 2.5.

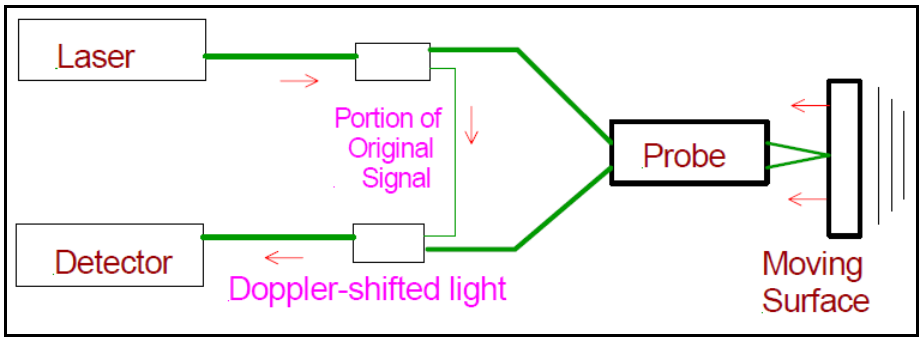

Figure 2.5 PDV Method [27]

Average velocity measurements utilize rather simple techniques like time of arrival detection [14, 18, 33] or high speed photography [23, 29, 34]. These techniques are all based on determining the time at which flyer plate reaches to a specific point. This specific point is usually defined as the exit of the barrel. Knowing the time for initial

movement of flyer plate, average velocity can be calculated by simply dividing flight distance (e.g. barrel length) to duration of flight. Determination of initial movement differs in all above techniques.

Nappert [19] measured average velocity with a TOAD. He described TOAD as a small piezoelectric sensor which generates voltage when struck by flyer plate. The voltage was recorded on an oscilloscope simultaneously with current and voltage recordings. Time of initial motion of the flyer plate was considered as the peak point of voltage measured from EFI system. In other words, it was assumed flyer plate's motion begins just after the burst of the metallic bridge foil. Time corresponding to the rise of voltage from TOAD is taken as the end of flyer plate's motion (Figure 2.6). Nappert [19] mentioned that at low firing voltages the average velocities of flyer plates are overestimated because flyer plate begins moving before burst of the metallic foil.

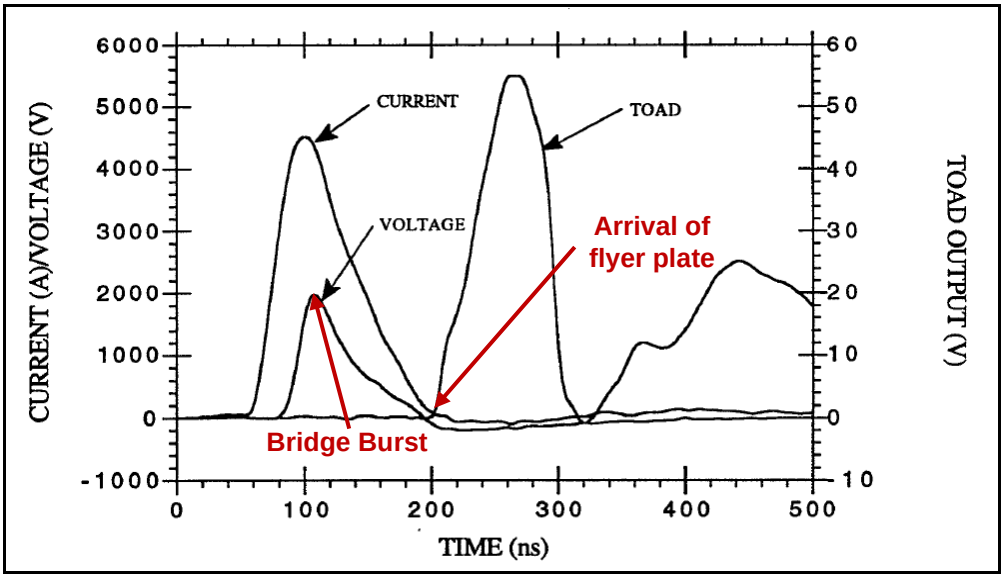

Figure 2.6 Current, Voltage and TOAD Output in [19]

Another time of arrival detection method is electrical breakwire technique. Podlesak [18] constructed a system using a copper wire which is electrically charged at low voltages. Voltage on the wire was monitored on oscilloscope and when the flyer plate hit the wire, the wire was damaged or broken, changing the monitored voltage waveform. This gives the time of arrival of the flyer plate. This kind of a system has the advantage of being simple and inexpensive; however problems regarding voltage recordings can be faced due to electromagnetic interferences caused by large currents flowing over the metallic bridge. A possible result of electromagnetic interference may be having difficulties to distinguish the time of breaking wire because of the noisy voltage waveform obtained from measurements.

To overcome the problems stated for breakwire technique, another simple method was represented by Di Marzio *et al.* [33]. In their work, fiber optic cables were used to determine the average velocity of flyer plates driven by exploding foils. Basically, a fiber optic cable senses the light and light is converted into voltage signal with optical-to-electrical converter photodiodes.

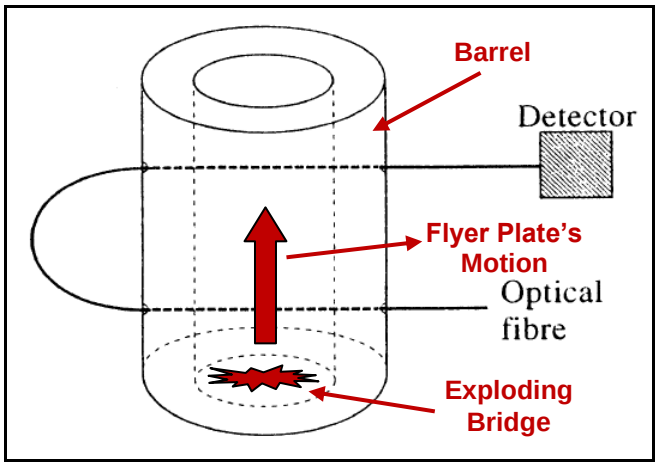

(a)

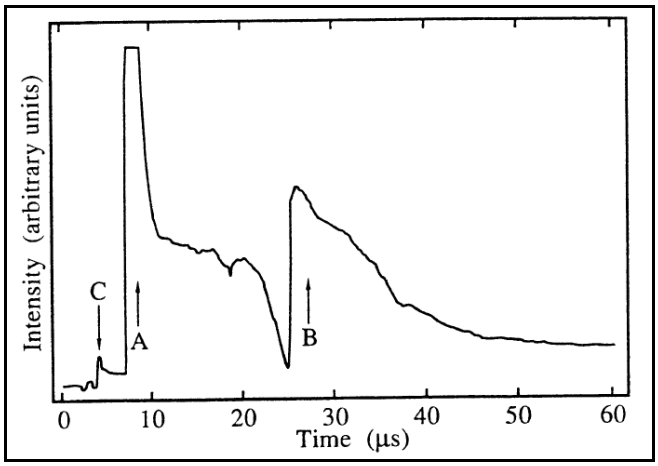

(b)

Figure 2.7 First Method for Average Velocity Measurement in [33]
(a) Arrangement of Optic Fibers inside the Barrel (b) Recorded Voltage Data Obtained from Optic Fibers

Figure 2.7 (a) shows the velocity measurement technique and Figure 2.7 (b) gives the results obtained from the optic fiber measurements. Di Marzio *et al.* [33] used a large barrel and they could manage to mount two fibers horizontally as shown in Figure 2.7 (a). It was aimed to record two points; first of which is the flyer impact to lower fiber and second is the flyer plate impact to upper fiber. Time between these two impacts gives the flight time of the flyer plate. However, Di Marzio *et al.* [33] realized that there occurred three rises in optic fiber's voltage waveform (*A*, *B*, *C* in Figure 2.7 (b)) and they interpreted the point *C* corresponds the light sensed from burst of the bridge. *A* and *B* are the impact points for lower and upper fibers respectively. The authors discussed that this method is somehow not efficient since flyer plate definitely decelerates when it hits the lower fiber. So they decided to construct another system for average velocity measurements shown in Figure 2.8. Like in the first method, they arranged optic fibers horizontally inside the barrel, but this time optic fibers were not placed on the trajectory of the flyer plate. The signal from optic fibers were collected and transformed by photodiodes and it was amplified for recording in the oscilloscope. Similar results obtained as in the first method.

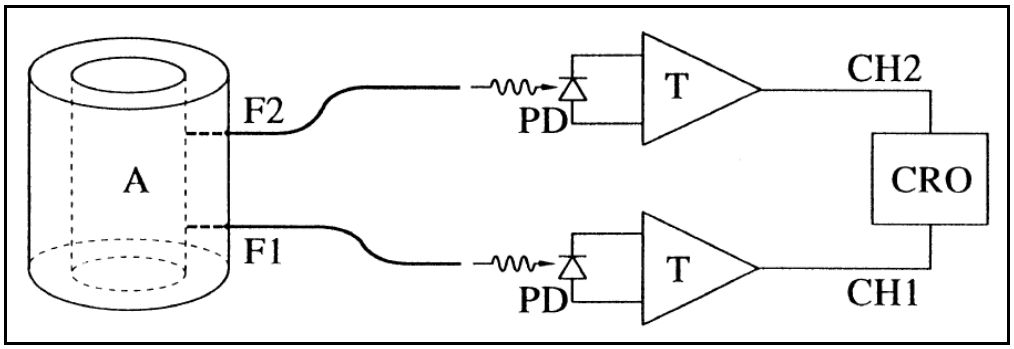

Figure 2.8 Second Method for Average Velocity Measurement in [33]
F: Optic Fiber, PD: Photodiode, T: Amplifier, CH: Channel, CRO: Oscilloscope

High speed photography was utilized by Davies *et al.* [23]; the aim was recording the motion of the flyer plate from the exit of the barrel. Schematic of experimental setup used in the study is shown in Figure 2.9.

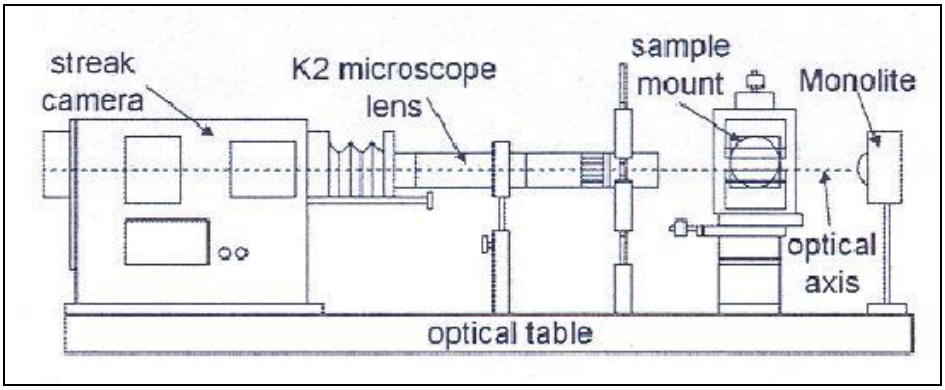

Figure 2.9 High Speed Photography used by Davies *et al.* [23]

An example to measured distance from the exit of a 0.1 mm long barrel is shown in Figure 2.10. The linear behavior of displacement is the result of constant velocity of the flyer plate. Assuming also a linear behavior inside the barrel, one can take the experimentally measured velocity as the final velocity of the flyer plate.

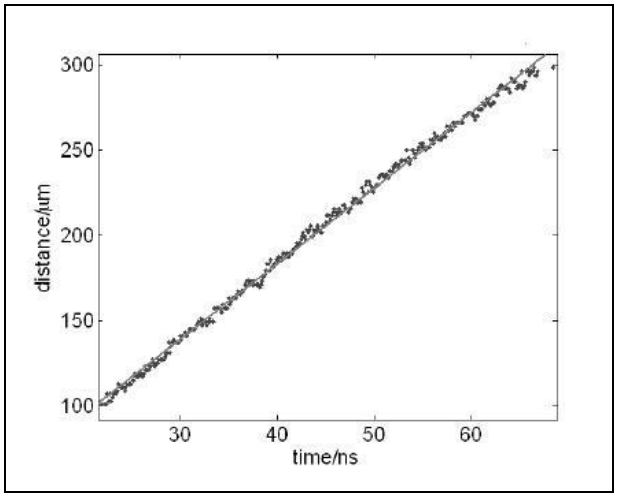

Figure 2.10 Measurement of Distance from the Exit of a 0.1 mm Barrel by High Speed Photography System [23, 29, 34]

Saxena *et al.* [35] used a Fabry – Perot Velocimeter in their study. They also tried to determine the flatness of flyer plate at the impact surface. Four multimode fibers oriented in a circular position were used at the exit of the barrel. A copper foil was adjusted between the fibers and the barrel exit. So when flyer reached the exit of the

barrel, it hit the copper foil creating a shock breakout at the fiber fronts. By measuring the time with optic fibers output voltage, Saxena *et al.* [35] determined the orientation of the flyer plate at the impact surface.

Also there have been techniques for determining the function time of EFIs. Nappert [19] was used an ionization switch which was mounted on the output surface of the explosive pellet. There was an electrical open path through the switch which was closed upon highly ionized detonation shock wave breakout from the pellet surface. Again the measurement of detonation time was accomplished simultaneously with current and voltage measurements in order to find the function time of the detonator.

Another method uses streak cameras to visualize detonation shown in Figure 2.11. Recording of the detonation event should be made simultaneously with current and voltage measurements.

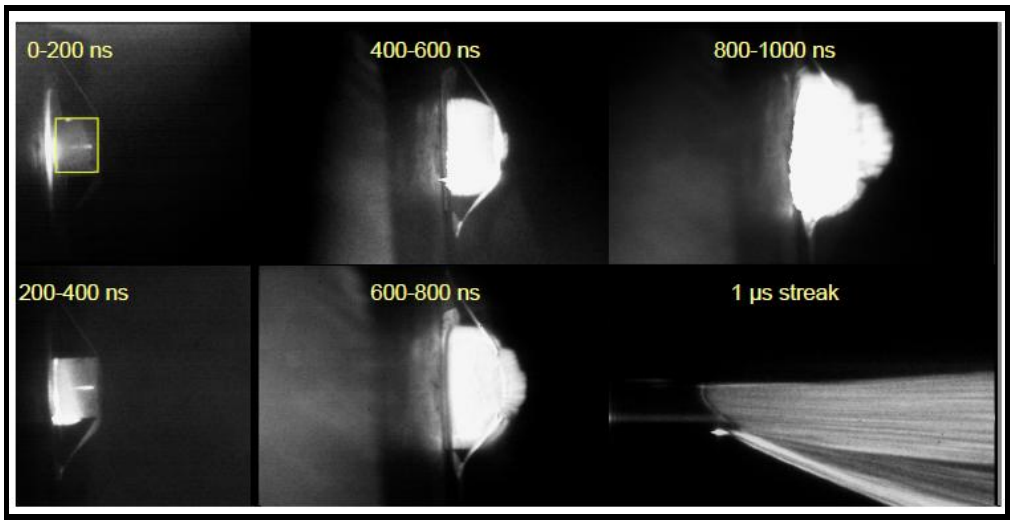

Figure 2.11 Streak Camera Record for Detonation of EFI Used in [31]

2.3.2 More Information for Numerical Study

There have been several approaches for the theoretical modeling of operation of an EFI system. In theoretical modeling, the first aim is to model the electrical behavior of the system and then relating the resulting electrical energy to the final velocity of the flyer plate. Finally, the major goal is to find the impact energy of the flyer plate - explosive interface.

In all literature data, the electrical system is taken as a simple RLC (Resistance – Inductance – Capacitance) circuit. Using Kirchhoff's Voltage Law, circuit equation is written based on the rule that sum of voltages around a closed network is zero.

Some simplistic approaches assume the resistivity of bursting bridge is constant with time; however, these approaches are far from the real situation and they give poor results. Efforts have been made to model the dynamic resistivity of metallic bridge. Lee [28] defined a Gaussian function to the resistivity of the bridge with four parameters that are determined empirically. He defined specific action parameter which is a very useful parameter that can be measured experimentally without getting into thermodynamic state of the metallic bridge. Also it is cited that specific action to burst is constant for a specific foil material.

Nappert [19] utilized Lee's dynamic electrical resistivity model in his work. He measured voltage and current simultaneously from the system and he plotted resistance versus specific action. He then made a curve fitting and defined the above stated four parameters equation to his EFI system.

Another study that uses a Gaussian function was presented by Furnberg *et al.* [10]. The authors also suggested subtracting out the initial inductive voltage that does not correspond to performance as in [19].

In his study Nappert [19] related burst current density and final velocity of flyer plate by using Gurney theory. Gurney theory was modified to be used for electrically accelerated flyer plates by Tucker and Stanton [11]. He also calculated impulse pressure at the interface of explosive and flyer plate. He then used a famous explosive initiation criterion to check what conditions and configurations are enough to initiate a specific explosive. In his study, he made the calculations for HNS - IV explosive pellet.

Tucker and Stanton [12] took electrical Gurney energy to a step further and they formulated time dependent acceleration of flyer plate relating it to time dependent energy deposition in the system. The formulation also includes their first formulation for final velocity of flyer plate stated above. The results of the formulation were compared with experimental data and changing the polytropic gas constant in the formulation, best match was tried to be obtained.

Sarkisov *et al.* [36] set a thermodynamical model for exploding wires. They formulated the deposited energy in the bridge during the ohmic heating process based on current and resistance of exploding wire or foil. They modeled resistivity and specific heat of exploding wire or foil with respect to temperature from the available literature data.

Richardson *et al.* [14] introduced possible lost energies of an EFI system. They discussed the contribution of those lost energies to the deposited energy during ohmic heating.

Schmidt *et al.* [13] used both electrical Gurney energy and time dependent energy deposition approach to build up a theoretical model for the flyer plate's velocity. Particularly for the latter approach, the authors claimed that the energy deposited in the bridge up to burst is spent to fusion, vaporization and ionization and one should use the energy after burst to find the velocity history. Furthermore they showed a relation for modifying post - burst power waveform in order to obtain much more accurate results compared with the experimental ones.

Finally, Christensen and Hrousis [37] started a work that includes three dimensional magnetohydrodynamics to better understand the behavior of flyer plate inside the

barrel which is really very difficult to realize in experiments or in 2-D simulations. They used different equations of state for modeling of both current and velocity of the flyer plates of large scale and small scale EFI systems. Results of simulations and experiments were in good agreement.

CHAPTER 3

EFI DESIGN

This chapter mainly introduces the design considerations and manufacturing steps of EFIs used in this study.

3.1 EFI STRIPLINE

Regarding the literature, to be able to have low inductance EFI striplines, it is a major rule to use flat electrical transmission paths and closely laminated stripline layers in the design. Many different types of EFI striplines can be attained by altering numerous parameters stated in CHAPTER 2.

In this study, stripline configurations which contain bridge part and electrical transmission lines are designed. The striplines were manufactured in Flexible Circuit Technologies Company settled in United States. An overview of present sample EFI stripline is shown in Figure 3.1.

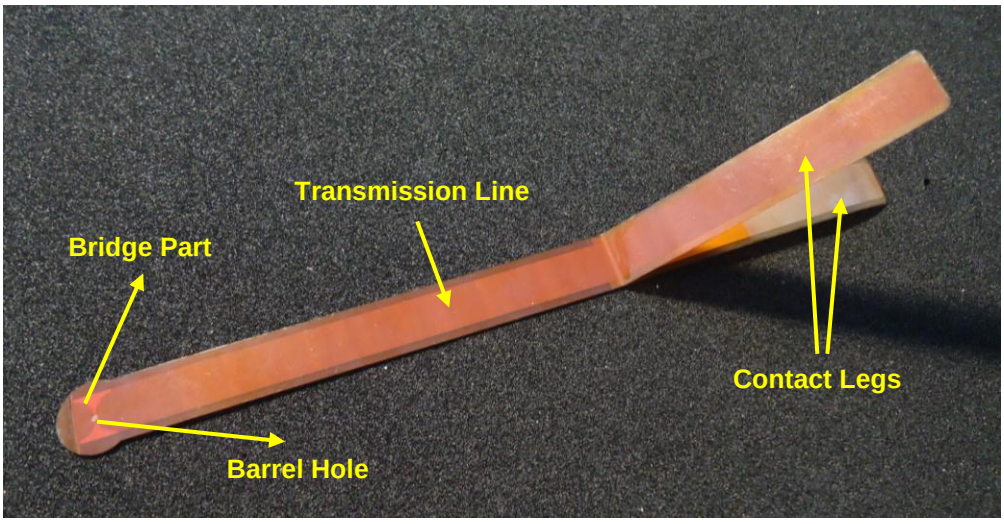

Figure 3.1 EFI Stripline

EFI stripline occurs from closely laminated layers. Exploded view of lamination layers of present EFI stripline design is shown in Figure 3.2.

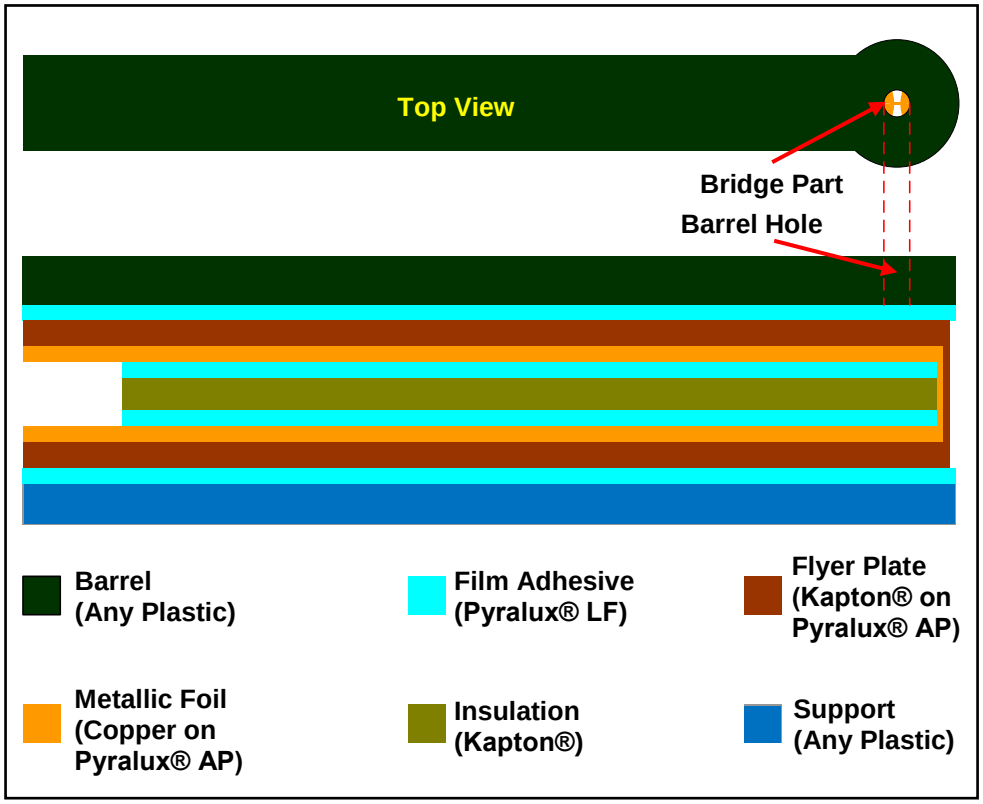

Figure 3.2 Lamination Layers of EFI Striplines

3.1.1 Exploding Foil and Flyer Plate

The core of the stripline is copper-Kapton® lamination which is produced by DuPont in the name of Pyralux® AP. Pyralux® AP is a two-sided copper-Kapton® lamination; that is, two layers of copper is insulated with a Kapton® layer in between. Thicknesses of copper and Kapton® vary in a large range on commercial Pyralux® AP.

To have a one-sided Pyralux® AP, the copper on one side of Pyralux® AP is chemically etched. It remains only a layer of copper and Kapton®. Then bridge shape is given on the desired location of copper sided front. The material is folded as the outer surfaces remain Kapton® and inner ones remain copper. Finally, a layer of Kapton® insulation is folded and bonded between copper layers to insulate them from each other. Insulation layer does not lie till the end of copper layers in order to enable making electrical connections with these uncovered portions (contact legs).

In this study, several stripline configurations are manufactured. These configurations are given in Table 3.1. Configurations will be referred to as their type numbers given in the table hereafter in the text.

Table 3.1 EFI Stripline Configurations

Type No	*Copper Thickness (μm)*	*Bridge Dimensions (mm)*	*Barrel Length (mm)*	*Flyer Plate's Thickness (μm)*
1	5	0.2 X 0.2	0.25	25
2	9	0.1 X 0.1	0.25	25
3	9	0.2 X 0.2	0.10	25
4	9	0.2 X 0.2	0.25	25
5	9	0.2 X 0.2	0.40	25
6	9	0.2 X 0.2	0.25	50

Bridge land areas are manufactured as half circles with a radius of 2.5 mm. Corners of bridge part are rounded approximately 0.01 mm in radius. Bridge part is shown in Figure 3.3.

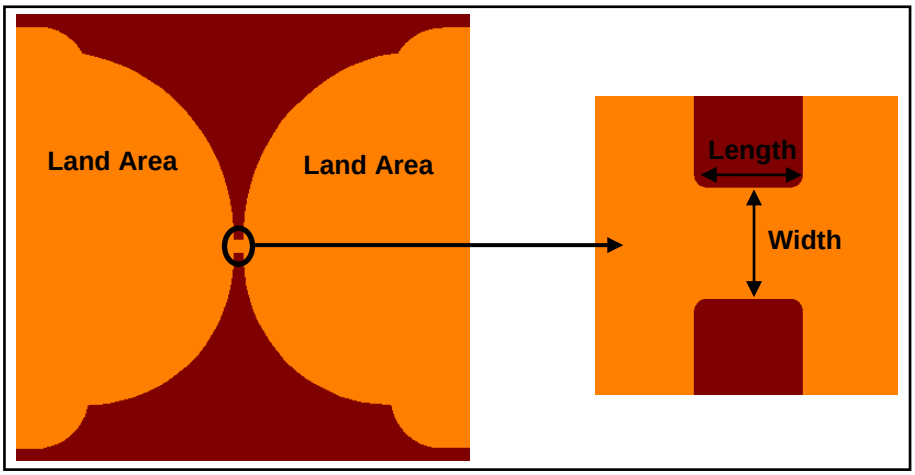

Figure 3.3 Bridge Part of EFI Stripline

Insulation plastic is chosen as 50.8 μm thick Kapton®. Insulation layer also acts as a tamper that supports the bridge underneath.

25.4 μm thick Pyralux® LF acrylic sheet adhesive is used to bond the layers closely.

By the way, as a rule of thumb, it is hard to provide high accuracy in producing the bridge part of especially Type 2 stripline since etching of copper on Pyralux® AP gets complex when the copper thickness increases (as Type 2 stripline has 9μm copper thickness). Due to this fact, excluding Type 1 stripline, it is possible for all types of striplines to have dimensional inaccuracies resulted during etching process. To better

take the control of dimensional variations and to be able to compare the performances with the commercial products in a future study, Type 1 striplines are used in explosive tests.

3.1.2 Barrel and Support

Since barrel is an important component that enhances EFI performance, diameter and length (thickness) of the barrel should be carefully decided. In this study, a barrel diameter of 1 mm and lengths (thicknesses) of 0.10 mm, 0.25 mm and 0.40 mm are chosen. The barrel can be considered as an infinite barrel because the ratio of barrel diameter to bridge length is 5 for all types of striplines except Type 2. The ratio is 10 for Type 2 stripline since it has 0.1 mm bridge length.

As a barrel, a polyimide material is employed in the design. A smooth barrel diameter is formed at the desired location. Barrel plastic is at the same length with folded Pyralux® AP to provide structural integrity. Barrel is bonded to Kapton® side of Pyralux® AP.

Most important operation in lamination of barrel is to face the center of the barrel to the center of the bridge area. Some little amount of misalignments can be tolerable because it is an infinite barrel. Since the final velocity of the flyer plate is characterized by the length (thickness) of the barrel, lamination should be accomplished perfectly not remaining intolerable room in between Pyralux® AP and barrel compared to the length (thickness) of the barrel.

There is a 75 μm thick support plastic under the stripline that has no significant effect on performance but is just believed to conserve the structural integrity of the stripline.

All layers are laminated using 25.4 μm thick Pyralux® LF acrylic sheet adhesive.

3.1.3 Stripline Inductance Calculations

Richardson *et al.* [14] gives the formulation for calculation of a specific stripline's inductance L_{sl} as

$$L_{sl} = \frac{\mu_0 \times d}{W} \times l_{sl} \tag{3.1}$$

where μ_0 equals to $4\pi \times 10^{-7}$ H/m, d is the separation between the conductors and W is the width of the conductor in the stripline. Since formulation is given per unit length, length of the total conductor l_{sl} is inserted into the formulation.

In present stripline design, W = 7 mm, and l_{sl} = 275 mm. Distance between conductors d are calculated by considering thicknesses of insulation plastic and adhesive layers. So a separation distance d of 0.127 mm is used in calculations. With all these data, inductance of striplines is found to be 6.4 nH.

3.2 EXPLOSIVE

A specific stripline type is used to detonate HNS - IV secondary high explosive pellets. In this study, HNS - IV pellets of Teledyne RISI are used. Explosive pellets have a diameter of 7.63 mm and a thickness of 5.15 mm. The pellets weigh approximately 370 mg and their densities are around 1.59 g/cc.

Another explosive used in explosive tests is PBXN – 5. PBXN – 5 powders are pressed into pellets which have a diameter of 5.0 mm and a thickness of 5.10 mm. PBXN – 5 pellets weigh approximately 185 mg and their densities are around 1.82 g/cc.

3.3 CASING AND OTHER AUXILIARY COMPONENTS

Both explosive pellets and the striplines are confined in Stainless Steel – Grade 304 two – piece casings. The mechanical casing design is accomplished in a way that EFIs can be mounted on any explosive train with proper bolts. Figure 3.4 shows the schematic view of a sample EFI assembly containing explosive pellet.

Bolts are used to fasten the upper and lower casing together. Rubber tamper is a highly compressible but rigid material that it ensures the barrel of the stripline to face with the explosive pellet closely. That is, no free space between the barrel and explosive is allowed when the bolts are fastened.

3.4 COST

An EFI assembly utilizing an HNS – IV explosive pellet roughly costs 300 USD whereas utilizing a PBXN – 5 explosive pellet, it costs 250 USD. The costs include transportation costs for explosives and non – recurring engineering costs for striplines, casings and auxiliary components.

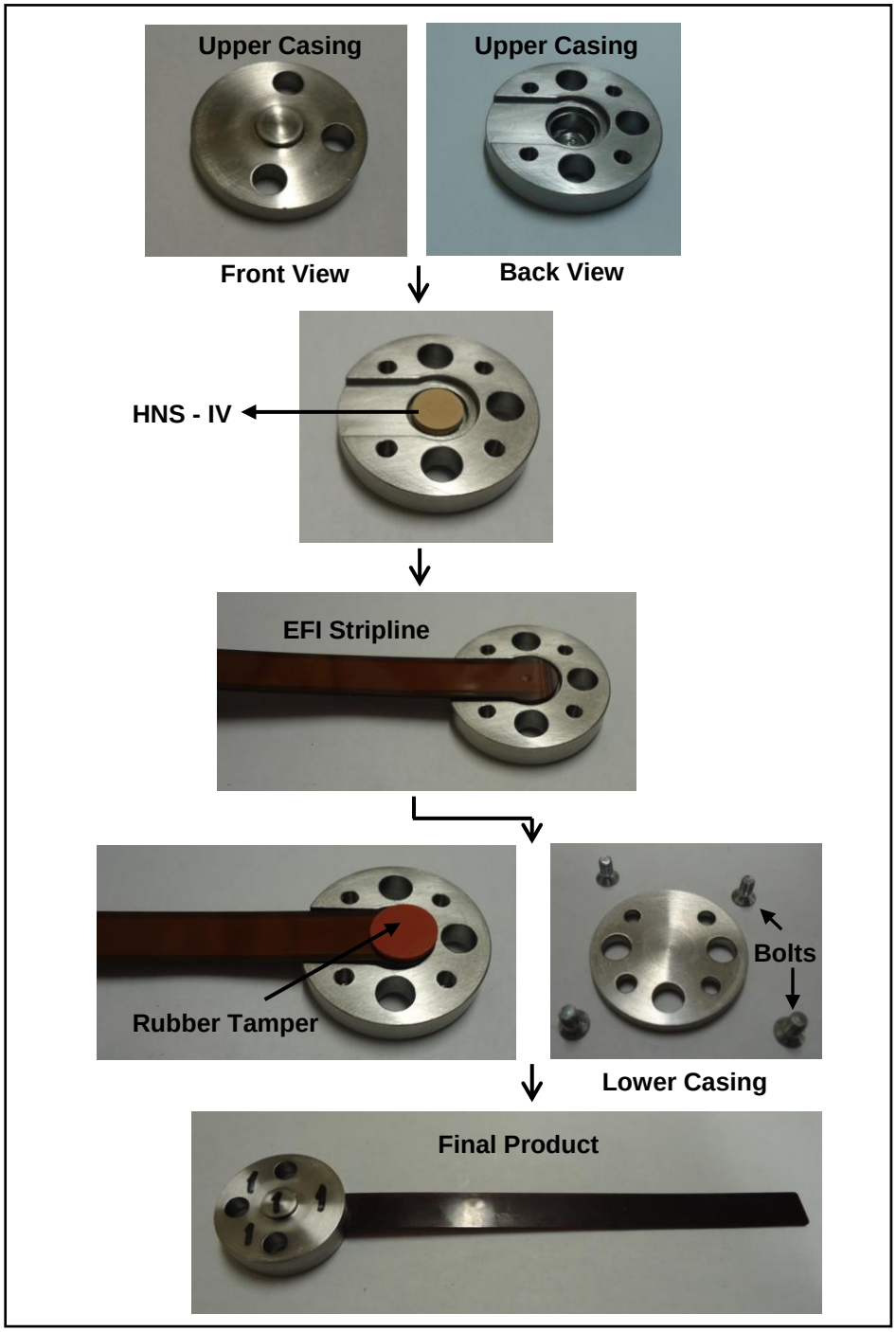

Figure 3.4 EFI Assembly

CHAPTER 4

EXPERIMENTAL STUDY

This chapter introduces the important characteristics of each part and equipment used in experimentation in detail.

4.1 EXPERIMENTAL SETUP

The experimental setup used in this study conserves both firing means of EFI striplines and the related measurement apparatus. Experimental setup is introduced in Figure 4.1.

The experimental setup given in Figure 4.1 is mainly for firings and tests of inert EFI striplines. Actually, same configuration is used in explosive tests with only minor changes like the orientation of optic fiber. Both optic fiber adjustments will be represented after all of the components of the setup are introduced.

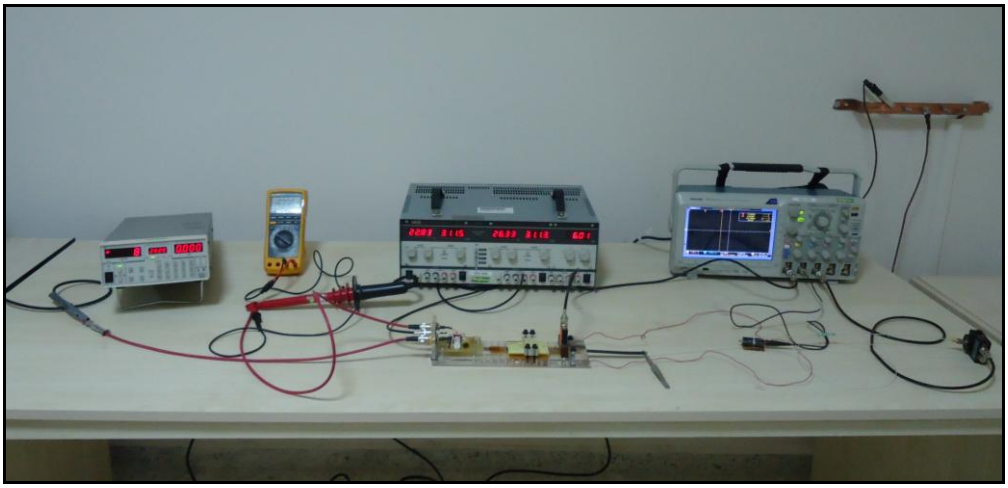

(a)

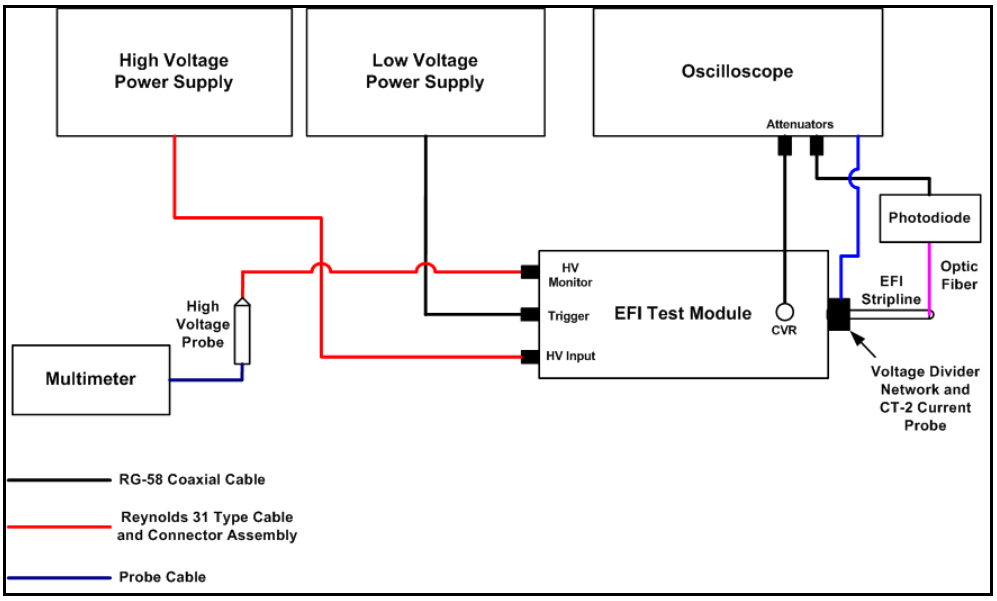

(b)

Figure 4.1 Experimental Setup
(a) General View (b) Schematic Display

An EFI Test Module (P/N 188-4421) was purchased from Teledyne RISI (Figure 4.2 (a)). The module mainly consists of a high energy vacuum spark - gap switch and its trigger unit, a high energy capacitor, an EFI stripline output and a CVR. Connections to the test module are made with a High Voltage Input Connector, a Trigger Input

Connector and a High Voltage Monitor Connector (Figure 4.2 (b)). The module is basically designed for firing EFI striplines while measuring current from the circuit.

(a)

(b)

Figure 4.2 EFI Test Module
(a) General View (b) Integrated Connectors

To load the high voltage capacitor inside EFI Test Module, a High Voltage Power Supply (PS350) was purchased from Stanford Research Systems. The device can supply maximum 5000 volts. It is connected to High Voltage Input Connector with a Type C coaxial cable and Reynolds 31 Type High Voltage Connector.

To trigger the spark – gap switch inside EFI Test Module, TTI Thurlbly Thandar power supply is used. The device can supply maximum 32 volts which is quite sufficient for the trigger circuit of the spark – gap switch. A RG - 58 coaxial cable is used for the connection between the power supply and Trigger Input Connector.

In order to check whether the capacitor is loaded with the desired voltage level, a high voltage probe which can measure a maximum voltage level of 40 kV and has 1000:1 attenuation is connected to High Voltage Monitor Connector on one end and its other end is connected to a Fluke 112 digital multimeter.

CVR is a 0.00517 ohm resistor which is connected in series with the rest of the circuit. It has a BNC connector on it for connection to the scope. To be able to get accurate and very low noise measurement results, CVR is connected to the scope with a RG-58 coaxial cable terminated with a Tektronix attenuator (P/N 011005903). The attenuator is simply a voltage probe that has 50 ohm termination level.

Voltage measurements are made by using a simple custom designed voltage divider network and a Tektronix CT-2 current probe. CT-2 has a fast rise time, quite good sensitivity and it can measure a maximum current pulse peak of 36 amperes. CT-2 current probe is used together with P6041 probe cable which has a 50 ohm termination. Voltage divider network and the probe are connected to the contact legs of EFI striplines. The display and schematic of the system constructed with voltage divider network and current probe is given in Figure 4.3.

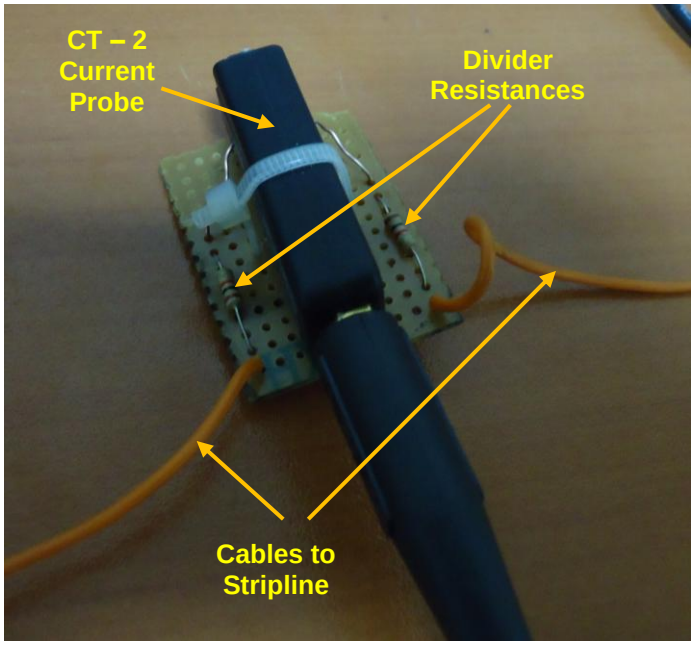

(a)

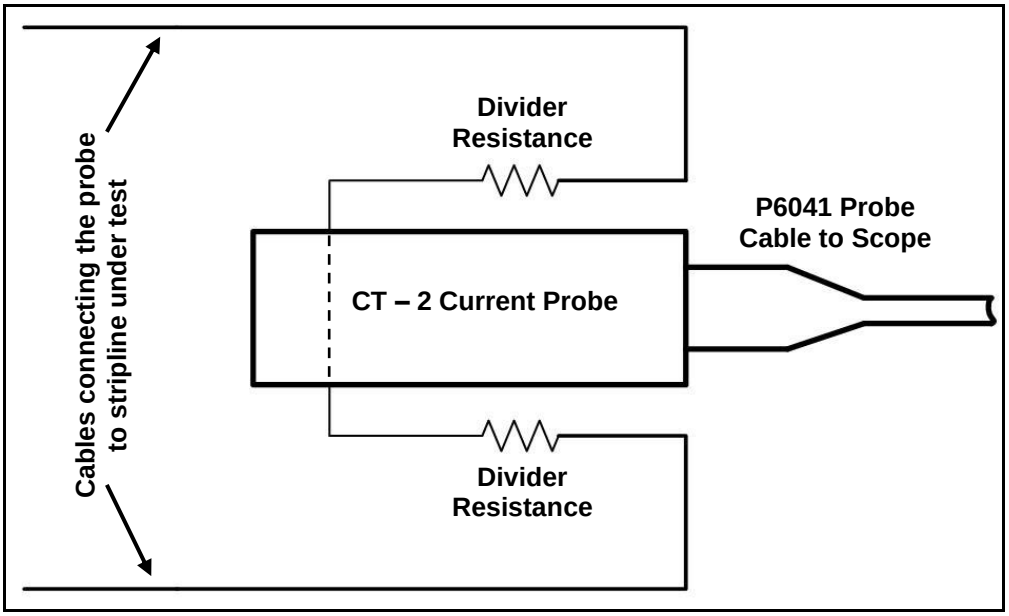

(b)

Figure 4.3 Voltage Measurement Technique
(a) General View (b) Schematic Display

One of the major goals of this study is measuring the average velocity of the flyer plate for a specific EFI stripline. A fast photodiode (Thorlabs / DET10A) is chosen and a multimode fiber optic cable (Thorlabs / BFH48-1000) that has 1 mm core diameter is mounted on it. Photodiode is used to convert the optic signals into the electrical signals collected from the optic fiber. Photodiode is connected to the scope with a RG-58 coaxial cable terminated with a Tektronix attenuator (P/N 011005903).

For non - explosive firings with EFI striplines, average velocity of the flyer plate is obtained by measuring flight time of the flyer plate. Optic fiber is arranged horizontally at the exit of the barrel such that when the flyer plate hit the optic fiber, the created shock breakout at the surface of the optic fiber results a rise in the voltage output which is recorded by the scope. Burst of the bridge is taken as the initial time for flyer plate's motion. This initial time is obtained from simultaneously recorded voltage peak of a specific stripline. Knowing the barrel length and flight time, one can obtain the average velocity by simply dividing the thickness to the flight time.

The schematic of the measurement technique is provided in Figure 4.4.

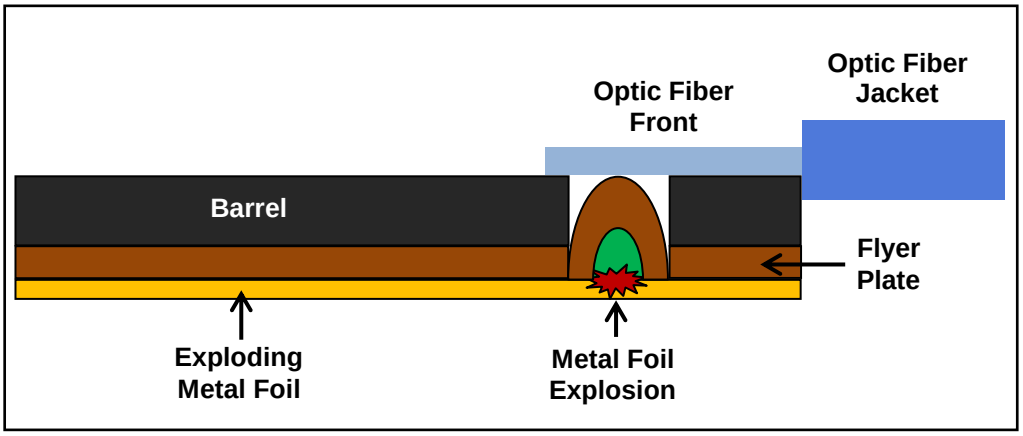

Figure 4.4 Velocity Measurement Technique

For explosive tests, detonation times of the explosive pellets are measured. It is aimed to find the time that passes from voltage peak (burst time) and detonation time to determine the function time of a single detonator. Again a simultaneous measurement of voltage and detonation time is accomplished. Detonation time measurement utilizes the same optic fiber arrangement but this time optic fiber is arranged just near the outer surface of the explosive pellet shown in Figure 4.5. Optic fiber senses the light resulted from detonation of the explosive pellet and this situation is realized as the output voltage rise of the optic fiber recorded by the scope.

In addition to function time measurement, 32 mm square and 16 mm thick steel witness plate pertinent to MIL-STD-331C is used to explore the degree of detonation.

Witness plate is placed in contact with the outer surface of lower casing which confines the explosive pellet. Resulting depth of the dent is measured with special gauges.

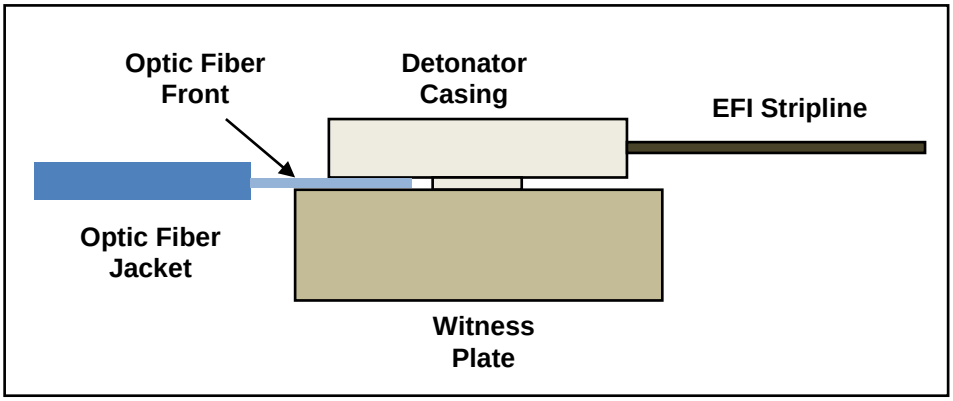

Figure 4.5 Schematic for Detonation Time and Dent Measurements

All aforementioned data is recorded with a Tektronix DPO 3054 model oscilloscope. It has a sample rate up to 2.5 Gs/s and a bandwidth of 500 MHz with four channels connection option.

4.2 COST

Experimental setup used in this study is relatively cheap since it does not utilize expensive velocity measurement techniques. An investment of approximately 30.000 USD is placed to have such an experimental setup. Furthermore, testing an EFI assembly with an HNS – IV explosive pellet costs 350 USD whereas it costs 250 USD for testing an EFI assembly that has a PBXN – 5 explosive pellet. These costs for testing include labor costs and costs for consumable items like one shot EFI assembly, optic fiber and dent block.

4.3 CHARACTERIZATION OF EXPERIMENTAL SETUP

As a common word, every EFI is characterized by its own firing and testing unit. So before conducting experiments with EFI striplines the characteristics of experimental setup should be well determined.

The main part of experimental setup is considered as EFI Test Module. EFI performance is directly affected by the parameters of this test module.

EFI Test Module has a trigger circuit on it which actually needs to be fed by a voltage signal greater than 20 volts in amplitude. The trigger circuit has a voltage transformer and auxiliary circuit elements. Voltage transformer transforms low voltage trigger signal to several kilovolts and transmits the signal to high energy vacuum spark – gap switch. In this study a voltage pulse of 30 volts in amplitude is used to trigger the switch.

The switch is one of the most critical components of the test module. The switch is believed to have a dynamic resistance which starts from a very high value and falls to some small value in a short time just at the beginning of the process. This dynamic resistance should be measured before the experiments if possible. However, EFI Test Module does not give the chance of making such a measurement because of the orientation of the switch inside the module. Nappert [19] used a similar switch in his system and he gives the dynamic resistance of the switch at different firing voltage levels obtained by experiments. Furthermore the switch has a negligible inductance compared to whole system. A known fact for vacuum spark – gap switches is that they have an operational life limit; in this case it is given as 600 shots if 6000 amperes level is not exceeded with the firings. So using EFI Test Module, one should be careful not to use high voltage levels that result current levels greater than 6000 amperes. Otherwise, failure of the switch is inevitable before 600 shots.

The capacitor on the test module is specially designed low inductance *micapacitor* that can easily be mounted on flat transmission lines. It has a capacitance value of 0.269 nF and a very low inductance value of approximately around a few nanohenries. The capacitor has a maximum voltage rating of 3000 volts.

It is important to know resistance and inductance values for CDC of EFI Test Module. A number of ringdown tests were performed at different voltage levels by using a piece of copper to short the circuit. A sample ringdown test curve at 2000 volts is given in Figure 4.6.

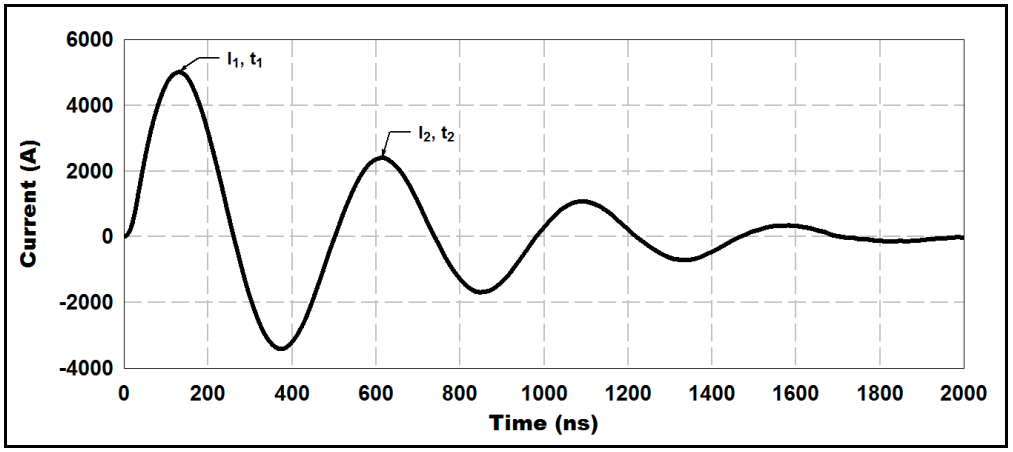

Figure 4.6 Ringdown Test at 2000 Volts

Inductance and resistance of the capacitor discharge circuit is computed using below formulas given by Nappert [19].

$$L_{cdc} = \frac{T_{fd}^{\ 2}}{C[4\pi^2 + \ln(\frac{I_m}{I_{m+1}})]} \tag{4.1}$$

$$R_{cdc} = \frac{2L_{cdc}}{T_{fd}} \ln(\frac{I_m}{I_{m+1}}) \tag{4.2}$$

$$T_{fd} = t_{m+1} - t_m = \frac{1}{f_d} \tag{4.3}$$

where I_m and I_{m+1} represent the peak values for two consecutive positive or negative current peaks; t_m and t_{m+1} are time values at that peaks. f_d is the oscillating frequency of the ringdown current. In this study, positive peak values are used in calculations.

Ringdown tests are carried out between 1000 volts and 2000 volts with increments of 200 volts. Results of the tests are adapted into above formulas and they are plotted in Figure 4.7.

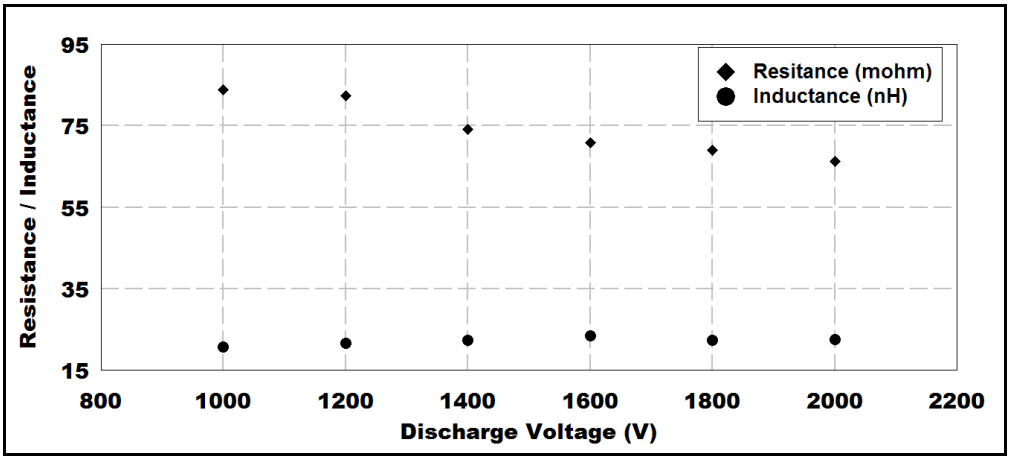

Figure 4.7 Ringdown Test Results at Different Discharge Voltages

From ringdown tests, it is realized that first peak point in current is increasing rapidly as the voltage level increases. At 2000 volts, current value for the first current peak is determined around 5000 amperes. So increasing voltage level any further may cause defects in the switch. For higher voltage levels, a simple two point extrapolation

scheme up to 3000 volts is carried out for resistance values. As inductance remains nearly same for all voltage levels, its average value 22.1 nH is used for all voltage levels. Resistance values are summarized in Table 4.1

Table 4.1 Ringdown Test Results at Discharge Voltage Levels Greater than 2000 Volts

Voltage (V)	*Resistance (mΩ)*
2000	66.2
2200	63.4
2400	60.5
2600	57.7
2800	54.9
3000	52

CHAPTER 5

NUMERICAL STUDY

In this chapter, a theoretical model for predicting performance of EFI striplines will be presented.

The numerical study of the present work involves electrical performances of specific EFI striplines by predicting current, voltage, power and energy waveforms. Moreover, average and final velocities of the flyer plate are predicted. Finally from impact pressure calculations, criterion for the detonation of HNS - IV explosive is checked.

All of the equations represented in this section are implemented into numerical computing program Matlab.

5.1 ELECTRICAL PERFORMANCE CALCULATIONS

Basic electrical circuit of EFI system used in this study is formed by CDC of EFI Test Module and EFI stripline. Whole representative circuit elements are shown in Figure 5.1 schematically.

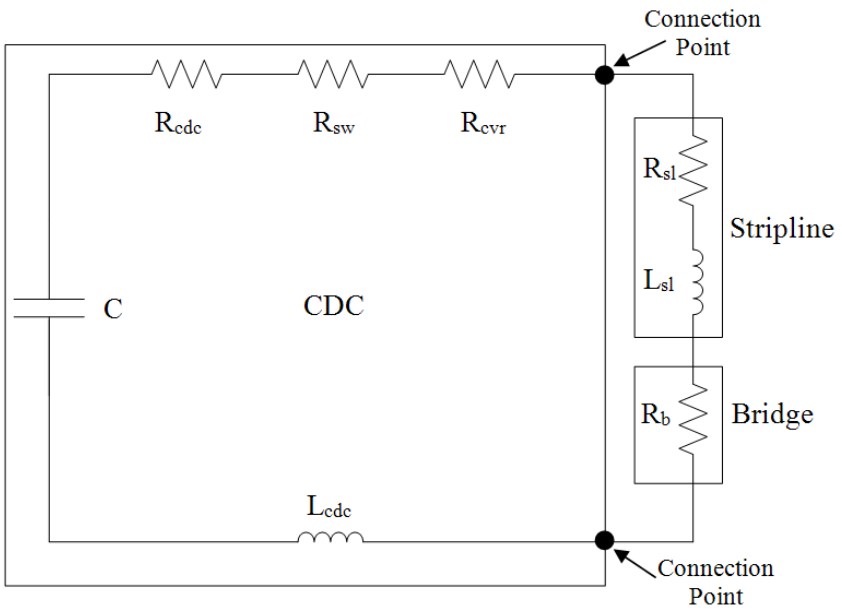

Figure 5.1 Equivalent Circuit Diagram of EFI System

From Kirchhoff's Voltage Law, circuit equation is written as

$$L_t \frac{dI}{dt} + [R_t + R_d(t)]I(t) + \frac{1}{C}\left(\int_0^t I(t)dt + Q_0\right) = 0 \tag{5.1}$$

Also a further relation between electrical charge *Q(t)* and current *I(t)* is defined as

$$\frac{dQ(t)}{dt} = I(t) \tag{5.2}$$

In Equation (5.1), L_t is the total inductance of the system including stripline inductance L_{sl} and CDC inductance L_{cdc} calculated from Ringdown tests at the specific discharge voltage of the capacitor V_0. Inductances of CVR and switch are neglected. *C* is the capacitance of the capacitor in CDC. Two parameters, L_t and *C* are assumed to be constant throughout the process.

$$L_t = L_{sl} + L_{cdc} \tag{5.3}$$

On the resistance point of view, R_t includes constant CVR resistance R_{cvr}, constant CDC resistance R_{cdc} obtained from Ringdown tests, constant stripline resistance R_{sl} calculated from the specific stripline properties excluding initial bridge resistance R_{b0}; $R_d(t)$ includes dynamic switch resistance $R_{sw}(t)$ and dynamic bridge resistance $R_b(t)$.

$$R_t = R_{cvr} + R_{cdc} + R_{sl} + R_{sw} \tag{5.4}$$

$$R_d(t) = R_{sw}(t) + R_b(t) \tag{5.5}$$

R_{b0} is calculated by using bridge dimensions defined in CHAPTER 3 and initial electrical resistivity ρ_0.

$$R_{b0} = \frac{\rho_0 \times l}{l \times w} \tag{5.6}$$

Equations (5.1) and (5.2) become a set of two first order differential equations, which are based on time dependent variables *I(t)* and *Q(t).* Those equations can be solved together by using a high order Runge - Kutta scheme. In this study, Runge – Kutta - Gill method is used with the initial conditions given below.

$$I(0) = 0 \tag{5.7}$$

$$Q(0) = C \times V_0 \tag{5.8}$$

In each time step, current values are obtained by altering dynamic resistances of switch and bridge with the models explained in following sections. Voltage across EFI stripline *V(t)* is calculated using Ohm's Law in each time step.

$$V(t) = [R_{sl} + R_b(t)] \times I(t) \tag{5.9}$$

Similarly, power and energy are obtained by using basic relations given below.

$$P(t) = I^2(t) \times [R_{sl} + R_b(t)] \tag{5.10}$$

$$E(t) = \int_0^t P(t) d(t) \tag{5.11}$$

5.1.1 Dynamic Switch Resistance Model

Richardson [38] realized that experimental ringdown waveforms were different with the ones calculated theoretically. He then developed a general idea of modeling the effect of switch resistance on the ringdown waveform of a slapper system. In his study, he assumed an instantaneous fall of the switch resistance to some value R_{sw0} which is quite a high value compared to the rest of the circuit. He assumed a linear drop in R_{sw0} to 0 after a certain time of t_{sw} passes.

Nappert [19] also figured switch resistance behavior for different voltage levels. Behavior of the switch resistance in his study is consistent with Richardson's [38] assumptions except two points. First, a considerable time passes between initial drop of resistance from infinity; second, switch resistance does not reach 0 after some time t_{sw} but it reaches nearly a constant value of around 0.1 ohm.

In this study the switch resistance is modeled by combining two above references. Three assumptions are made;

- Infinite switch resistance falls to R_{sw0} instantaneously.
- Switch resistance falls linearly from R_{sw0} to a constant resistance value R_{swf} in a time t_{sw}.
- R_{sw0}, R_{swf} and t_{sw} may change for different system parameters like firing voltage.

With above assumptions, formulation for dynamic switch resistance calculations is given as

$$R_{sw}(t) = R_{sw0} \times \frac{t_{sw} - t}{t_{sw}} \quad t \le t_{sw} \tag{5.12}$$

$$R_{sw}(t) = R_{swf} \quad t > t_{sw} \tag{5.13}$$

5.1.2 Dynamic Bridge Resistance Model

In this study, a temperature based bridge resistance model is set. A basic relationship given for resistance is

$$R_b(t) = R_{b0} \times [1 + \alpha \times (T(t) - T_0)] \tag{5.14}$$

where α is first temperature coefficient of resistance, T_0 is the initial temperature of striplines and $T(t)$ is the time dependent temperature. The model involves basic energy equation based on ohmic heating of bridge given in Equation (5.15). That is, electrical energy provided to bridge results temperature changes in the bridge proportionally with its mass M_b and specific heat capacity $C_p(T)$.

$$M_b \times C_p(T) \times dT = \int_0^t [I^2(t) \times R_b(t)]dt \tag{5.15}$$

Mass of the bridge M_b is constant and specific heat capacity of copper $C_p(T)$ is formulated in terms of temperature with data obtained from [39]. $T(t)$ is computed by solving Equation (5.15) using a fourth order Runge - Kutta method.

In the theoretical model, temperature at burst T_b is used as a control point for burst. After burst, resistance of bridge plasma is assumed to be constant. The burst resistance and temperature are obtained empirically.

5.2 VELOCITY CALCULATIONS

Velocity calculations of EFI system is related with electrical energy obtained from electrical performance calculations. An advanced Gurney analysis is performed to find velocity histories of flyer plate inside the barrel. Formulation given by Stanton and Tucker [12] is as follows;

$$\ddot{x}(t) = \frac{n-1}{1+A} \times \frac{M_b}{M_f} \times \frac{1}{x(t)} \times \left[E(t) - \frac{\dot{x}(t)}{2 \times CF^2} \right] \tag{5.16}$$

$$A = \frac{M_b + 2 \times M_f}{M_b + 2 \times M_{tamp}} \tag{5.17}$$

$$CF^2 = \frac{M_b}{M_f + M_{tamp} \times A^2 + M_b \times (1 - A + A^2)} \tag{5.18}$$

In above formulations, acceleration of flyer plate $\ddot{x}(t)$ is basically related with displacement of flyer plate $x(t)$ and its velocity $\dot{x}(t)$, energy given to the system per unit bridge foil mass $E(t)$, mass of bridge foil M_b, mass of flyer plate M_f, mass of tamper M_{tamp} and polytropic gas exponent n.

Using the simple relation between acceleration, velocity and displacement, Equation (5.16) turns out to be a set of two differential equations which is solved by a fourth order Runge-Kutta method to obtain displacement and velocity histories of the flyer plate.

Energy given to the system *E(t)* has several important features. First of all, the energy provided to the system is given as

$$E(t) = \int_0^t [I^2(t) \times R_b(t)]dt \tag{5.19}$$

The system is thought to be at rest initially, that is, no flyer plate motion occurs before burst of the bridge. Up to burst, total electrical energy deposited in the system E_b can be defined as

$$E_b = \int_0^{t_b} [I^2(t) \times R_b(t)]dt \tag{5.20}$$

However, it is assumed that bridge foil changes phase during ohmic heating process. Some certain energy losses occur during ohmic heating of bridge up to burst point. These losses do not contribute to the performance of EFI system and they should be subtracted from deposited electrical energy. These losses are namely;

1. Energy needed to heat bridge foil up to melting point T_{mp}

$$E_{mp}(t) = M_b \times \int_{T_0}^{T_{mp}} C_P(T)dT \tag{5.21}$$

2. Energy needed to change bridge foil's phase from solid to liquid

$$E_{fus} = M_b \times L_f \tag{5.22}$$

   where L_f is latent heat of fusion.

3. Energy needed to heat bridge foil up to boiling point T_{bp}

$$E_{bp}(t) = M_b \times \int_{T_{mp}}^{T_{bp}} C_P(T)dT \tag{5.23}$$

4. Energy needed to change bridge foil's phase from liquid to vapor

$$E_{vap} = M_b \times L_v \tag{5.24}$$

where L_v is latent heat of vaporization.

5. Energy needed to ionize bridge foil to transform into plasma

$$E_{ion} = I_p \times M_b \times \alpha_i \tag{5.25}$$

where I_p is the first ionization energy and α_i is the ionization degree.

Total loss energy is the sum of above loss energies.

$$E_{loss} = E_{mp} + E_{fus} + E_{bp} + E_{vap} + E_{ion} \tag{5.26}$$

In this study, two methods for contribution of the above stated energy calculations to the flyer plate's velocity are utilized. These two methods are clarified in the following sections.

5.2.1 First Method for Contribution of Energy in Velocity Calculations

In the first method, total electrical energy up to burst is calculated by Equation (5.20) and the total loss energy calculated by Equation (5.26) is subtracted from total electrical energy up to burst. There remains some energy deposited in the formed plasma by the explosion of the metallic foil. The energy term in Equation (5.16) *E(t)* is formed by adding this pre - burst excess energy to the post – burst energy (energy added to the system after burst). The formulations for pre - burst excess energy and post – burst energy are given below.

$$E_{pre} = E_b - E_{loss} \tag{5.27}$$

$$E_{post}(t) = \int_{t_b}^{t_a} [I^2(t) \times R_b(t)] dt \tag{5.28}$$

5.2.2 Second Method for Contribution of Energy in Velocity Calculations

For the second method, it is inspired from the work in [13] that the whole energy deposited up to burst is used for the ohmic heating process and energy deposited in the system after burst should be taken into consideration for the velocity calculations of the flyer plate. Second method solely utilizes Equation (5.28) for the energy term *E(t)* in Equation (5.16). Results obtained by two methods are represented in CHAPTER 6.

5.2.3 Closure of Velocity Calculations

Using first and second methods stated above in Equation (5.16), displacement, velocity and acceleration histories for flyer plate are calculated. Average velocity of the flyer plate is obtained by simply dividing the barrel length to the time that flyer plate

reaches the exit of the barrel. Final velocity V_f is defined as the velocity of the flyer plate at the exit of the barrel.

Using Equation (5.16), one should note that *x(t)* term is at the denominator. If one takes *x(0)* = 0 by considering the vertical axis (motion axis of flyer plate) starts at flyer plate - metallic bridge interface, then Equation (5.16) approaches infinity. To overcome this problem, calculations are started by assuming that vertical axis originated at the base of the metallic bridge. Then metallic bridge thickness is subtracted from the displacement history of the flyer plate. This phenomenon is shown in Figure 5.2.

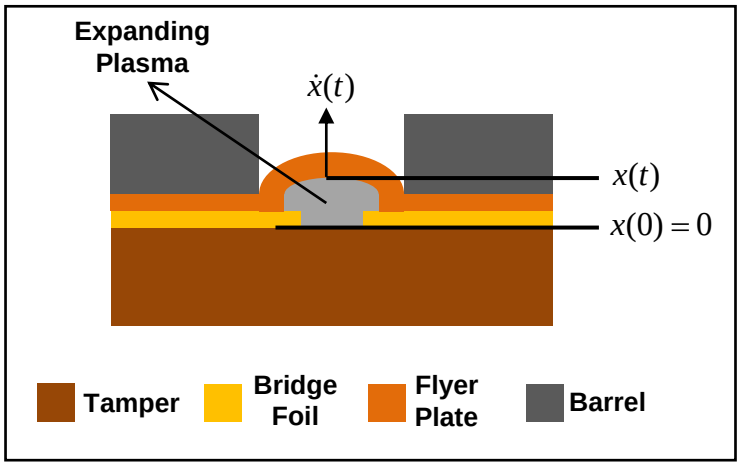

Figure 5.2 Definition of the Vertical Axis for the Motion of Flyer Plate inside the Barrel

5.3 PRESSURE PULSE CALCULATIONS AND INITIATION CRITERION CHECK

After calculating the final velocity V_f of flyer plate, pressure imparted to explosive located at the exit of the barrel is obtained with formulations given by Nappert [19]. From momentum conservation equation, pressure pulse on explosive P_e is given as

$$P_e = \rho_{0e} \times (C_{0e} + S_e \times U_{pe}) \times U_{pe} \tag{5.29}$$

Initial density of the explosive ρ_{0e} and initial sound speed in the explosive C_{0e} are known parameters for a specific explosive. S_e is determined experimentally and unknown particle velocity U_{pe} will be determined.

Definitions in pressure pulse equation for flyer plate are similar to that for explosive. Pressure pulse equation for flyer plate is given as

$$P_f = \rho_{0f} \times [C_{0f} + S_f \times (V_f - U_{pf})] \times (V_f - U_{pf}) \tag{5.30}$$

Since pressure and particle velocity for explosive and flyer plate at explosive-flyer interface are equal, equating above pressure pulse equations gives

$$\rho_{0f} \times [C_{0f} + S_f \times (V_f - U_p)] \times (V_f - U_p) = \rho_{0e} \times (C_{0e} + S_e \times U_p) \times U_p \quad (5.31)$$

Determination of the only unknown U_p from Equation (5.31) leads the pressure pulse value by either solving Equation (5.29) or equation (5.30).

Initiation criterion for a specific explosive is related to pressure imparted to the explosive and duration t_p of this pressure pulse. The formulation is given as

$$P_e^{x_i} \times t_p \geq const. \quad (5.32)$$

t_p is related with flyer plate thickness th_f and final velocity of flyer plate V_f.

$$t_p = 2 \times th_f \times [C_{0f} + S_f \times (V_f - U_p)] \quad (5.33)$$

Initiation criterion is determined experimentally for a specific explosive. One can check whether a particular EFI system will initiate that specific explosive or not by utilizing Equation (5.32).

CHAPTER 6

RESULTS, VALIDATION AND DISCUSSIONS

In this section, results obtained from experimental and numerical studies are represented.

Primarily, experimental results covering both electrical performance of the striplines and measured average velocities of flyer plates belonging to those striplines are given. Moreover, results of the explosive tests are presented.

Results of numerical study that cover the configurations and the parameters utilized in experimental study are introduced. Outcomes of both studies are compared. Finally, a case study using the numerical code is represented.

6.1 EXPERIMENTAL RESULTS

Utilizing experimental setup introduced in CHAPTER 4 and stripline configurations defined in CHAPTER 3, tests were performed to present effects of some parameters on EFI performance. In general, an EFI performance is characterized by its flyer plate's final velocity and impact of this flyer plate to the intended target which is a secondary high explosive in this study. Detonation of a specific explosive is expected for a particular energy level applied to an EFI. However, measurements in this study can only indicate average velocities of flyer plates because of the type of velocity measurement technique. It is not possible to measure the quantity of flyer plate's impact either. Numerical study is utilized to determine the final velocity and impact characteristics of the flyer plate.

All striplines are fired at the same voltage level (2000 volts). Also two types of striplines are fired at different voltage levels (2400 and 2800 volts). Results of these firings are represented in a manner that all the configurations are introduced comparatively for brevity.

6.1.1 Recorded Data Manipulation

Since the waveforms should represent all significant points in EFI experiments, recording system is adjusted such that enough data is gathered in measurements. Some trials are carried on to determine the minimum number of points that the scope should collect. Although minimum number of points is collected, results indicate substantial noise in recorded data. Noise does not affect to realize the form of the waveforms; however, it complicates manipulating the data. This part clarifies the manipulation of the noisy data and further treatment of the manipulated data. As an illustration, result of one of the firings for Type 1 striplines is given. The process is identical for all stripline configurations.

Figure 6.1 represents a sample firing with Type 1 stripline at 2000 volts. 60 step smoothed version of raw data with DPlot graphing program is also shown. Figure 6.2 shows the waveforms of the smoothed data of Figure 6.1.

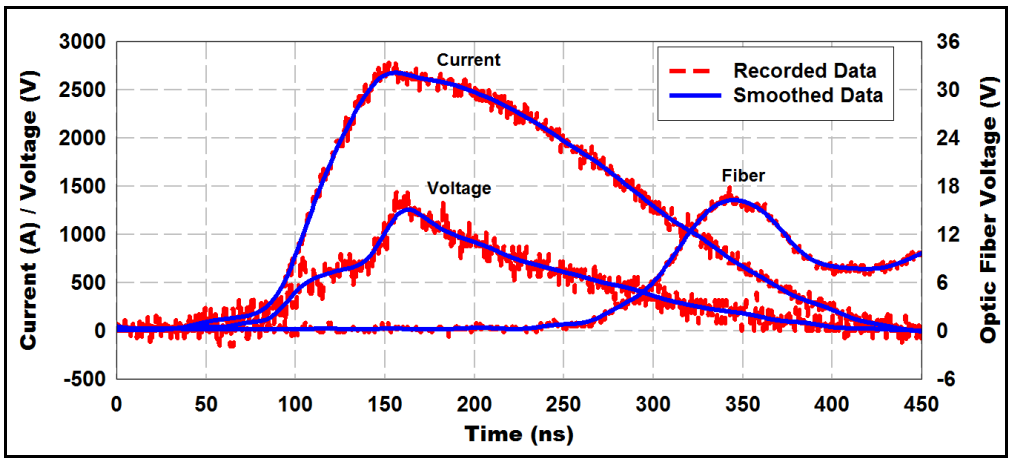

Figure 6.1 Comparison of Raw Data and Smoothed Data for Sample Firing at 2000 Volts

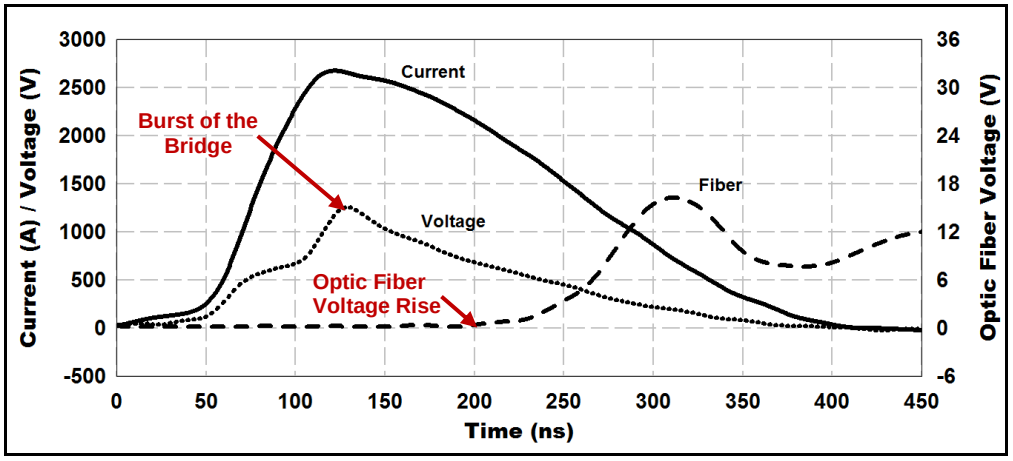

Figure 6.2 Measured Current, Voltage and Optic Fiber Waveforms for Sample Firing at 2000 Volts (Smoothed Data)

In this study, time of voltage peak is considered as the burst time of the metallic bridge and the rise of optic fiber voltage is considered as the arrival of the flyer plate to the exit of the barrel. Calculation of flyer plate's average velocity is done by simply finding

the flight time (time passes between the voltage peak and the initial optic fiber voltage rise) and dividing barrel length to that flight time as stated in above sections. For this sample firing, flight time and average velocity of the flyer plate are summarized in Table 6.1.

Table 6.1 Average Velocity Calculation Results for Sample Firing at 2000 Volts

Type No.	*Barrel Length (mm)*	*Flight Time (ns)*	*Average Velocity (km/s)*
1	0.25	70	3.57

It is noted from the recorded voltage data that there occurs an unwanted induced voltage. This is certainly due to inductive coupling created between the voltage measurement probe and the circuit [20]. This phenomenon is shown in Figure 6.3.

It is further stated by Nappert *et al.* [20] that inductive coupling occurring in current rise region does not contribute to the performance of EFI, so they suggested a technique to subtract that induced voltage from the recorded data. First thing to do is to determine the inductance of the voltage measurement probe.

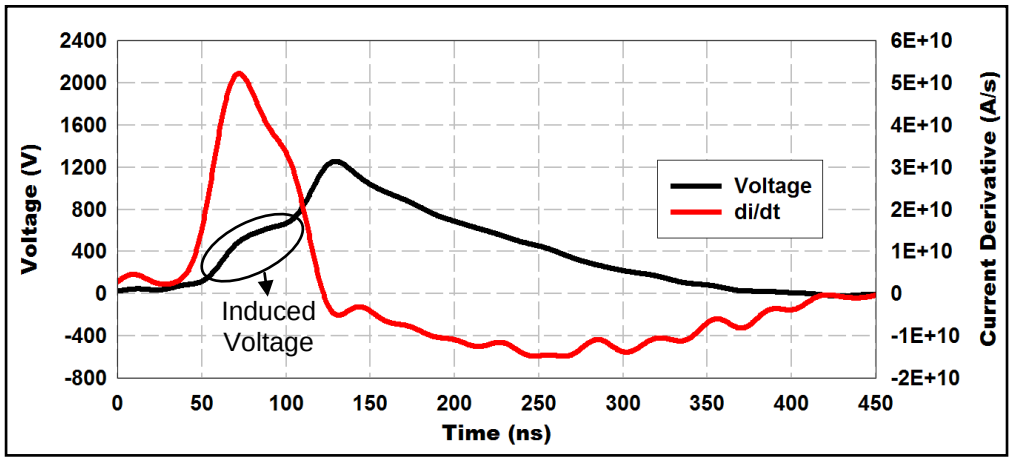

Figure 6.3 Induced Voltage in Voltage Waveform for Sample Firing at 2000 Volts

Relation between voltage, current and inductance is given by Hatt *et al.* [16] and Nappert *et al.* [20] revised as

$$V_i(t) = L_p \times \frac{dI}{dt} \tag{6.1}$$

For the first guess, V_i is determined for a random point considering the tendency of the voltage waveform as if there is no inductive coupling and then for that point L_p can be found by dividing that induced voltage to the corresponding derivative of the current.

Table 6.2 gives input parameters and resulting L_p for voltage waveform shown in Figure 6.3.

Table 6.2 Inductance of Voltage Measurement Probe for Sample Firing at 2000 Volts

Type No.	*Voltage (V)*	*dI/dt (A/s)*	*Probe Inductance (nH)*
1	V_i = 299	4.6e10 (Figure 6.3)	L_p = 6.5

Using Equation (6.2) [20], corrected voltage waveform is obtained and shown in Figure 6.4.

$$V_{corrected} = V_{measured} - L_p \times \frac{dI}{dt} \tag{6.2}$$

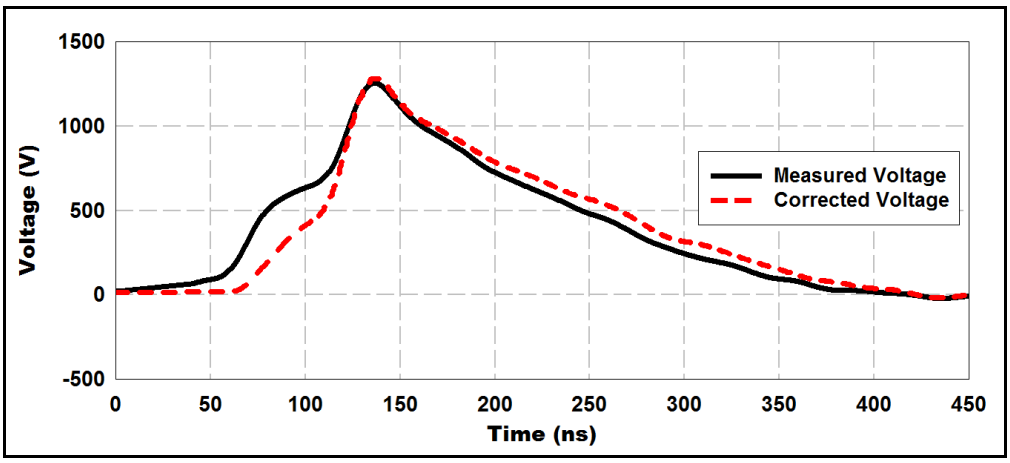

Figure 6.4 Corrected Voltage Waveform for Sample Firing at 2000 Volts

One should note that time of peak point does not change after correction; however, burst voltage level slightly increases with the correction in voltage waveform. Corrected voltage data is used in finding burst resistances of striplines. Burst resistance of the bridge is calculated as

$$R_{burst} = \frac{V_{burst}}{I_{burst}} - R_{sl} \tag{6.3}$$

Since voltage is measured across the stripline contact legs, resistance of the stripline is subtracted to find the bridge resistance at burst. Using Equation (5.9) with the corrected burst voltage, resistance at burst for firing voltage range is obtained. Furthermore, Equation (5.14) gives temperature at burst with utilizing the ratio of burst resistance to initial resistance of the bridge. For this sample firing values at burst are summarized in Table 6.3. Experimentally obtained burst resistance and temperature values are used in numerical study.

Table 6.3 Burst Values for Sample Firing at 2000 Volts

Type No.	t_b *(ns)*	V_{burst} *(V)*	I_{burst} *(A)*	R_{burst} *(ohm)*	T_b *(K)*
1	136.8	1280	2651	0.347	25908

Furthermore, it is observed that same configurations may result different waveforms and values at same firing voltage levels. This fact is clarified in Figure 6.5.

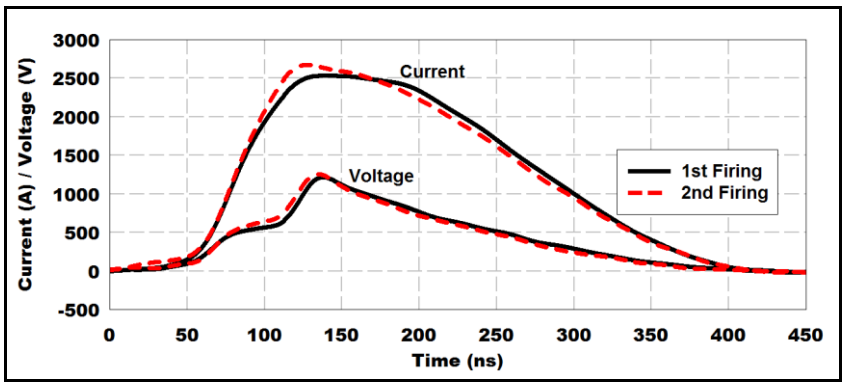

(a)

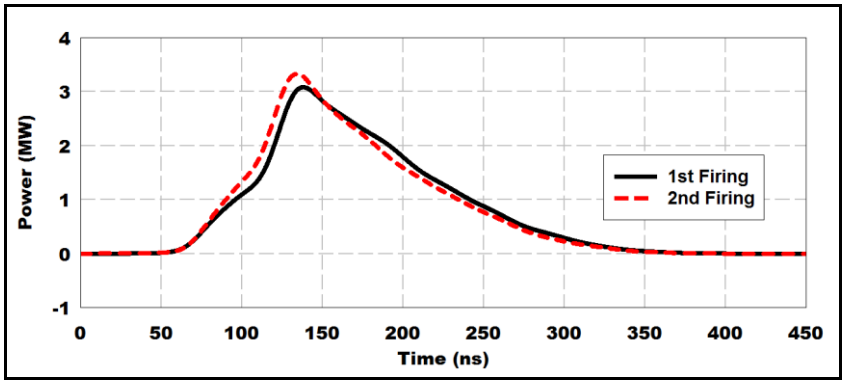

(b)

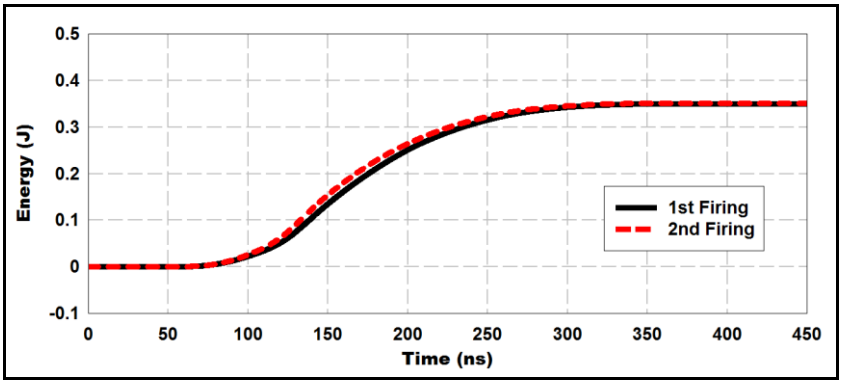

(c)

Figure 6.5 Comparison of Two Firings at 2000 Volts for Type 1 Striplines
(a) Current and Voltage Waveforms (b) Power Waveform (c) Energy Waveform

Above figures are illustrative examples for possible deviations of electrical performances of same stripline configurations. From Figure 6.5 (a), it is obvious that even though the voltage waveforms are similar, current waveforms differ in burst value. This results a higher peak power value at burst for second firing (Figure 6.5 (b)). This difference reflects in energy as well. Due to this difference, average velocities of the flyer plates obtained from these two firings alter. Average velocities of the flyer plates for first and second firings are measured as 3.3 km/s and 3.9 km/s respectively. The difference in the peak current value and resulted average velocities can be explained by the dimensional variations in metallic bridges of tested two striplines. Table 6.4 summarizes the values for above two firings.

Table 6.4 Measured Values of Type 1 Striplines for Two Firings at 2000 Volts

Firing No	*Burst Time (ns)*	*Burst Current (A)*	*Peak (Burst) Power (MW)*	*Energy at Burst (mJ)*
1	139.2	2533.0	3.1	99.5
2	135.2	2651.4	3.3	104.6

6.1.2 Electrical Performance Comparison of Stripline Configurations

This part introduces electrical performances of Type 1, Type 2 and Type 3 (or Type 4, Type 5 and Type 6 as they have the same configuration considering electrical performances) striplines. Current, power and energy waveforms obtained at a firing voltage level of 2000 volts are compared. Also electrical performance at different firing voltage levels of Type 1 and Type 3 striplines are presented.

Figure 6.6 shows current, power and energy waveforms for aforementioned stripline configurations. For brevity, voltage waveforms are not included in the plots. However, burst times obtained from voltage waveforms are represented on the plots.

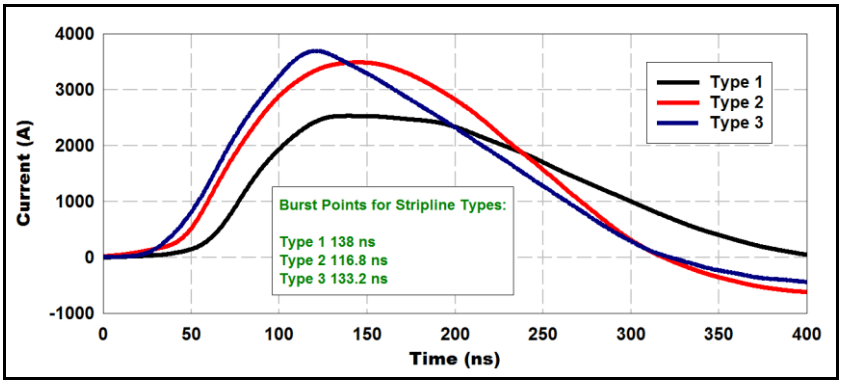

(a)

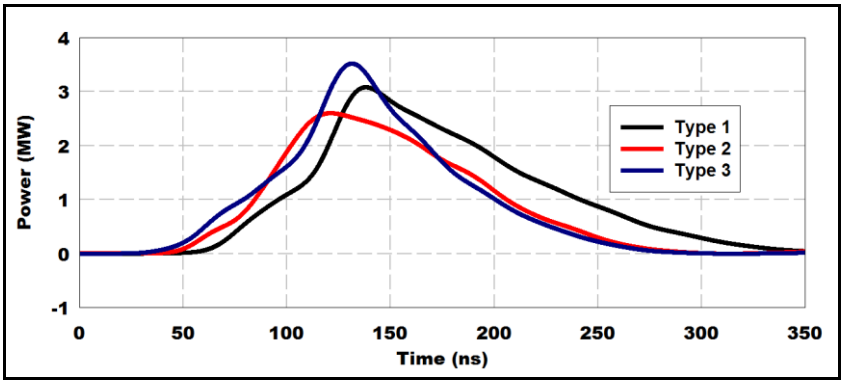

(b)

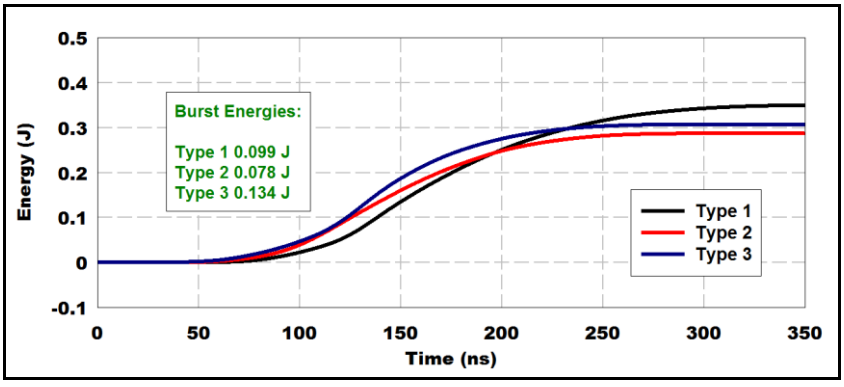

(c)

Figure 6.6 Electrical Performance Comparison of Stripline Types Fired at 2000 Volts
(a) Current Waveforms (b) Power Waveforms (c) Energy Waveforms

Figure 6.6 is a good example for realizing the effect of bridge dimensions on electrical performance. Comparing Type 1 and Type 3 striplines, it is clear that as thickness of the bridge is increased from 5 μm to 9 μm, larger currents are obtained since thicker bridges need more energy for burst because of the larger mass. It is hard to comment on burst times of these two types since burst times are significantly depend on switching time of the spark – gap which seems larger for Type 1 in this case.

Comparing Type 2 and Type 3, again due to larger mass of Type 3, current level of this type is slightly over according to Type 2. This time, one can comment on the burst times because even the switching time of the spark – gap is larger for Type 2, its burst time is earlier. Another interesting point may be, for Type 2, burst occurs during current rise whereas burst occurs after current peak for other types. This explains the low energy need for burst of Type 2.

Another comparison for Type 1 and Type 3 striplines are given in Figure 6.7 and Figure 6.8, respectively. Results of firings at 2000, 2400 and 2800 volts are represented. Not surprisingly higher firing voltage levels result higher current and energy levels for both stripline types which will further be clarified by flyer plates' velocities in the following sections.

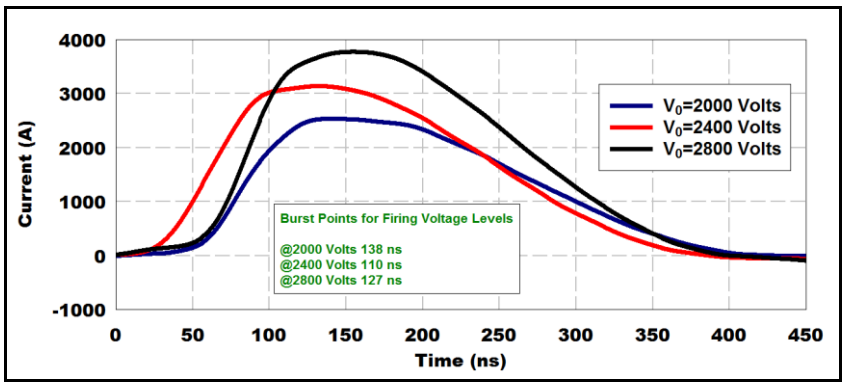

(a)

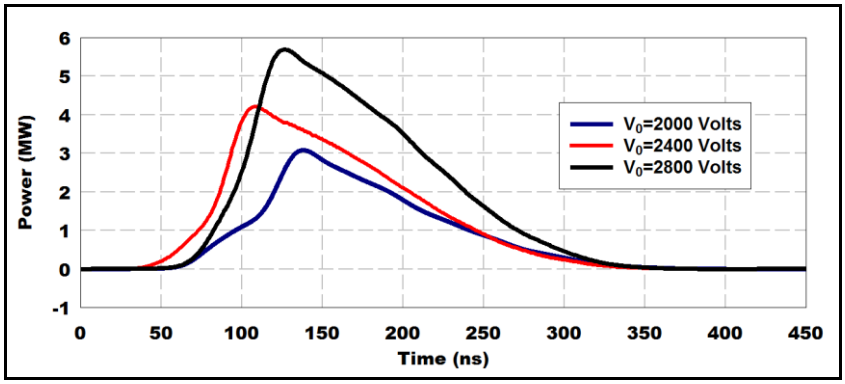

(b)

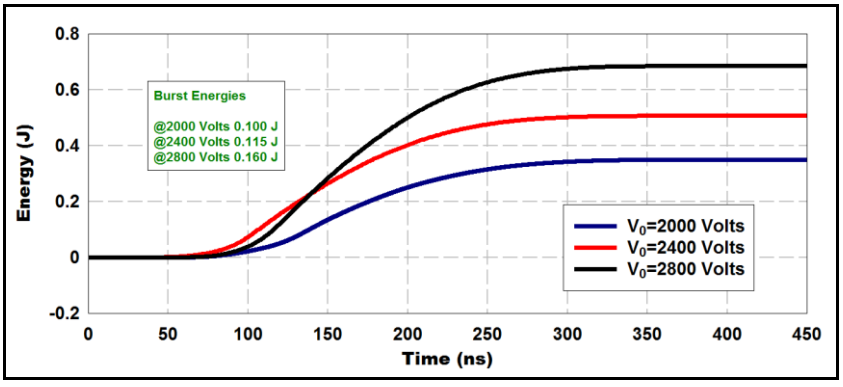

(c)

Figure 6.7 Electrical Performance Comparison of Type 1 Striplines Fired at 2000, 2400 and 2800 Volts
(a) Current Waveforms (b) Power Waveforms (c) Energy Waveforms

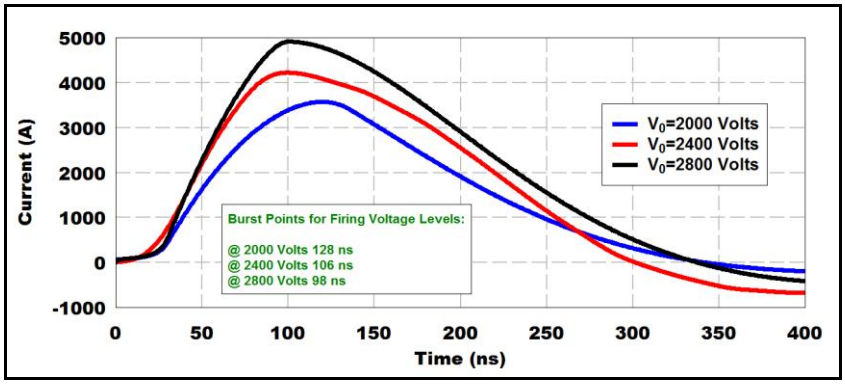

(a)

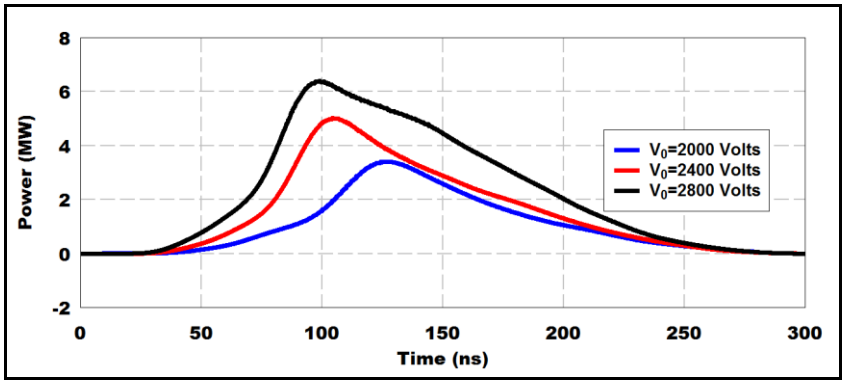

(b)

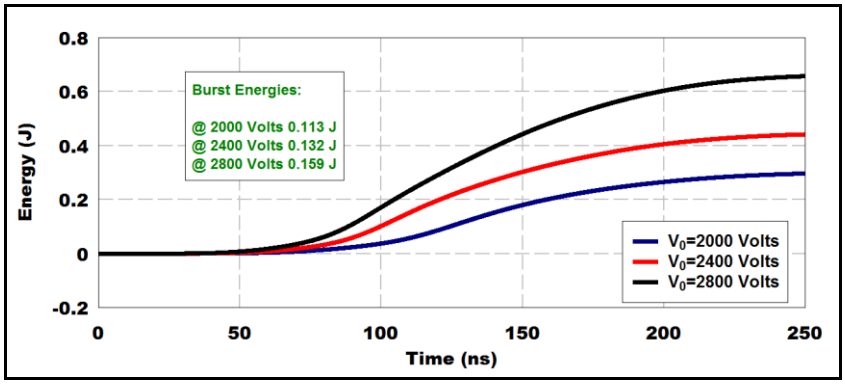

(c)

Figure 6.8 Electrical Performance Comparison of Type 3 Striplines Fired at 2000, 2400 and 2800 Volts
(a) Current Waveforms (b) Power Waveforms (c) Energy Waveforms

From Figure 6.7, it is clear that switching times for three firings are different. Actually it is expected that the higher the firing voltage levels, the sooner the bridge bursts. This phenomenon holds for Type 1 striplines if the result of the firing at 2400 volts is shifted right by considering as if it has the same switching time with the other two firings. The switching times for the firings of Type 3 striplines are closer as seen in Figure 6.8 which supports the above phenomenon without any manipulations.

Figure 6.9 depicts burst resistance and burst temperatures for Type 1, Type 2 and Type 3 striplines fired at 2000 volts. Referring to burst temperatures, it is obvious that increasing metallic bridge mass results a higher burst temperature. Also regarding the initial resistances of three types of striplines, there is no such a constant ratio between the burst resistances and initial resistances as stated in [24].

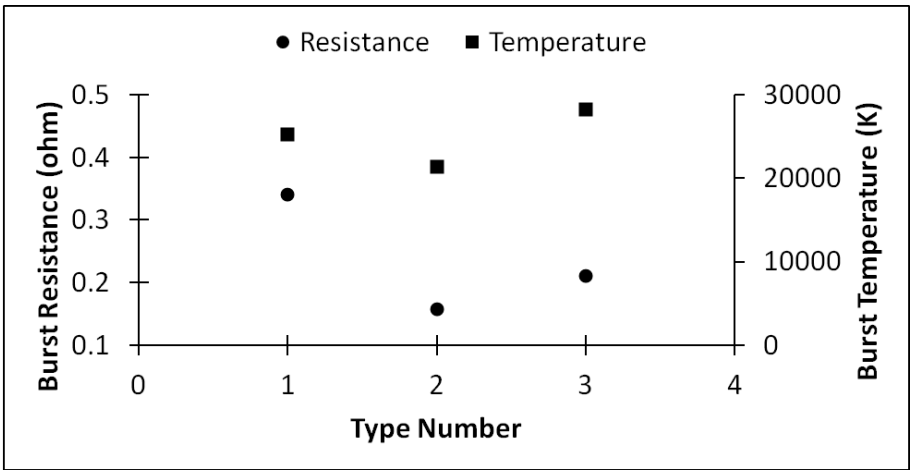

Figure 6.9 Resistances and Temperatures at Burst for Type 1, Type 2 and Type 3 Striplines

Furthermore, another study for Type 1 and Type 3 striplines shows that at firing voltage levels higher than 2000 volts, resistance and temperature values at burst remain nearly same. That is, for Type 1, resistance at burst is around 0.310 ohm and temperature at burst is around 23000 K; for Type 3, resistance at burst is around 0.210 ohm and temperature at burst is around 28000 K.

6.1.3 Comparison of Average Flyer Plate's Velocities

This section presents average velocities of flyer plates measured from different types of striplines including aforementioned bridge dimensions, firing voltage levels, barrel lengths and also flyer plates' thicknesses.

Error bars are used to point out the overall distribution of the measured data. The function "*std()"* in Matlab is used for standard deviation calculations and error bars are then plotted around the mean values of measured data.

Figure 6.10 shows average velocities for Type 1 and Type 4 striplines. At a firing voltage level of 2000 volts, copper thickness effect is not so clear from the experiments. However, at larger firing voltage levels 9 μm thick bridges seems to be more advantageous in terms of average velocity of the flyer plates.

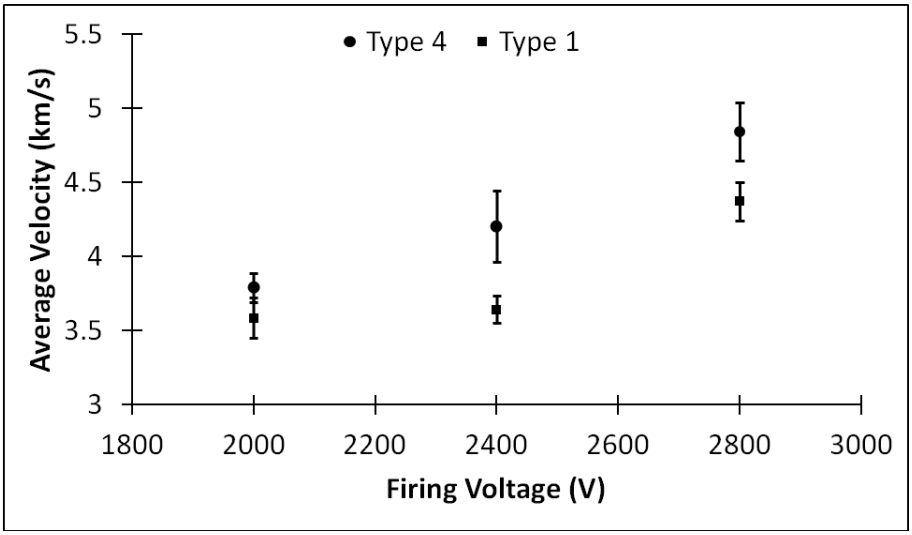

Figure 6.10 Effect of Copper Thickness on Measured Average Velocities at Various Firing Voltage Levels

Figure 6.11 represents the effect of bridge dimensions on average velocities of the flyer plates. Since less energy is spent for bridge burst in Type 2 striplines, remaining amount of energy is spent for the acceleration of the flyer plate through the barrel which indeed results a higher average velocity. Considering the momentum, impact of the flyer plate should be checked whether using small bridge dimensions are advantageous or not. This will be accomplished in numerical study.

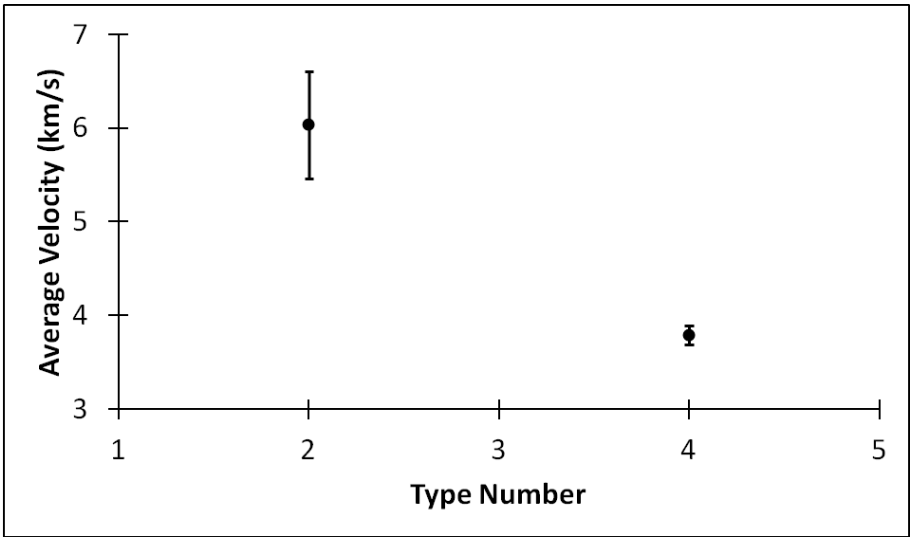

Figure 6.11 Effect of Bridge Dimensions on Measured Average Velocities at 2000 Volts

Figure 6.12 shows the effect of the barrel length on the measured average velocities of the flyer plates. Not surprisingly, as barrel length increases, average velocity increases. However, since there is rather a small rise in velocity through 0.25 mm to 0.40 mm barrel length, it can be commented that 0.40 mm barrel length is so close to the optimum barrel length value.

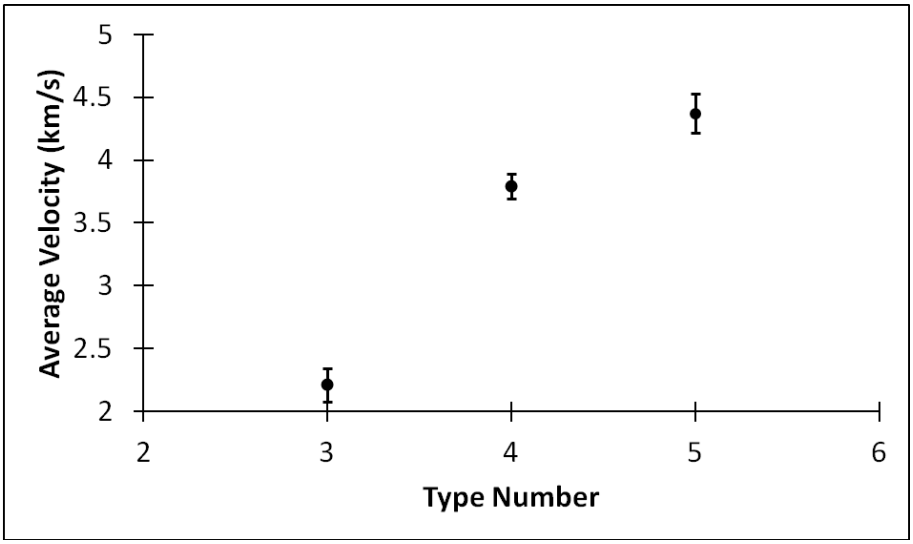

Figure 6.12 Effect of Barrel Length on Measured Average Velocities at 2000 Volts

Effect of flyer plate's thickness to average velocity is shown in Figure 6.13. Since the mass of thicker flyer plate is larger than the thinner one, its velocity is expected to be lower. However, impact of thicker flyer plate should be considered. This will be accomplished in numerical study.

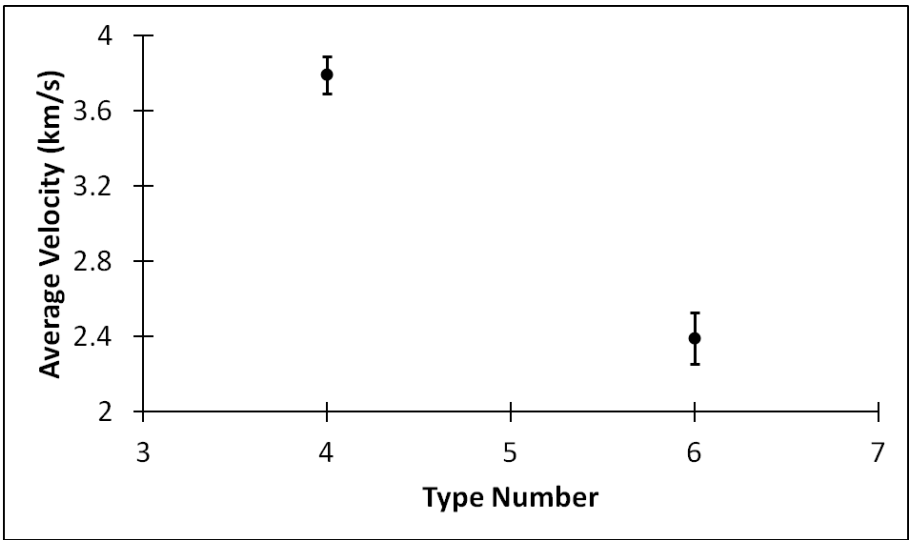

Figure 6.13 Effect of Flyer Plate's Thickness on Measured Average Velocities at 2000 Volts

Comparison of all stripline types are shown in Figure 6.14. It is realized that Type 2 striplines result the higher average velocity whereas they have the most deviation in average velocity measurements.

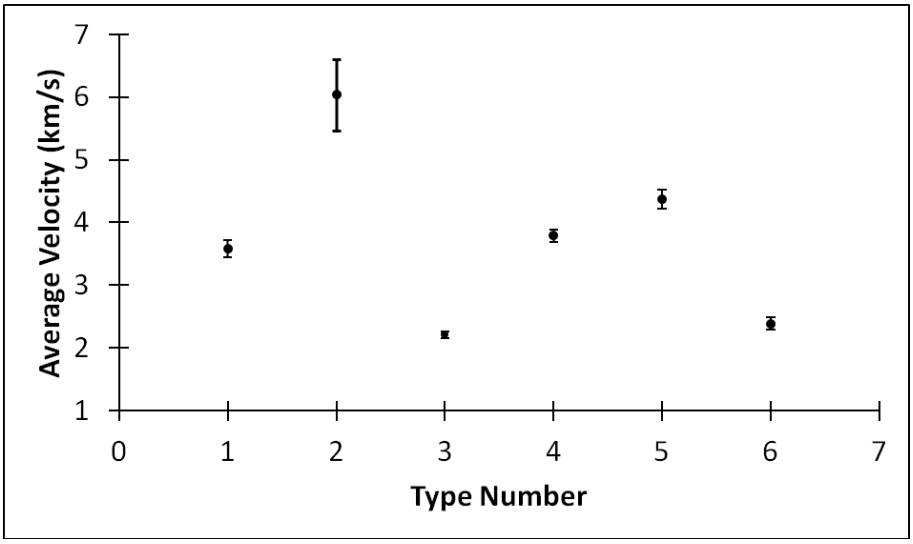

Figure 6.14 Comparison of Measured Average Velocities for All Striplines at 2000 Volts

6.1.4 Results of Explosive Tests

With the given configurations in CHAPTER 3, Type 1 striplines are mounted together with HNS – IV and PBXN – 5 explosive pellets for explosive tests.

Type 1 striplines are fired at 2000 volts. Current, voltage and optic fiber data are collected simultaneously as for inert firings. Smoothed recorded data for the first firing is shown in Figure 6.15.

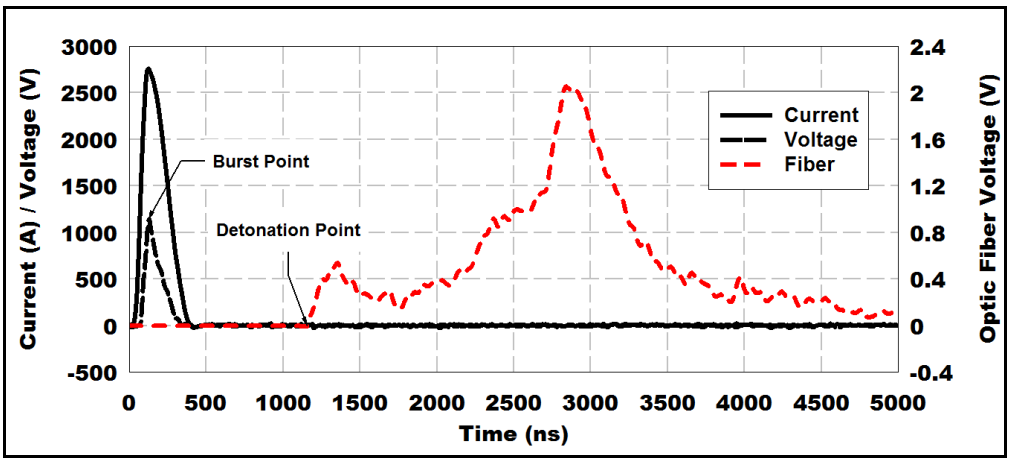

Figure 6.15 Explosive Test at 2000 Volts with Type 1 Stripline and HNS – IV Explosive Pellet

Referring to Figure 6.15, current and voltage waveforms are similar in terms of peak current values, peak voltage values and burst times with the inert firings represented in above sections. As it is stated, the time of initial rise of optic fiber voltage is taken as the detonation time and function time of the detonator is the time difference between voltage peak (burst) and detonation time. Results of the two firings are summarized in Table 6.5. Two HNS – IV explosive pellets are detonated and the results show good agreement with the ones in [19]. It was Nappert [19] who used almost the same HNS – IV explosive pellet (regarding the dimensions, density and weight of the explosive pellet which play crucial roles in the detonation output). He measured the function times of his detonators approximately around 1 μs.

As expected, detonation of the explosives cause a cavity on the dent block shown in Figure 6.16. The resulted depths of these cavities for both firings are measured.

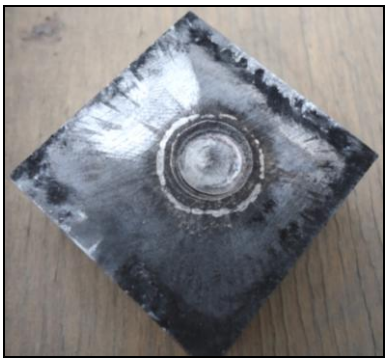

Figure 6.16 Dent Block after Detonation of HNS – IV Explosive Pellet in First Firing

Table 6.5 Results of Explosive Tests with Type 1 Striplines and HNS – IV Explosive Pellets

Firing No.	*Firing Voltage (V)*	*Burst Time (ns)*	*Detonation Time (ns)*	*Function Time (μs)*	*Depth of Dent (mm)*
1	2000	128	1156.4	1.03	0.50±0.03
2	2000	135	1178.2	1.04	0.51±0.02

Two firing trials are done with Type 1 striplines and PBXN – 5 pellets; however, the explosive pellets do not detonate at 2000 and 2800 volts firing level. Even, Type 2 striplines, which indeed has the highest average velocity, are used to detonate PBXN – 5 pellets at 2800 volts firing voltage level but the result is again no detonation. This behavior of PBXN – 5 explosive pellets may be explained with several reasons. First of all, it is actually known that plasticized explosives are more insensitive to shock initiations. This phenomenon is depicted in [1] for PBX – 9407 which is expected to have closer insensitive behavior with PBXN – 5 (Figure 6.17).

Another reason may be that PBXN – 5 powders are pressed to form high density pellets which are approximately 95.9% of their theoretical mean density. Especially for EBWs, it is known that a low density explosive is used in contact with gold bridgewire which can be readily detonated by the shock waves created as a result of explosion of the bridgewire. Due to this fact, it may be possible to detonate PBXN – 5 explosive pellets which are pressed to lower densities for a future study.

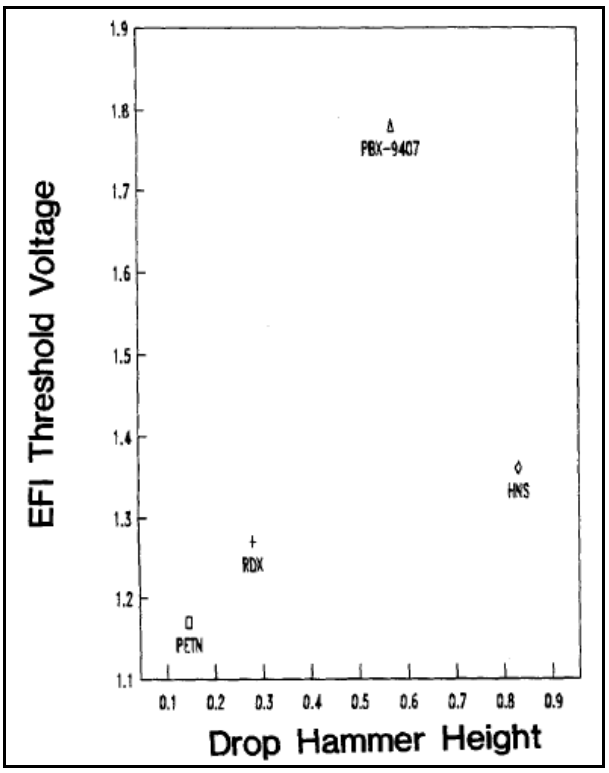

Figure 6.17 Sensitivity Comparison of Several Secondary Explosives [1]

(y – axis in kilovolts and x – axis in meters)

6.2 NUMERICAL RESULTS

In this section, results of the numerical study are represented by giving comparisons with the experimental results. Then the numerical code is utilized for a parametric case study.

Here are some important assumptions made in this numerical study;

- Volume and dimensions of the bridge are assumed to be constant throughout the process. This assumption also leads to a constant bridge density.
- Resistances of CDC, CVR and striplines (except the metallic bridge) are taken as constants throughout the process.
- In resistance calculations, first coefficient of temperature is used. Second coefficient is neglected.
- Resistance of the bridge is assumed to be constant after burst. This constant value is adapted from experimental data.

- Initial temperature value for the calculations is taken as 300 K approximately at which experiments are carried out.
- Degree of ionization of the metallic bridge is taken as 20% [14].
- Flyer plate is assumed to begin its motion just after the burst of the bridge.
- Flyer plate dimensions are taken same as bridge dimensions.

Results in this section are obtained by firing at least three striplines of each type.

6.2.1 Electrical Performance Predictions

Electrical performance predictions for the stripline types given in Section 6.1.2 are represented in following figures. For comparisons, only one experimental result is shown for a specific stripline. That representative experimental result is chosen in such a way that it gives the closest outcome to the numerical result.

Initial and constant values used in the calculations are summarized in Table 6.6. The calculations are carried out with a time step of 0.4 ns. It is also observed that using higher time steps like 1 ns causes overshoots in current peaks. Using lower time steps like 0.05 ns does not result any changes in the results.

Table 6.6 Some Constants Used in Electrical Performance Calculations [40]

Constants	*Values*
ρ_b	8.93 g/cc
α	0.0039 1/K
ρ_0	1.72E-6 Ωcm
T_0	300 K
T_{mp}	1358 K
T_{bp}	2835 K
L_f	208.7 J/g
L_v	4730 J/g
I_p	11.8 J/g

Figure 6.18, Figure 6.19 and Figure 6.20 demonstrate electrical performance predictions for Type 1 striplines. Considering the current waveforms, theoretical model shows a good agreement in predicting the current rise part. Empirical values used for switch and a proper adaptation of formulations play significant roles in this nice simulation. However, after burst, the model shows a poor simulation since resistance after burst is taken constant whereas it decreases as realized from experiments. Burst times and energy estimations are also in good agreement with the experimental ones which play important roles in calculation of flyer plate's velocities.

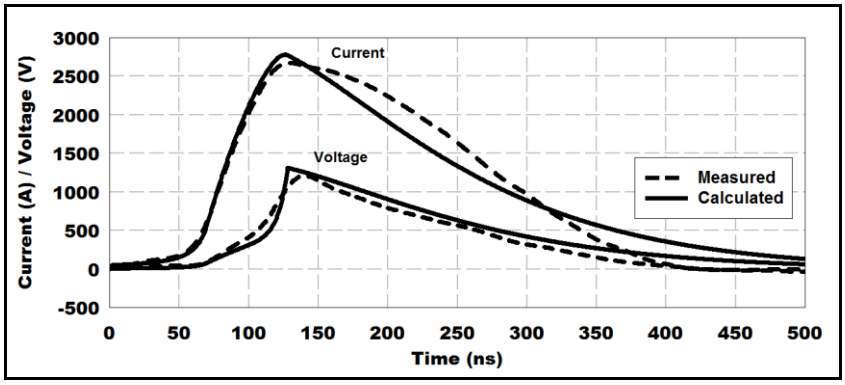

(a)

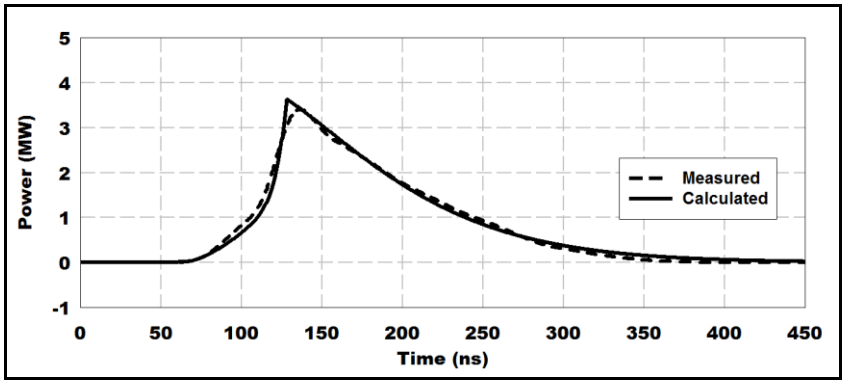

(b)

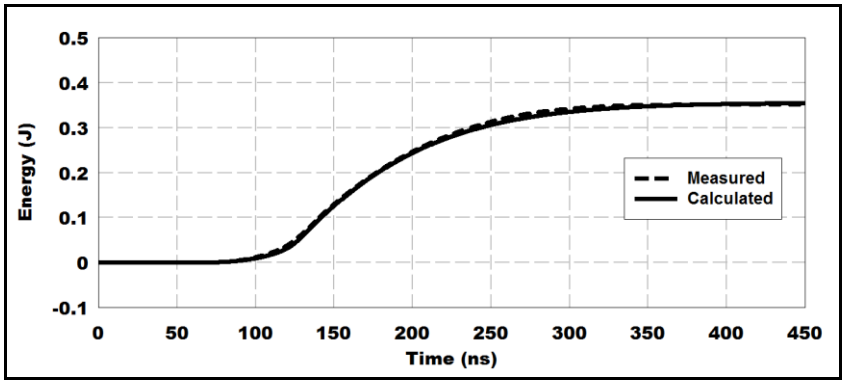

(c)

Figure 6.18 Measured and Calculated Electrical Performances for Type 1 Striplines at 2000 Volts
(a) Current and Voltage Waveforms (b) Power Waveforms (c) Energy Waveforms

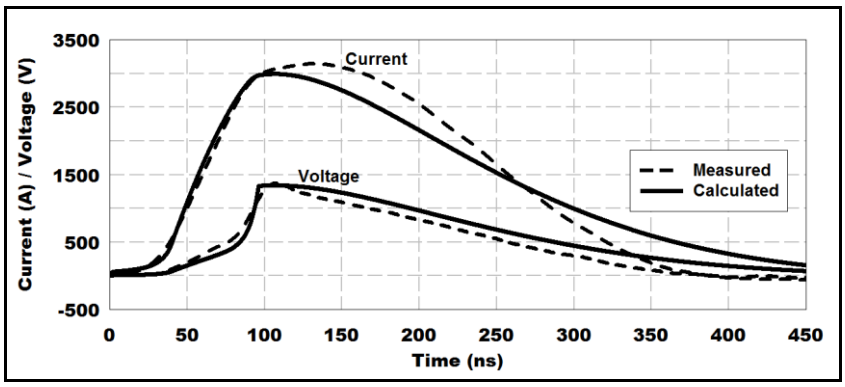

(a)

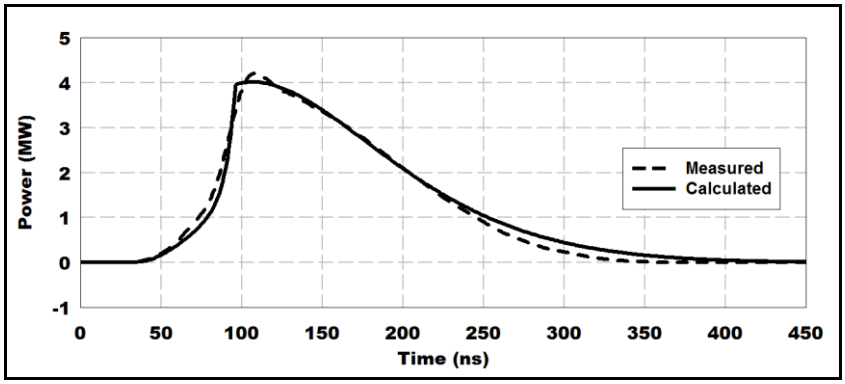

(b)

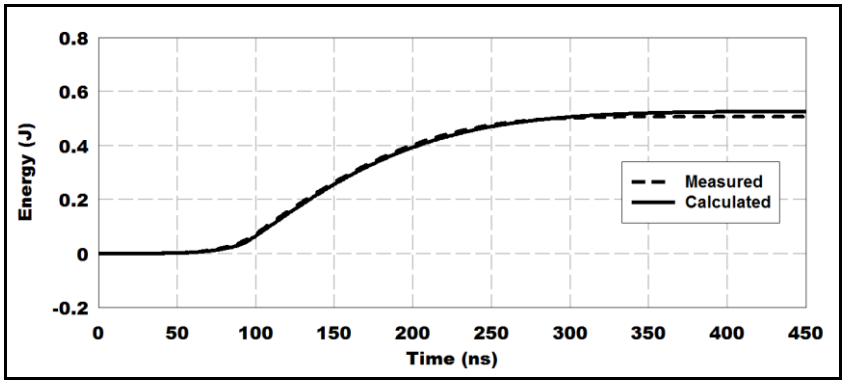

(c)

Figure 6.19 Measured and Calculated Electrical Performances for Type 1 Striplines at 2400 Volts
(a) Current and Voltage Waveforms (b) Power Waveforms (c) Energy Waveforms

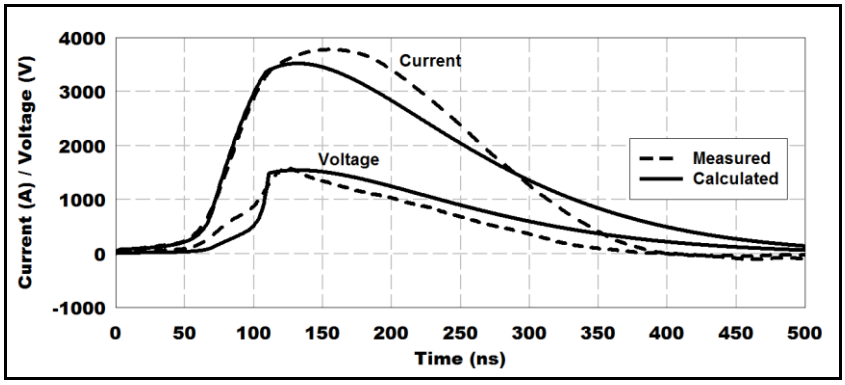

(a)

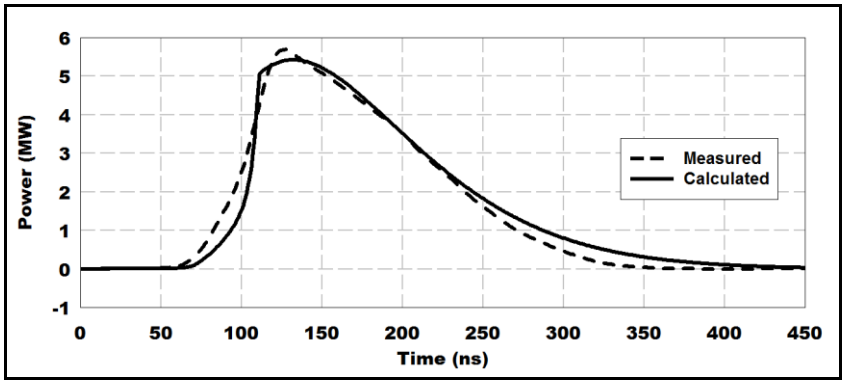

(b)

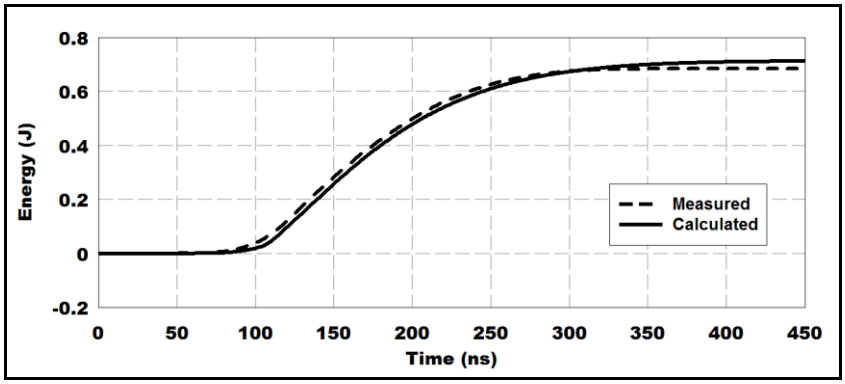

(c)

Figure 6.20 Measured and Calculated Electrical Performances for Type 1 Striplines at 2800 Volts
(a) Current and Voltage Waveforms (b) Power Waveforms (c) Energy Waveforms

Figure 6.21 shows electrical performance predictions for Type 2 striplines. It is observed that predicted current waveform has a higher deviation from the measured one. The lower predicted current levels result a lower energy prediction. Furthermore, estimation of the burst time from voltage peak gives an earlier value compared to the experimental burst time value.

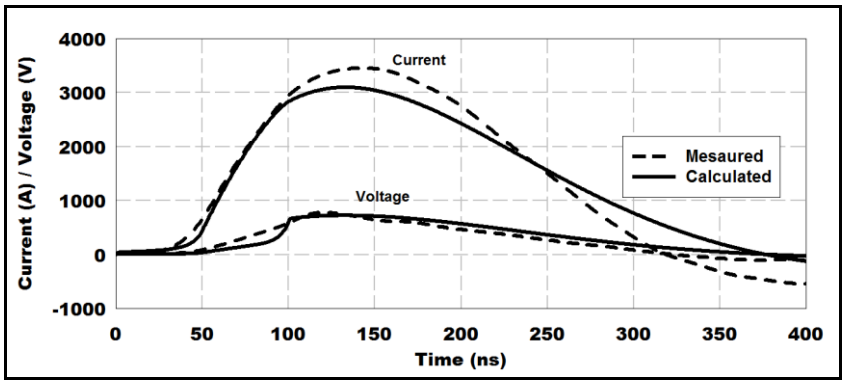

(a)

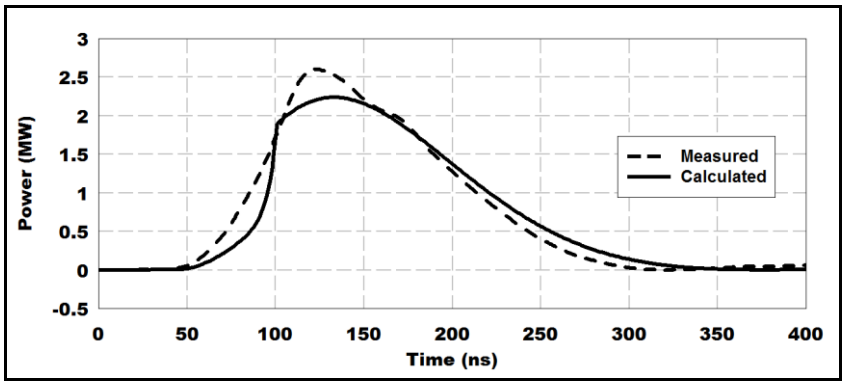

(b)

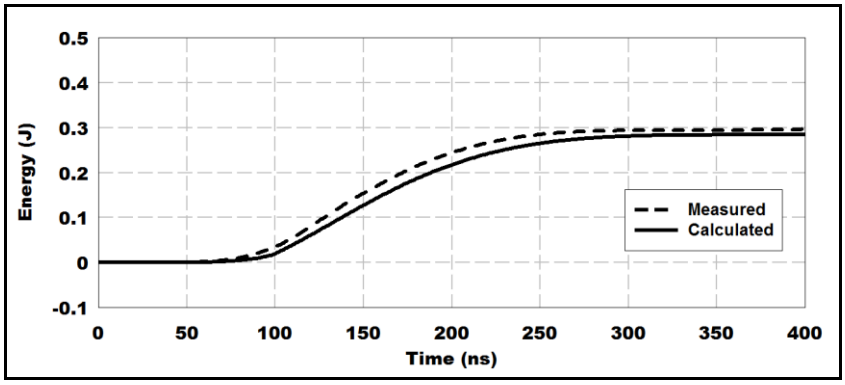

(c)

Figure 6.21 Measured and Calculated Electrical Performances for Type 2 Striplines at 2000 Volts
(a) Current and Voltage Waveforms (b) Power Waveforms (c) Energy Waveforms

Figure 6.22, Figure 6.23 and Figure 6.24 demonstrate electrical performance predictions for Type 3 striplines. Unlike predictions for Type 1 striplines, theoretical model shows rather a poor agreement in predicting the current rise part. One possible explanation for this situation may be the higher inductance level of striplines which can be caused by inadvertently lamination of layers. Furthermore the poor prediction in current waveform is reflected onto energy predictions and the model results lower values for energy.

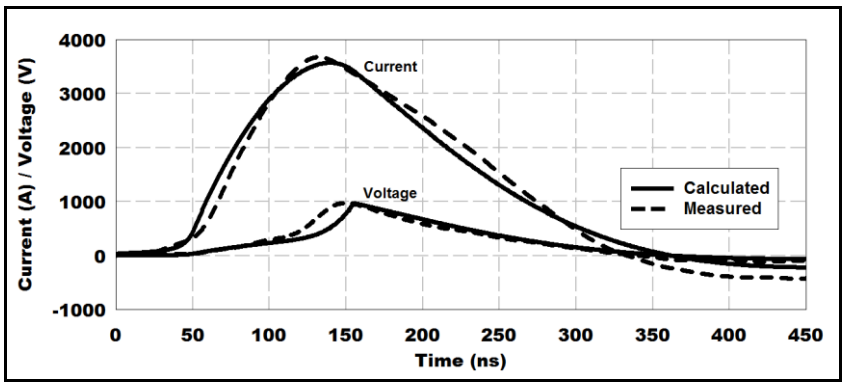

(a)

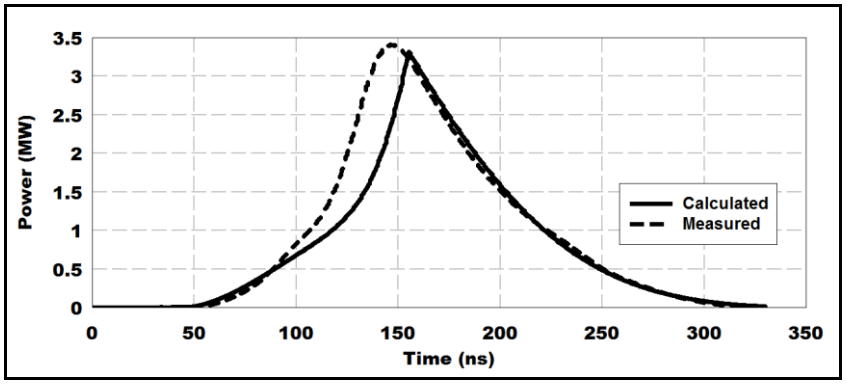

(b)

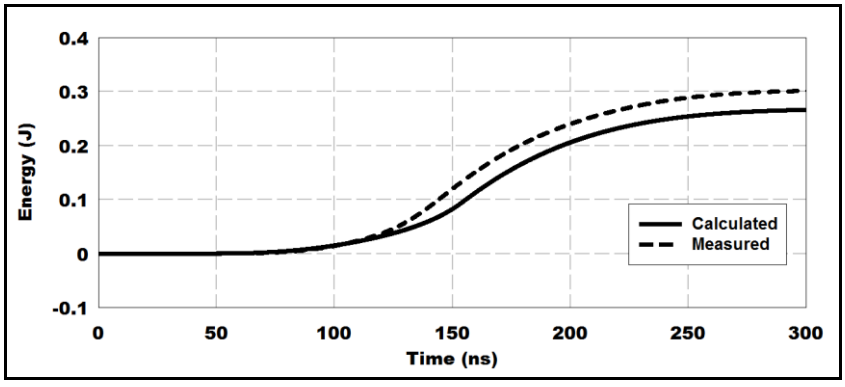

(c)

Figure 6.22 Measured and Calculated Electrical Performances for Type 3 Striplines at 2000 Volts
(a) Current and Voltage Waveforms (b) Power Waveforms (c) Energy Waveforms

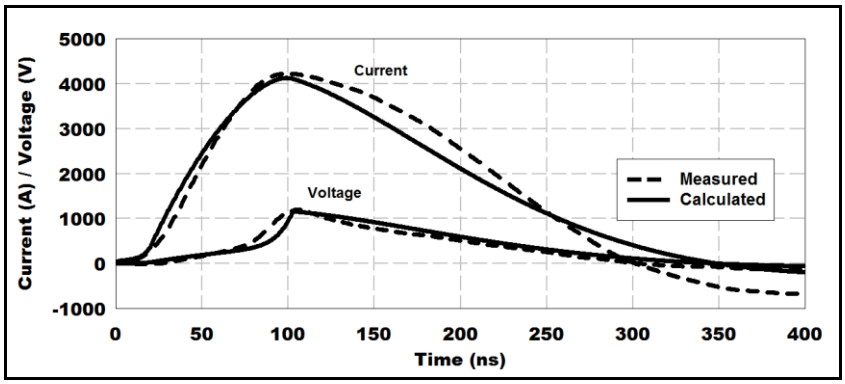

(a)

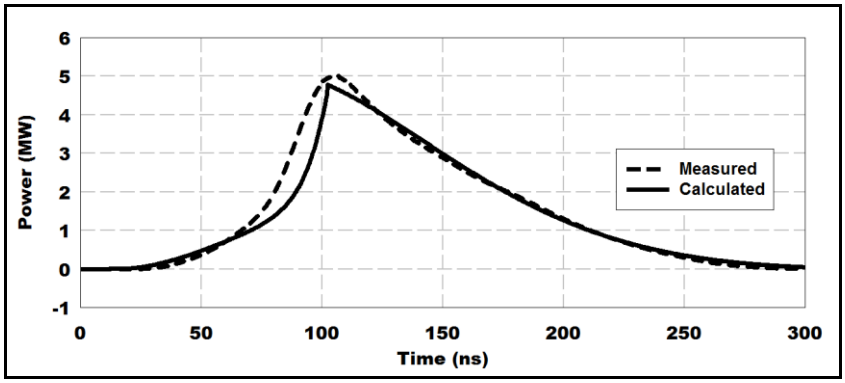

(b)

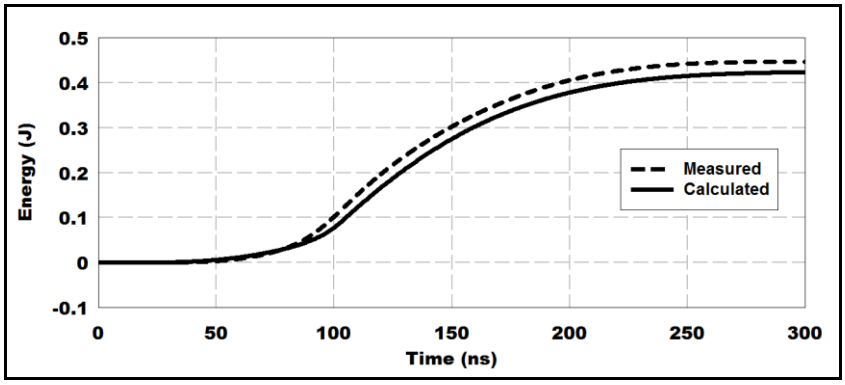

(c)

Figure 6.23 Measured and Calculated Electrical Performances for Type 3 Striplines at 2400 Volts
(a) Current and Voltage Waveforms (b) Power Waveforms (c) Energy Waveforms

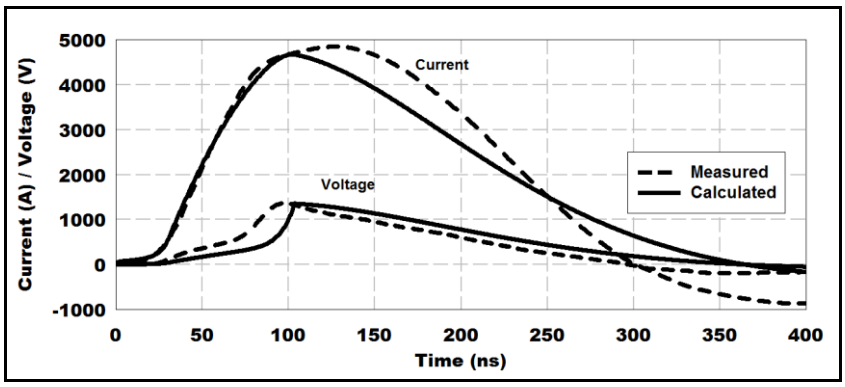

(a)

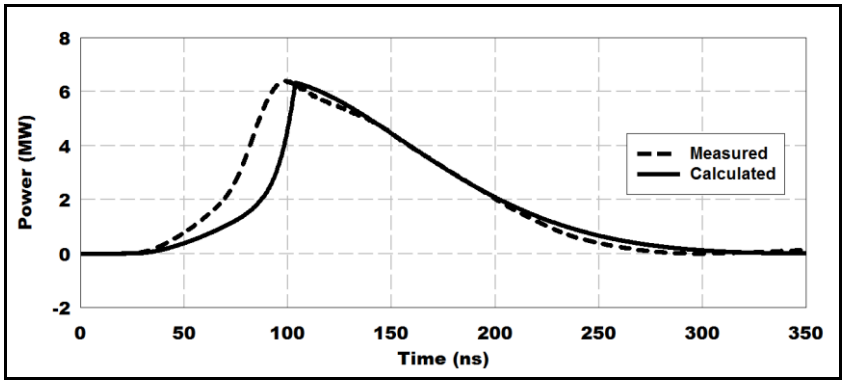

(b)

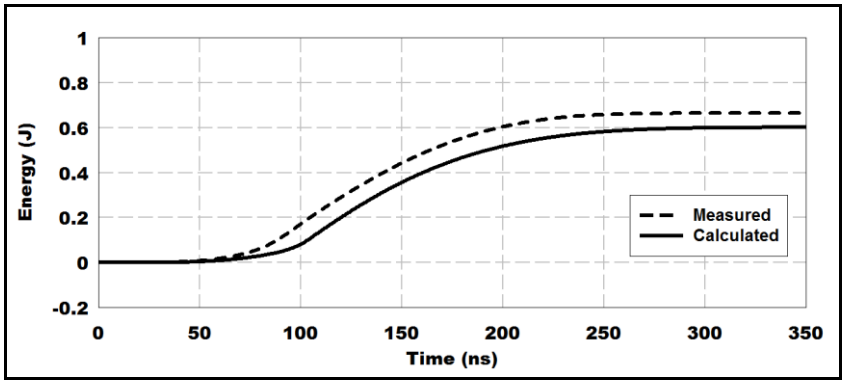

(c)

Figure 6.24 Measured and Calculated Electrical Performances for Type 3 Striplines at 2800 Volts
(a) Current and Voltage Waveforms (b) Power Waveforms (c) Energy Waveforms

Table 6.7 gives relative percentage errors in current and voltage comparisons shown in above plots. Results for burst time, burst current and burst voltage are obtained from measurements and numerical study. Relative percentage errors are calculated using Equation (6.4) given below.

$$E_{RPE} = \left| \frac{x_{bm} - x_{bc}}{x_{bm}} \right| \times 100 \tag{6.4}$$

Table 6.7 Relative Percentage Errors in Electrical Performance Calculations

Stripline Type	*Firing Voltage (V)*	*Relative Error %*		
		Burst Time	*Burst Current*	*Burst Voltage*
Type 1	2000	8.3	5.8	4.2
Type 1	2400	9.4	2.8	3.1
Type 1	2800	8.7	4.7	4.9
Type 2	2000	13.3	13.3	13.2
Type 3	2000	3.5	0.5	1.1
Type 3	2400	1.5	2.4	4.6
Type 3	2800	6.2	1.1	0.5

To summarize the electrical performance predictions, the theoretical model results good estimations for Type 1 and Type 3 striplines in burst time values (relative percentage errors below 10%, given in Table 6.7) whereas it deviates from the measured data for Type 2 striplines. Trends of Type 1 stripline waveforms are more likely to match with the recorded data than the other two types. These deviations are more likely to occur from defective manufacturing of striplines as stated in CHAPTER 3. That is, especially the dimensions and the constants used for the striplines in the model may differ from the real case.

It should be noted that in order to anticipate the discharge voltage level for a specific stripline which will be used for detonating a high explosive, the initiation criterion of that particular explosive should be checked by the theoretical model. Therefore predicted energy levels should be in good agreement with the measured ones even the current or voltage waveforms deviate since energy strongly affects the impact characteristics.

6.2.2 Velocity Predictions

Using the equations given in CHAPTER 5, velocity histories of the flyer plates for different striplines are determined by the numerical code. From displacement histories

average velocities are calculated and compared with the ones obtained from experiments.

The constants used in the calculations are given in Table 6.8.

Table 6.8 Some Constants Used in Velocity Predictions [19]

Constants	*Values*
ρ_f	1.414 g/cc
ρ_{tamp}	1.414 g/cc

As stated in CHAPTER 5, two methods are utilized in numerical calculations with different polytropic gas constants [12]. Results of the numerical study obtained with these two methods compared by the experimental ones are given in Figure 6.26 for all stripline types fired at 2000 volts.

Before representing the average velocity comparisons, an example for the calculated displacement history of the flyer plate belonging to Type 1 stripline is shown in Figure 6.25. As stated several times before, first, time difference is found between the arrival point and burst point which gives the flight time of the flyer plate. Then the barrel length is divided to that flight time to obtain the average velocity of the flyer plate. One should note that displacement of the flyer plate shown in Figure 6.25 starts at 5 μm (not zero) which actually corresponds to the thickness of the metallic bridge. The reason for this situation is explained in CHAPTER 5.

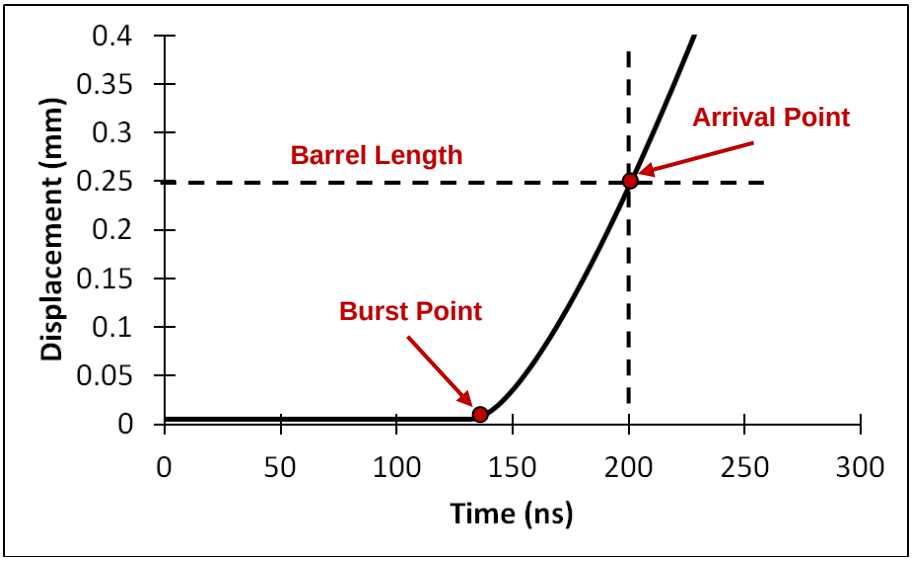

Figure 6.25 A Sample Calculated Displacement History of the Flyer Plate Belongs to Type 1 Stripline Fired at 2000 Volts

Figure 6.26 (a) shows the average velocity comparison for two numerical methods that utilize a polytropic gas constant n = 1.2. From this figure, it is clear that Second Method estimates the average velocities better. First Method generally gives higher values since it uses the excess energy at burst. Moreover, predictions for Type 1 striplines seem the best whereas Type 2 striplines are the worst. This situation can be related with electrical performance predictions. It is expected from the measured and calculated energy waveforms that Type 1 striplines are expected to give good estimates for average velocities. It is further expected that since measured energy values are greater than the calculated ones for Type 2 striplines, they have higher measured average velocities. As for Type 1, for electrically same stripline configurations (Type 3, 4, 5, 6) Second Method should be used because it gives closer results to measured values. Second Method also underestimates the average velocities that should be preferred to be on the safe side in design considerations.

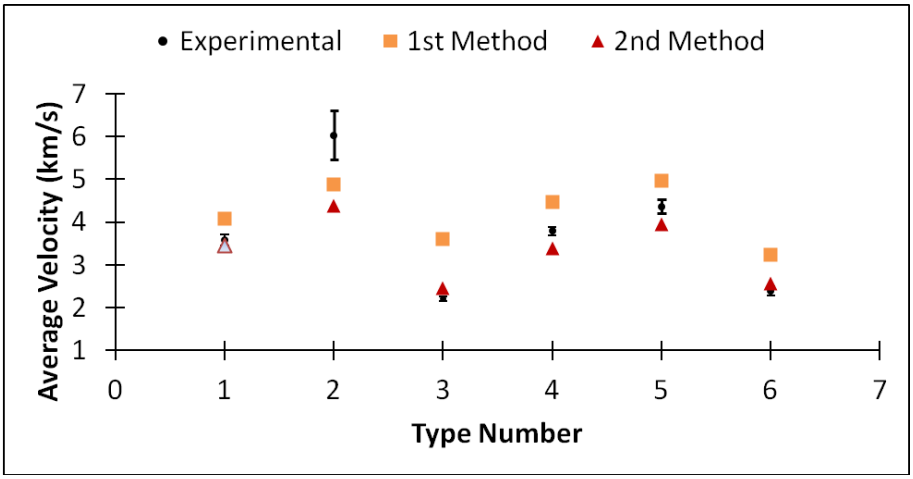
Experimental
1st Method
2nd Method
Average Velocity (km/s)
Type Number
0
1
2
3
4
5
6
7

(a)

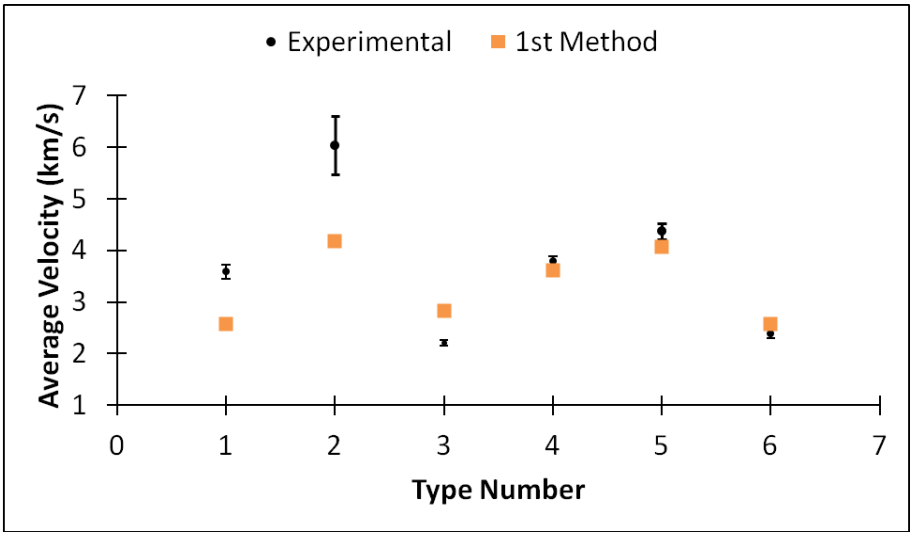
Experimental
1st Method
Average Velocity (km/s)
Type Number
0
1
2
3
4
5
6
7

(b)

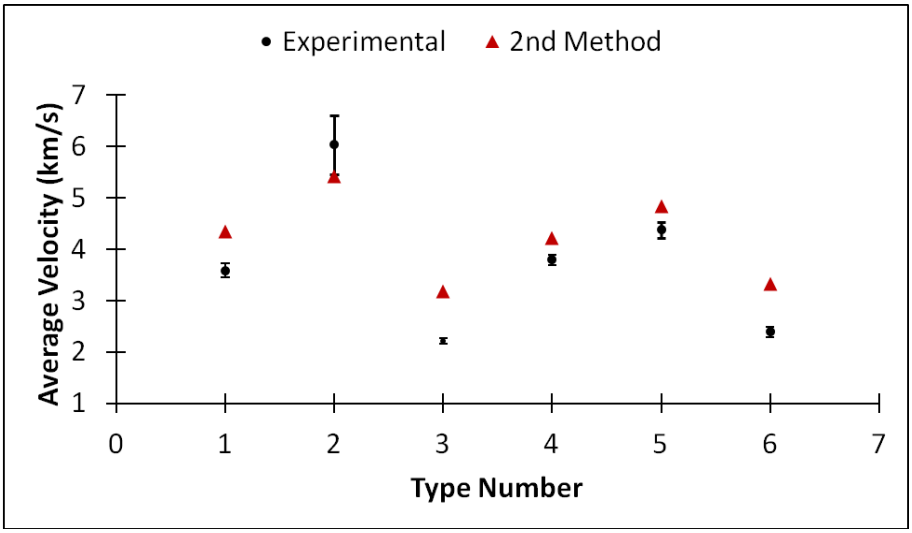

(c)

Figure 6.26 Comparison of Measured and Calculated Average Velocities for All Stripline Types at 2000 Volts
(a) n = 1.2 (b) n = 1.1 (c) n = 5/3

In Figure 6.26 (b), it is checked whether using a lower n value in First Method decreases the estimated average velocities. The result is positive; however, still using Second Method with n = 1.2 is preferred.

Then in Figure 6.26 (c), same phenomenon in First Method is sought in Second Method to realize whether the estimated values can be perfectly fit to measured ones by using n = 5/3. However, this time Second Method gives greater values and it is decided not to go on further by changing n.

Figure 6.27 also depicts comparison of average velocities calculated by two numerical methods at various firing voltage levels for Type 1 and Type 4 striplines.

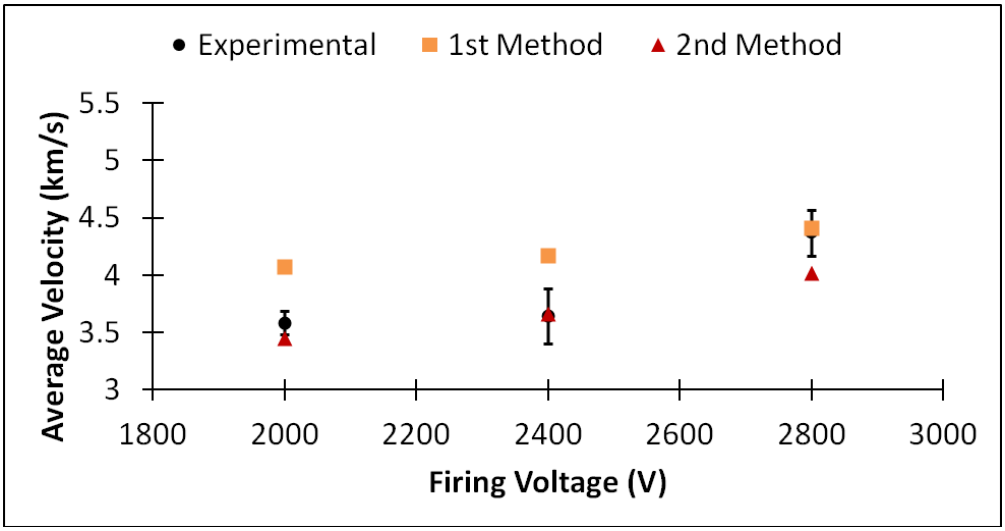

(a)

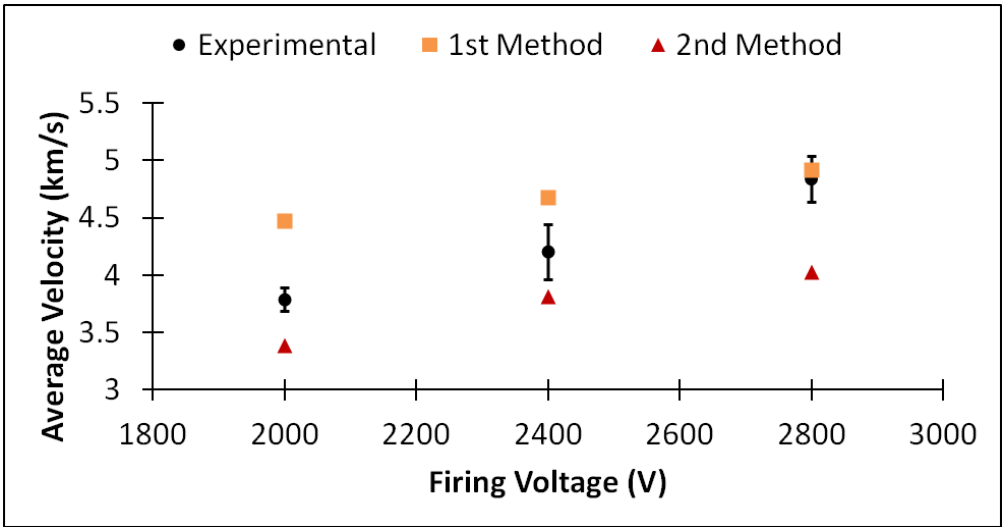

(b)

Figure 6.27 Comparison of Measured and Calculated Average Velocities at Various Firing Voltage Levels
(a) Type 1 Striplines (b) Type 4 Striplines

Final velocity of the flyer plate is defined as the velocity just at the exit of the barrel. First, the time when the flyer plate reaches the exit of the barrel is found and at that time final velocity is determined from the velocity history. Figure 6.28 shows both velocity history and velocity versus displacement plots.

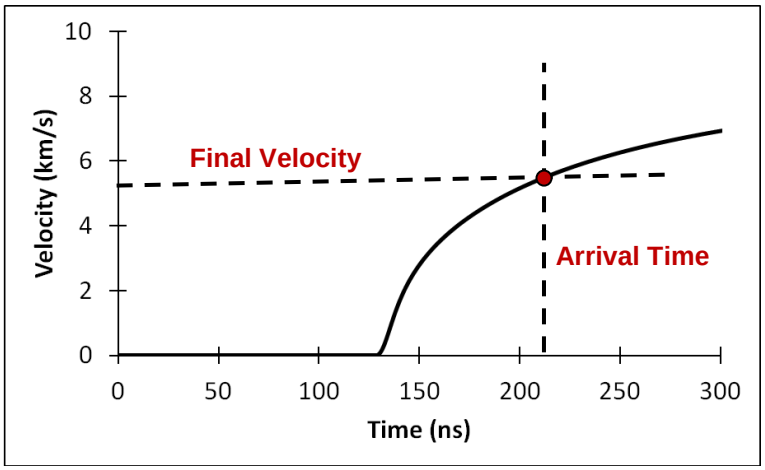

(a)

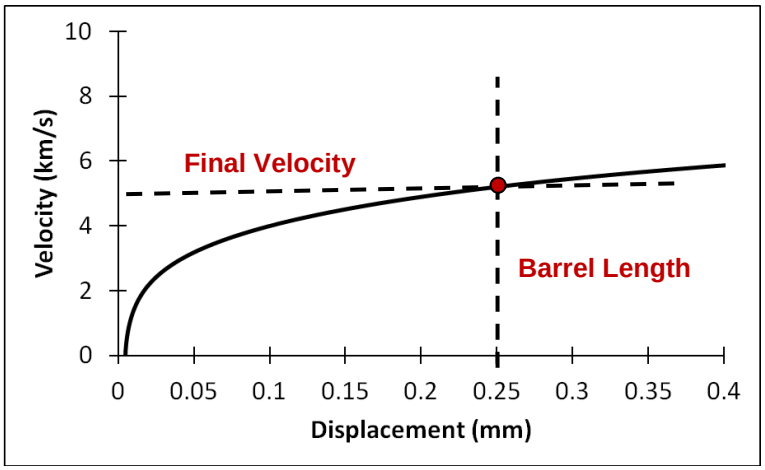

(b)

Figure 6.28 Calculated Flyer Plate's Velocity Plots for Type 1 Striplines Fired at 2000 Volts
(a) Velocity versus Time (b) Velocity versus Displacement

Figure 6.29 demonstrates final velocities of the flyer plates calculated by both methods for all striplines. Referring the final velocities of Type 1, Type 2, Type 4 and Type 5

striplines, regardless of the dimensions of the metallic bridge, using a low height barrel and a thicker flyer plate result rather low velocities.

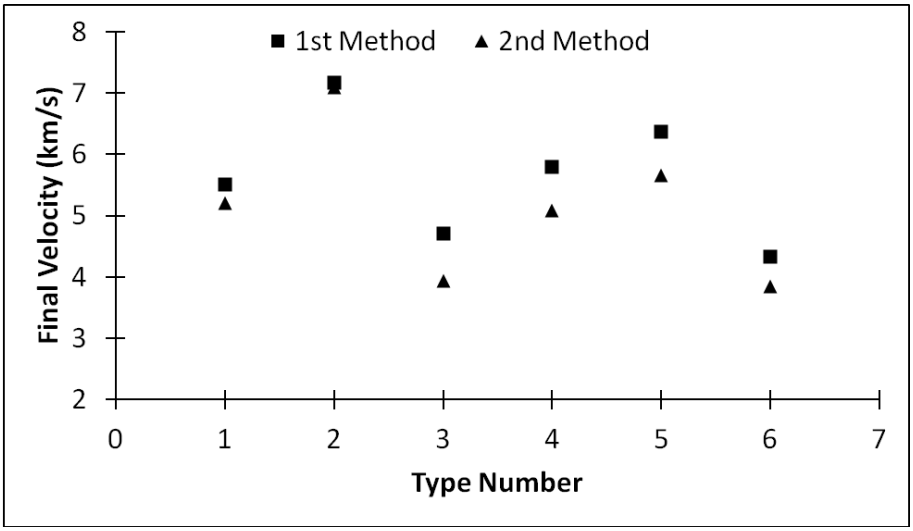

Figure 6.29 Comparison of Final Velocities of Flyer Plates Belong to All Striplines at 2000 Volts for Two Numerical Methods

Figure 6.30 gives final velocities for Type 1 and Type 4 striplines at various firing voltage levels. At 2000 volts, final velocities are close; however, as voltage level increases Type 4 striplines have a greater increase compared to Type 1 striplines. Still there seems no significant increase in final velocities for both types of striplines.

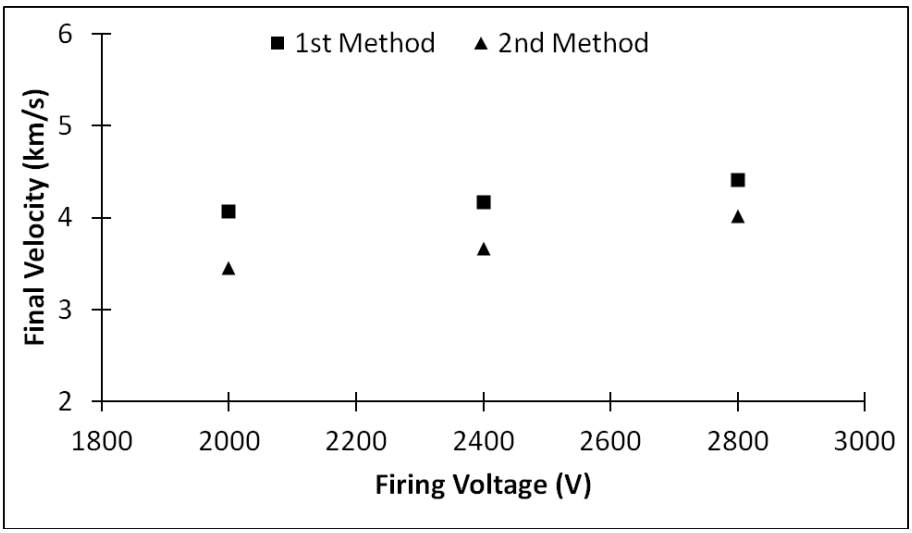

(a)

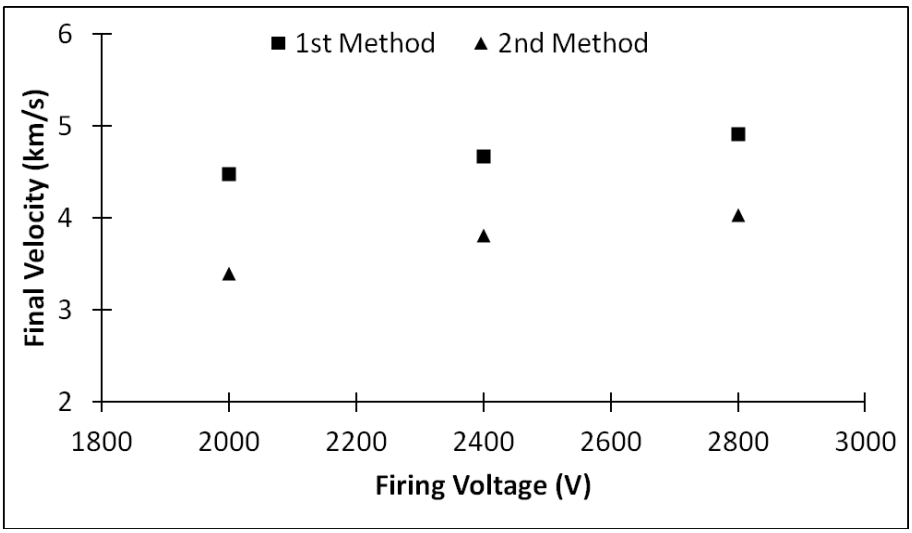

(b)

Figure 6.30 Comparison of Final Velocities of Flyer Plates Belong to Two Types of Striplines at Various Firing Voltage Levels for Two Numerical Methods
(a) Type 1 Striplines (b) Type 4 Striplines.

To sum up the velocity predictions, the theoretical model shows good estimations in average velocities with Second Method and n = 1.2. Comparing final velocities

obtained from numerical calculations, Type 2 striplines have the greater velocity whereas Type 6 is the worst.

Using shorter barrel lengths definitely lowers velocity. However, once more it should be noted that there is an optimum barrel length and beyond this length velocity of the flyer plates begins decreasing [14]. In this study, this length is thought to be slightly higher than 0.4 mm for 9 μm thick striplines. Moreover, when two different barrel lengths are compared in the case they both result sufficient velocities for the flyer plates, shorter one should be selected since longer barrels adds up extra time for detonation. This increases the function time of the detonator.

Higher firing voltage levels certainly results higher velocities; however, lowest possible voltage level that gives sufficient flyer plate's velocities should be determined.

6.2.3 Pressure Pulse Predictions and Initiation Criterion Check

Having defined the final velocity V_f of the flyer plate from the numerical study, equations stated in CHAPTER 5 is used to determine the impulse pressure. For all types of striplines and firing voltage levels, results are shown in Figure 6.31.

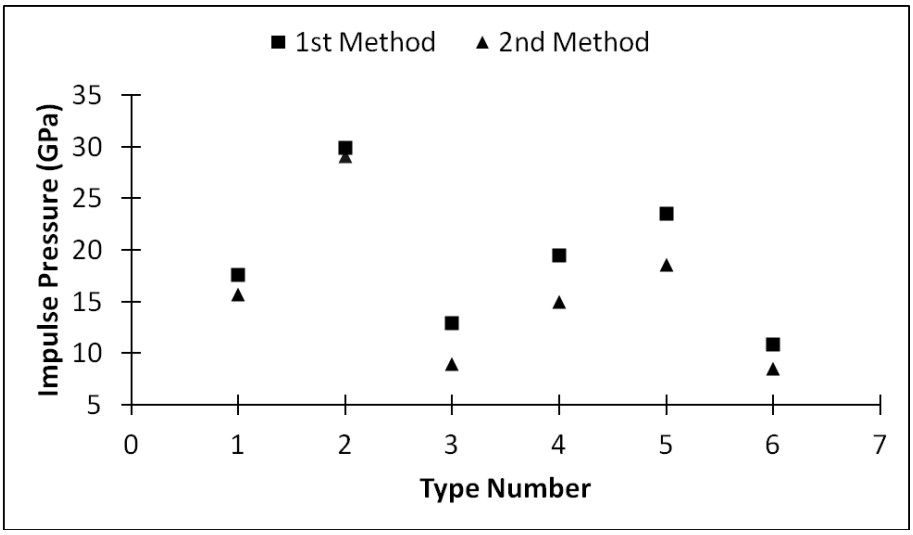

(a)

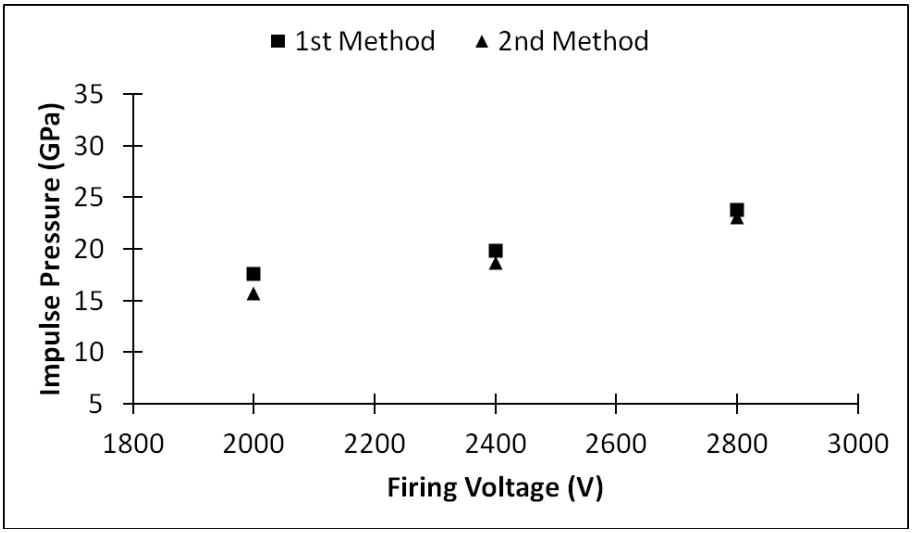

(b)

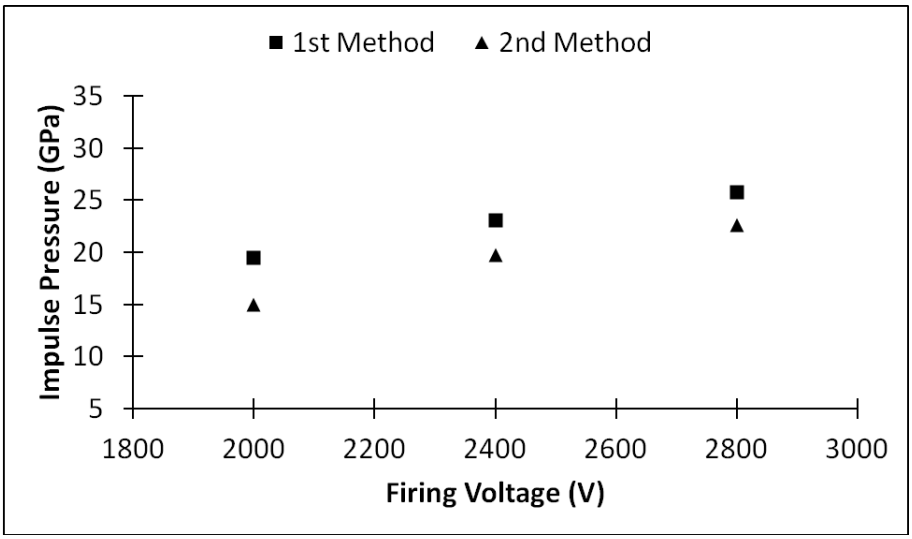

(c)

Figure 6.31 Impulse Pressure Calculation Results
(a) All Striplines at 2000 Volts (b) Type 1 Striplines at Various Firing Voltage Levels
(c) Type 4 Striplines at Various Firing Voltage Levels

HNS - IV is the intended secondary high explosive to be used with EFI striplines. In order to have a high degree detonation a certain criterion should be maintained. Initiation criterion for HNS - IV is given in [19] as

$$P_e^{2.36} \times t_p \geq 2.25 \text{ Gpa}^{2.36}\text{-}\mu\text{s} \tag{6.5}$$

Some constants used in the calculation of initiation criterion check are given in Table 6.9.

Table 6.9 Some Constants Used in Initiation Criterion Check [19]

Constants	*Values*
C_f	0.93E-5 cm/s
S_f	1.64
C_e	2.2E-5 cm/s
S_e	1.45
ρ_e (HNS - IV)	1.6 g/cc
C_f	0.93E-5 cm/s
S_f	1.64

For all type of striplines and at various firing voltage levels, initiation criterion check results are shown in Figure 6.32. All stripline types are simulated as they result detonation when fired at 2000 volts. Also it is understood that as firing voltage level increases, the calculated values is alienated from the critical no-detonation value as expected.

One interesting point in velocity, pressure and initiation criterion check calculations is that although Type 6 stripline has the lowest velocity, its $P_e^{2.36}t_p$ value is greater than the one for Type 3 stripline. One good reason for this situation is the role of flyer plate's thickness on the impact. That is, since the duration of impulse pressure is affected by the thickness which is formulated in Equation (5.33), $P_e^{2.36}t_p$ for Type 6 striplines give slightly higher values.

Also detonations of HNS – IV explosives with Type 1 striplines fired at 2000 volts are properly simulated by the initiation criterion check calculations since the model predicts that detonation will occur as a result of firing Type 1 striplines at 2000 volts.

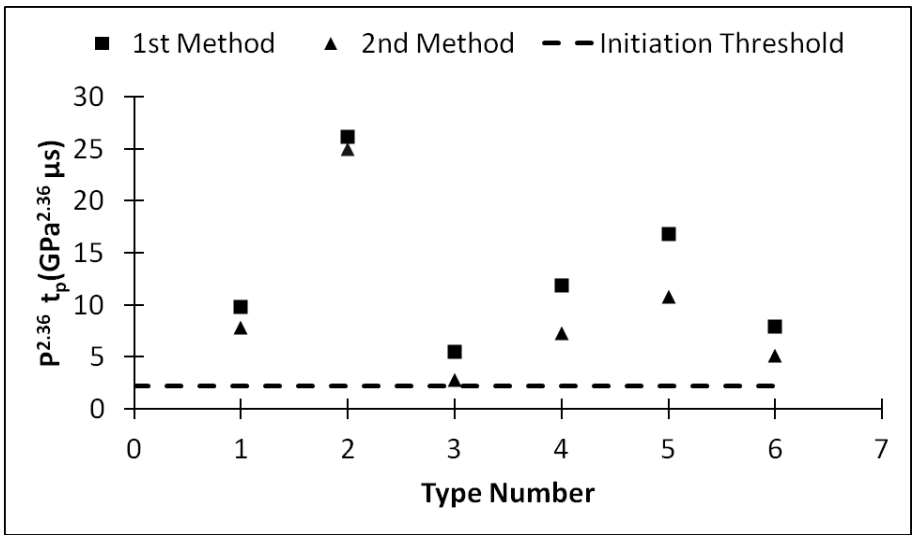
1st Method
2nd Method
Initiation Threshold
$P^{2.36} t_p (GPa^{2.36} \mu s)$
30
25
20
15
10
5
0
0
1
2
3
4
5
6
7
Type Number

(a)

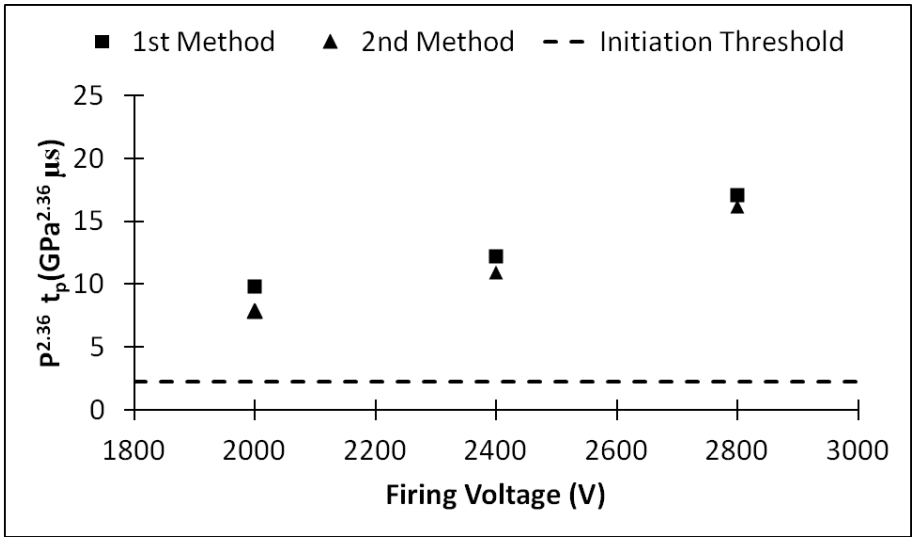
1st Method
2nd Method
Initiation Threshold
$P^{2.36} t_p (GPa^{2.36} \mu s)$
25
20
15
10
5
0
1800
2000
2200
2400
2600
2800
3000
Firing Voltage (V)

(b)

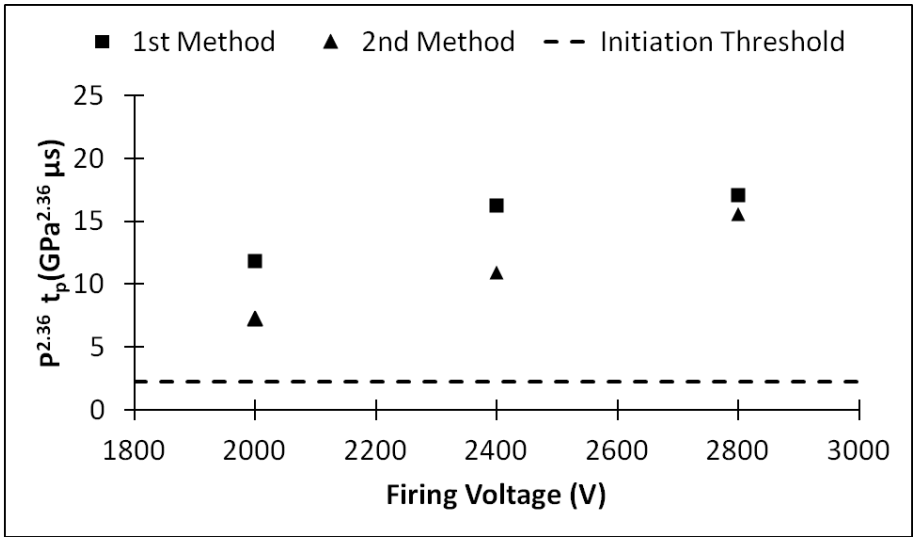

(c)

Figure 6.32 Initiation Criterion Check Results
(a) All Striplines at 2000 Volts (b) Type 1 Striplines at Various Firing Voltage Levels (c) Type 4 Striplines at Various Firing Voltage Levels

6.3 CASE STUDY

This section provides results of two parametric studies by utilizing the numerical code. The first study is about changing some electrical parameters in CDC to show the effects of these parameters on an EFI system. Type 1 striplines are used for the first study. The second one includes altering the discharge voltage levels below 2000 volts for Type 1 and Type 4 striplines to find out at which voltage level detonation of HNS – IV is not expected to occur.

Avoiding empiricism; switching effects are not considered and resistance and temperature values at burst are kept constant for the striplines.

6.3.1 First Case

Figure 6.33 shows the effect of resistance on current and voltage waveforms. It is obvious that increasing the resistance of the CDC while keeping inductance and capacitance constant, decreases current and voltage values resulting a decrease in the energy. Reduction in the energy definitely causes decrease in velocities and $P_e^{2.36}t_p$ values tabulated in Table 6.10.

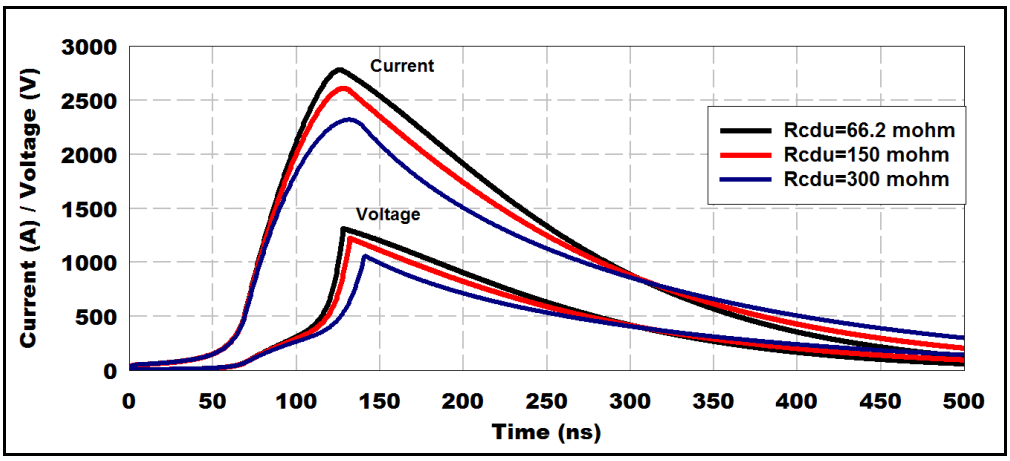

Figure 6.33 Effect of CDC Resistance on Current and Voltage Waveforms

Table 6.10 Effect of CDC Resistance on Velocity and $P_e^{2.36}t_p$

CDC Resistance (mohm)	V_f *(km/s)*	$P_e^{2.36}t_p$ *($GPa^{2.36}$ - μs)*
66.2	5.20	7.86
150	4.83	4.83
300	4.21	3.61

Figure 6.34 shows the effect of inductance on current and voltage waveforms. It is clear that increasing the inductance of the CDC while keeping resistance and capacitance constant, decreases current and voltage values resulting a reduction in the energy. Reduction in the energy definitely causes decrease in velocities and $P_e^{2.36}t_p$ values tabulated in Table 6.11.

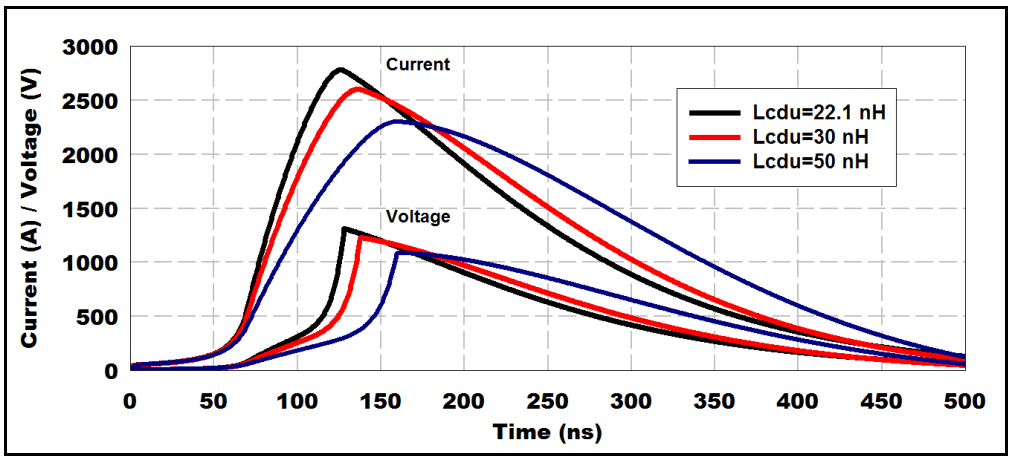

Figure 6.34 Effect of CDC Inductance on Current and Voltage Waveforms

Table 6.11 Effect of CDC Inductance on Velocity and $P_e^{2.36}t_p$

CDU Inductance (nH)	V_f *(km/s)*	$P_e^{2.36}t_p$ *($GPa^{2.36}$ - μs)*
22.1	5.20	7.86
30	5.08	7.24
50	4.82	5.94

Figure 6.35 shows the effect of capacitance on current and voltage waveforms. Besides the capacitance value used in this study, 0.1 μF is simulated since using a smaller capacitance value is suggested in military standards. It is obvious that as capacitance decreases while keeping resistance and inductance constant, current and voltage values decreases resulting a reduction in the energy. Reduction in the energy causes decrease in velocity and $P_e^{2.36}t_p$ values as tabulated in Table 6.12. Therefore using a 0.1 μF capacitance in CDC while keeping resistance and inductance at the levels stated in this study, striplines should be fired at a higher voltage level in order to have similar characteristics and most importantly to have detonation in the explosive.

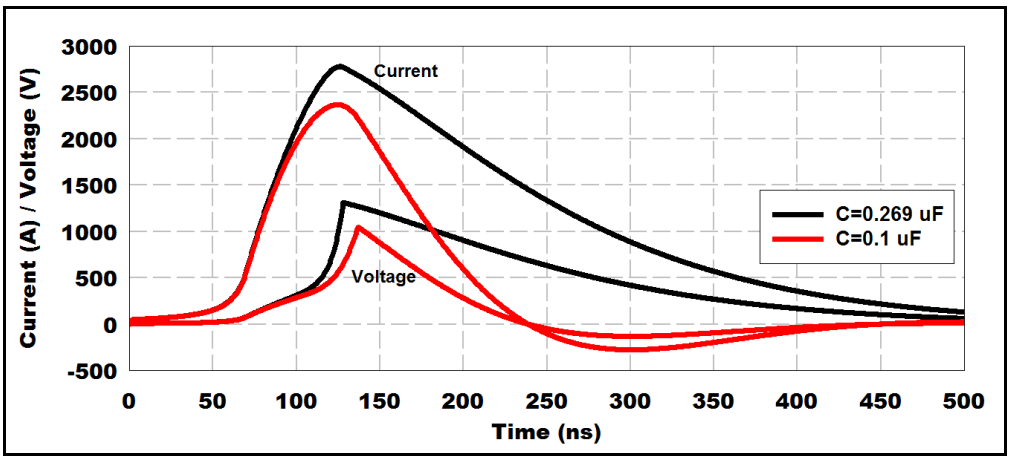

Figure 6.35 Effect of CDC Capacitance on Current and Voltage Waveforms

Table 6.12 Effect of CDC Capacitance on Velocity and $P_e^{2.36}t_p$

CDC Capacitance (μF)	V_f *(km/s)*	$P_e^{2.36}t_p$ *($GPa^{2.36}$ - μs)*
0.269	5.20	7.86
0.1	3.55	1.91

6.3.2 Second Case

Figure 6.36 shows the effect of discharge voltage on $P_e^{2.36}t_p$ value for Type 1 and Type 4 striplines. Second Method is used in the calculations.

From Figure 6.36 (a) it is observed that the critical discharge voltage for Type 1 striplines is 1400 volts. Below this level, it is impossible to detonate HNS – IV explosives.

During calculations it is discovered that metallic bridge of Type 4 stripline does not burst at discharge voltage levels 1200 volts and below. The critical discharge voltage level for Type 4 striplines is determined to be 1600 volts as expected to be higher than Type 1 striplines.

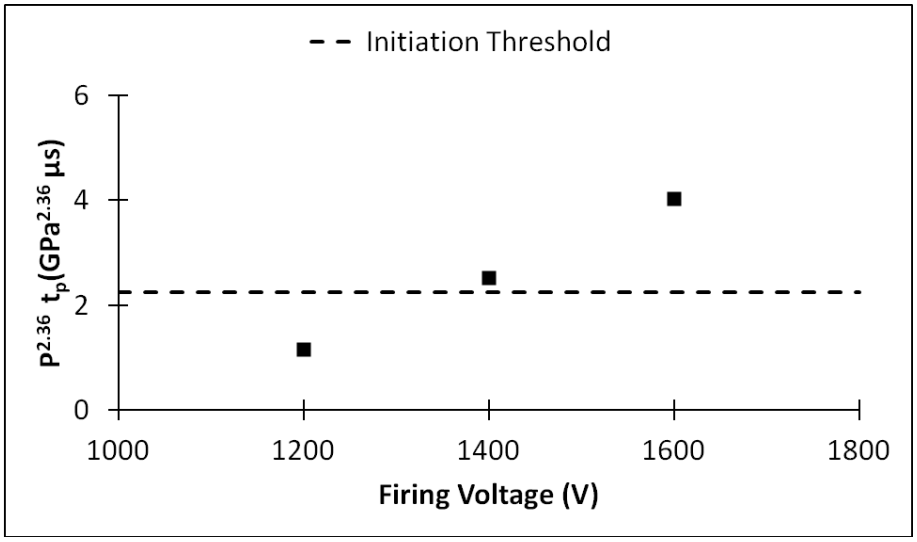

(a)

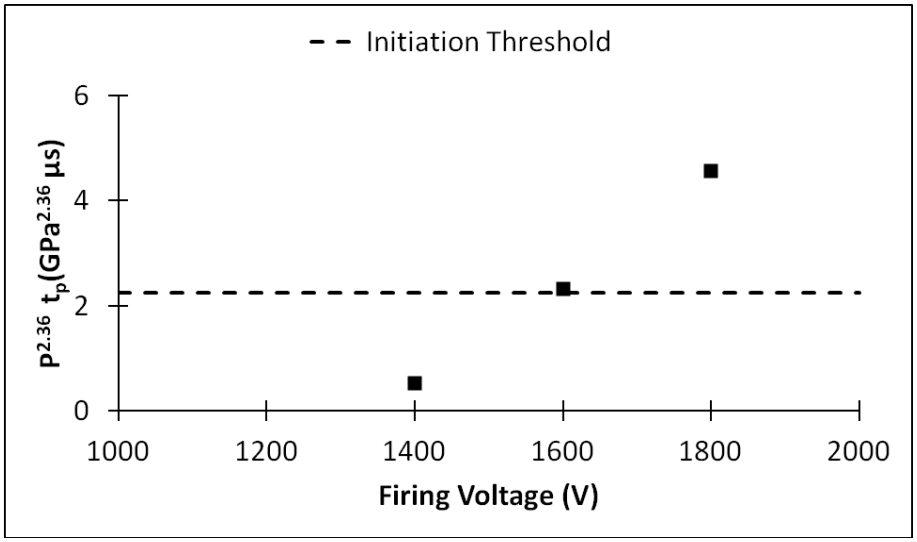

(b)

Figure 6.36 Initiation Criterion Check Calculations at Firing Voltage Levels below 2000 Volts
(a) Type 1 Striplines (b) Type 4 Striplines

CHAPTER 7

CONCLUSION

7.1 OVERVIEW OF THE STUDY

This thesis includes the studies that cover designing Exploding Foil Initiator (EFI) striplines and using these striplines in the detonation of two types of secondary high explosives. It also involves analyzing the electrical performances and impact characteristics of flyer plates with both experiments and theoretical calculations. Works accomplished in this thesis add a deep experience about design, manufacturing and analysis steps of EFIs.

Data obtained from open literature was so useful in both experimental and numerical study. Even old studies are still valid because there are lots of parametric surveys at the time when EFIs first invented and there have been little changes in the concept except commercial products. Most of the studies included laboratory testing and related development of experimental processes. Those were mostly for large scale EFIs. However, in recent years, it is realized that number of researches has been decreased in the world which may be because of the satisfactory investigations accomplished in the past.

In Turkey, there is indeed no academic work on EFIs or related high voltage applications. There is rare technology to produce EFIs and no experience about the manufacturing steps. Even the proper technology is developed; there will always be need for import sub - components in production stages of EFI striplines because of the insufficient facilities in the area of raw materials. Besides, explosives and related technologies should be transferred from experienced foreign countries. This great foreign – source dependency deeply affected the motivation of this study.

EFI striplines used in this study were manufactured in United States. In the meantime, the local production means were investigated but could not be utilized in the time limit of this study. Manufacturing striplines in another country was really tedious because of the very long import times and no chance of instantaneous intervention to possible poorly produced striplines.

Experimental setup was constructed from nothing with the help of literature data. Considerable number of striplines was fired to characterize the setup. Like in every experimentation there happened unexpected situations that resulted some unplanned loss of time. For instance, the initially used high voltage power supply was damaged after some tests because of the voltage reversals which were caused by the regular operation of the system. This power supply was immediately replaced with the one which is immune to stated voltage reversals. The situation caused a loss like five months with no tests. However, against all odds, an experimental setup that is fairly enough to characterize small scale EFIs is established.

Numerical study is based on previously derived useful formulas found in literature. Numerical model is mostly theoretical; however, adding some empiricism resulted to have a more substantial model. Results of the numerical study and experiments show good agreement so the model can be confidently used in predicting all performance characteristics of EFI striplines.

From the study, following results are derived;

- Using 9 μm thick bridge foils results higher flyer plate velocities than using 5 μm thick bridge foils. However, this does not mean further increasing bridge foil thickness will increase the flyer plate's velocity.
- As expected, smaller bridge dimensions give higher flyer plate velocities. Still the characteristics at impact for low mass bridge foils should be determined.
- Increasing the barrel length increases the velocity of the flyer plate. However, it should not be ignored that there is always an optimum barrel length beyond which the flyer plate's velocity will decrease because of the cooling plasma. Besides, using long barrels increases the time for detonation since the flyer plate spends more time to reach the explosive pellet.
- All literature survey, commercial products and results of this study show that optimum flyer plate thickness is 25.4 μm if Kapton® is used.
- Higher firing voltage levels definitely give higher flyer plate velocities, smaller burst and detonation times and increased probability for detonation of a specific explosive.
- As expected, HNS – IV explosive pellets were easily detonated at 2000 volts firing voltage level whereas PBXN – 5 explosive pellets did not. This is due to the insensitive behavior and high density of PBXN – 5 explosive pellets. As HNS – IV needs low firing energies and it is superior against harsh environments, it should be the choice in EFI applications.

The result of this thesis is an EFI which can be used in rocket motor and warhead initiation trains with appropriate Capacitor Discharge Circuits that has the similar characteristics with the one in this study.

7.2 FUTURE WORK

Possible future areas of interests are summarized below;

- Threshold, all – fire and no – fire voltage levels of EFIs with HNS – IV explosive pellets can be determined by using Bruceton Test method.
- Pelletization of PBXN – 5 powder to lower densities can be done and firings of these explosive pellets to specify an initiation criterion for PBXN – 5 can be accomplished (open literature lacks of such a data for PBXN – 5).
- Electrical performance and flyer plate's velocity measurements can be carried out with squib-wise (an alternative to stripline version) EFIs which will be produced in Turkey.

REFERENCES

[1] Varosh, R., *"Electric Detonators: EBW and EFI"*, Propellants, Explosives, Pyrotechnics 21, 150-154, 1996.

[2] Keller, D.V., Penning, J. R., Jr., *"Exploding Foils – the Production of Plane Shock Waves and the Acceleration of Thin Plates"*, Exploding Wires Vol. 2, 1962.

[3] Stroud, J.R, *"A New Kind Of Detonator – The Slapper"*, UCRL-7739, Lawrence Livermore National Laboratory, 1976.

[4] Chau, H.H., Dittbenner, W.W., Honodel, C.A., Steinberg, D.J., Stroud, J.R., Weingart, R.C., and Lee, R.S., *"Electric Gun: A Versatile Tool for High-Pressure Shock-Wave Research"*, American Institute of Physics, 1980.

[5] Chau, H., Dittbenner, G., Mikkelsen, K., Weingart, R., Froeschner, K., Lee, R., *"Performance of a 100 kV, 78 kJ, Electric – Gun System"*, UCRL-86259, Lawrence Livermore National Laboratory, 1981.

[6] Osher, J.E., Chau, H., Gathers, G.R., Lee, R.S., Pomykal, G.W., Weingart, R.C., *"Shock - Wave Studies Using Plastic Flyers Driven by an Electric Gun for Hypervelocity Impact on Selected Materials"*, UCRL-96498, Lawrence Livermore National Laboratory, 1987.

[7] Osher, J.E., Chau, H., Gathers, G.R., Weingart, R.C., *"Characteristics of Flyer Impact For One – Dimensional Shock Wave Study Applications"*, UCRL-100901, Lawrence Livermore National Laboratory, 1989.

[8] Osher, J.E., Barnes, G., Chau, H., Gathers, G.R., Lee, R.S., Lee, C., Speer, R., Weingart, R.C., *"Operating Characteristics and Modeling of the LLNL 100 – kV Electric Gun"*, IEEE Transactions on Plasma Science Vol. 17 No. 3, 1989.

[9] Lee, R.S., Osher, J.E., Chau, H.H., Pomykal, G., Speer, R.D., *"1 MJ Electric Gun Facility at LLNL"*, UCRL-JC-108530, Lawrence Livermore National Laboratory, 1992.

[10] Furnberg, C.M., Peevy, G.R., Brigham, W.P., Lyons, G.R., *"Computer Modeling of Electrical Performance of Detonators"*, Sandia National Laboratories, AIAA-95-28, 1995.

[11] Tucker, T.J., Stanton, P.L., *"Electrical Gurney Energy: A New Concept in Modeling of Energy Transfer from Electrically Exploded Conductors"*, Sandia National Laboratories, SAND-75-0244, May 1975.

[12] Tucker, T.J., Stanton, P.L., *"A Gas Dynamics Gurney Analysis for Modeling the Acceleration History of An Exploding System"*, Sandia National Laboratories, 1977.

[13] Schmidt, S.C., Seitz, W.L., Wackerle, J., *"An Empirical Model to Compute the Velocity Histories of Flyers Driven by Electrically Exploding Foils"*, Los Alamos National Laboratory, LA-6809, 1977.

[14] Richardson, D.D., Northeast, E.D., and Ryan, P. F. X., *"An Exploding Foil Flying Plate Generator"*, Materials Research Laboratory, MRL-R-1133.

[15] Hatt, D.J., Ryan, P.F.X., *"Calibration and Testing of a Large – Scale Electric Gun for Shock Hugoniot Measurements"*, Materials Research Laboratory, MRL-TR-93-24, 1993.

[16] Hatt, D.J., Wolfson, M.G., *"Construction, Characterization and Evaluation of the AMRL Flyer Sensitivity Test Apparatus"*, Aeronautical and Maritime Research Laboratory, DSTO-TR-0218, 1996.

[17] Hatt, D.J., *"A VISAR Velocity Interferometer System at MRL for Slapper Detonator and Shock Wave Studies"*, Materials Research Laboratory, MRL-TR-91-42, 1991.

[18] Podlesak, M., *"Breakwire Technique for Hypervelocity Measurement"*, MRL-TR-92-39, October 1993.

[19] Nappert, L., *"An Exploding Foil Initiator System"*, DREV-R-9502, March 1996.

[20] Nappert L., Fortier, C., *"A New Approach to Electrical Characterization of Exploding Foil Initiators"*, DREV-TM-9827, December 1998.

[21] Neyer, B.T., Adams, J.T., Edwards, J.C., Stountenborough, T.L., and Tomasoski, R.J., EG&G Optoelectronics, *"A Low Cost, Reliable, Hermetically Sealed, Chip Slapper Detonator Suitable for Various Aerospace Application"*, 35th AIAA/ASME/SAE/ASEE Joint Propulsion Conference and Exhibit, AIAA-99-2555.

[22] Logan, J.D., Lee, R.S., Weingart, R.C., and Yee, K.S., *"Calculation of Heating and Burst Phenomena in Electrically Exploded Foils"*, Lawrence Livermore National Laboratory, 1976.

[23] Davies, H.R., Chapman, D.J., Vine, T.A., and Proud, W.G., *"Characterisation of An Exploding Foil Initiator (EFI) System"*, CP1195, Shock Compression of Condensed Matter, 2009.

[24] Hasman, E., Gvishi, M., and Carmel, Y., *"Measurement of Shock Initiation Threshold of HNAB by Flyer Plate Impact"*, Propellants, Explosives, Pyrotechnics 11, 144-149, 1986.

[25] Clement, D., Rudolf, K.P., *"The Shock Initiation Threshold of HNS as A Function of Its Density"*, Propellants, Explosives, Pyrotechnics 32, No.4, 2007.

[26] Neyer, B.T., Cox, L., Stountenborough, T., and Tomasoski R., *"HNS-IV Explosive Properties and Characterization Tests"*, AIAA-2003-5138.

[27] Waschl, J.A., and Hatt. D.J, *"Characterization of A Small Scale Exploding Bridge Foil Flyer Generator"*, Int. J. Impact Engng, Vol. 14, pp. 785-796, 1993.

[28] Lee, R.S., *"An Analytical Model for the Dynamic Resistivity of Electrically - Exploded Foils"*, Proc. of the 13th Symposium on Explosives and Pyrotechnics", 1986.

[29] Davies, H.R., Vine, T.A., Williamson, D.M., *"Velocity Measurements of Exploding Foil Initiators (EFIs) Using High Speed Photography"*, New Trends in Research of Energetic Materials, Czech Republic, 2010.

[30] Murphy, M.J., *"Optical Diagnostic Techniques for Measuring Flows Produced by Micro – Detonators"*, M.S. Thesis, California State University Stanislaus, 2002.

[31] Scholtes, G., Prinse, W., *"Development of Exploding Foil Initiators and Micro Chip EFIs"*, Insensitive Munitions & Energetic Materials Technology Symposium, 2007.

[32] Hodgin R., May, C., Hanks, R., Hansen, D., Whitworth, T., *"Fabry Perot / PDV Comparison"*, 51th Annual Fuze Conference, 2007.

[33] Di Marzio, F., Szajman, J., Mazzolini, A., *"A Fibre Optic Sensor for High-Velocity Measurements of Projectiles Driven by Hot Gases"*, Aust. J. Physics., 48, 78-87, 1995.

[34] Davies, H.R., Chapman, D.J., Vine, T.A., and Proud, W.G., *"Development of An Optical System for High-Speed, Small-Scale Velocity Measurements"*, CP1195, Shock Compression of Condensed Matter, 2009.

[35] Saxena, A.K., Kaushik, T.C., Gupta, S.C., *"Shock Experiments and Numerical Simulations on Low Energy Portable Electrically Exploding Foil Accelerators"*, Review of Scientific Instruments 81, 2010.

[36] Sarkisov, G.S., Rosenthal, S.E, Struve, K.W., *"Thermodynamical Calculation of Metal Heating in Nanosecond Exploding Wire and Foil Experiments"*, Review of Scientific Instruments 78, 043505, 2007.

[37] Christensen, J.S., Hrousis, C.A., *"Three-Dimensional Magnetohydrodynamic Simulation of Slapper Initiation Systems"*, Lawrence Livermore National Laboratory, LLNL-CONF-425269, 2010.

[38] Richardson, D.D., *"The Effect of Switch Resistance on the Ringdown of A Slapper Detonator Fireset"*, Materials Research Laboratories, MRL-R-1004, December 1986.

[39] Logan, J.D., *EBF1: A Computer Simulation of the Preburst Behavior of Electrically Heated Exploding Foils"*, Lawrence Livermore Laboratory, UCRL-52003, 1976.

[40] Lide, D.R., *"CRC Handbook of Chemistry and Physics"*, 76th Edition, 1995-1996.